

Application of Photoluminescent Measurement Techniques for Quantitative Assessment of Turbine Film Cooling

THÈSE N° 4650 (2010)

PRÉSENTÉE LE 30 AVRIL 2010

À LA FACULTÉ SCIENCES ET TECHNIQUES DE L'INGÉNIEUR
LABORATOIRE DE THERMIQUE APPLIQUÉE ET DE TURBOMACHINES
PROGRAMME DOCTORAL EN ENERGIE

ÉCOLE POLYTECHNIQUE FÉDÉRALE DE LAUSANNE

POUR L'OBTENTION DU GRADE DE DOCTEUR ÈS SCIENCES

PAR

Magnus JONSSON

acceptée sur proposition du jury:

Prof. D. Favrat, président du jury
Dr P. Ott, directeur de thèse
Dr J. Krückels, rapporteur
Prof. J. R. Thome, rapporteur
Prof. B. Weigand, rapporteur



ÉCOLE POLYTECHNIQUE
FÉDÉRALE DE LAUSANNE

Suisse
2010

“All is flux; nothing stays still.”

Heracitus

Abstract

Reduction of the specific fuel consumption of gas turbines can be achieved by maximizing the turbine inlet temperature. However, this requires a detailed understanding of the cooling performance in order to ensure safe and economical operation of the engine. This is because the resulting temperature distributions in the blade walls dictate the thermal stresses and life-time of the hot section of the engine. Film cooling performance depends on a large number of parameters including turbulence making it complex to predict numerically. Moreover, the harsh flow conditions found in turbines situated directly downstream of the combustion chamber makes it difficult to obtain high resolution measurements of the relevant quantities. Therefore, simplified experiments are employed in order to simulate the engine situation by matching the most important flow similarity parameters. More specifically, the large difference in temperature between hot-gas and cooling air leads to considerable difference in density between the film cooling jets and hot-gas. This can be simulated at ambient temperatures by injecting a heavy foreign gas into a less dense main-flow of air.

This thesis aims at demonstrating the applicability of photoluminescent paints as sensing element for film cooling measurements. When this type of sensor is excited by ultraviolet light, the photoluminescent process leads to the emission of red-shifted light. The luminescence depends on oxygen pressure as well as temperature at the coating surface. A commercially available Pressure Sensitive Paint (PSP) is chosen for experimental characterization of the two fundamental quantities of film cooling:

- *Adiabatic film cooling effectiveness*
- *Heat transfer coefficients*

The adiabatic film cooling effectiveness is a measure of the mixing between coolant and mainflow. This quantity corresponds to concentration of gas species according to the analogy between heat and mass transfer. An oxygen-free coolant acts as tracer gas as it dilutes the oxygen of the main-flow, allowing for detailed measurements of the cooling gas concentration with PSP.

The corresponding convective heat transfer coefficient is measured by imposing step changes in heat flux and tracing the transient temperature

response of the wall. For this purpose, the same PSP-sensor is employed for thermography measurements by taking advantage of the inherent temperature sensitivity of this technology.

An engine-realistic test case illustrates the capability of the technique under complex flow conditions. It allows to demonstrate that measurements with high spatial resolution can be obtained over large portions of the surface within a short period of time. It turns out that the combination of oxygen pressure and temperature sensors, in the form of photoluminescent paint, is particularly advantageous in compressible flow experiments with moderate heat transfer at the wall. Another important advantage of the technique is the possibility to separate the adiabatic film cooling effectiveness from the wall heat transfer effects, without applying another coating for separate experiments. This ensures high geometrical tolerance of the small-scale cooling holes of the experimental models. However, the technique is limited by the maximum applicable temperature of the photoluminescent system making it first of all suitable for cold-flow measurements.

While both pressure and temperature sensitive paints have previously been employed in film cooling studies, the proposed combination of those techniques is unique in that it allows for simultaneous, yet decoupled measurement of the two fundamental quantities in film cooling.

In the present thesis, it is shown that the application of the presented technique allows to validate numerical flow models. Furthermore, conclusions can be transferred to the modelling of real engines in the form of technology trends. Ultimately, this allows to optimize film cooling performance and reduce the fuel consumption of gas turbines.

Keywords

Film cooling, convective heat transfer, photoluminescence, pressure sensitive paint, gas concentration, transient heating experiments

Version Abrégée

La réduction de la consommation en carburant des turbines à gaz peut être réalisée en maximisant la température des gaz à l'entrée de la turbine. Cela nécessite une meilleure analyse de la performance des systèmes de refroidissement afin d'assurer un fonctionnement sécurisé et économique du moteur. La distribution de la température à la surface des aubes impose en effet des contraintes thermiques agissant sur les parties chaudes du moteur ainsi que sur sa durée de vie. Les performances du refroidissement par film, ou film cooling, dépendent de nombreux paramètres de l'écoulement. Ainsi la turbulence complexifie les prédictions numériques. De plus, les conditions d'écoulement extrêmes rencontrées dans les étages de turbine situés directement à l'aval de la chambre de combustion ne permettent pas de réaliser des mesures précises de ces paramètres.

Par conséquent, des configurations d'essais simplifiées satisfaisant le plus grand nombre de paramètres de similitude sont employées pour simuler le fonctionnement des moteurs. L'important écart de densité entre le film de refroidissement et les gaz chauds, généré par la différence considérable de température entre les deux écoulements, est simulé à température ambiante en injectant un gaz lourd au sein d'un écoulement principal moins dense.

Cette thèse vise à démontrer l'applicabilité des peintures photo-luminescentes pour la réalisation de mesures visant à caractériser le film cooling. Lorsque ces peintures sont exposées à des rayons lumineux UV, le processus photo-luminescent engendre l'émission de rayons lumineux rouges. La luminescence dépend de la pression partielle d'oxygène ainsi que de la température de surface du revêtement.

Une peinture photo-luminescente sensible à la pression (PSP), disponible dans le commerce, est choisie pour la caractérisation expérimentale de deux quantités fondamentales dans le domaine du film cooling:

- *Efficacité du refroidissement par film*
- *Coefficients de transfert de chaleur*

L'efficacité (adiabatique) du film cooling permet d'évaluer le mélange entre le fluide réfrigérant et l'écoulement principal. En effet, cette quantité correspond à la concentration des espèces gazeuses, le transfert de chaleur étant analogue au transfert de masse. Le réfrigérant, qui ne contient pas d'oxygène libre, agit donc comme un traceur du gaz dans le film de refroidissement lorsqu'il est mélangé avec

le fluide de l'écoulement principal et permet d'obtenir des mesures détaillées de la concentration en gaz réfrigérant.

Le coefficient de transfert de chaleur correspondant est mesuré en imposant des impulsions de flux de chaleur sur la paroi et en mesurant l'évolution de la température transitoire. La même peinture photo-luminescente sensible à la pression est utilisée pour des mesures thermographiques en exploitant la sensibilité à la température de la technique utilisée.

Dans cette étude, une application réaliste illustre la faisabilité de cette technique sous des conditions d'écoulement complexes. Cette expérimentation démontre que des mesures avec une résolution spatiale élevée peuvent être obtenues sur de grandes surfaces au cours d'une courte période temporelle. Il s'avère que l'exploitation de la sensibilité de la peinture photo-luminescente à la pression partielle d'oxygène ainsi qu'à la température est particulièrement avantageuse lors des mesures au sein d'un écoulement compressible avec transfert de chaleur modéré à la paroi. Un autre avantage important de cette technique est la possibilité de considérer l'efficacité du film cooling indépendamment du transfert de chaleur à la paroi, sans avoir à appliquer un nouveau revêtement lors de mesures annexes. Ceci garantit la précision géométrique des orifices de refroidissement de très petite échelle sur les dispositifs expérimentaux. Cependant, cette technique est limitée par la température maximale applicable sur un système photo-luminescent. En effet, un tel dispositif est initialement adapté pour des mesures au sein d'un écoulement froid.

Les peintures photo-luminescentes sensibles à la pression (PSP) et à la température (TSP) ont déjà été utilisées dans le cadre d'étude sur le film cooling, néanmoins la combinaison de ces techniques est unique. Elle permet la mesure simultanée et découplée des deux quantités fondamentales dans le domaine du film cooling. Dans cette thèse, il est montré que l'application de la technique proposée permet de valider les modèles d'écoulement numériques. En outre, les conclusions obtenues peuvent être étendues à la conception de moteurs réels afin d'engendrer de nouvelles avancées technologiques. Au final, les résultats présentés ici vont permettre d'optimiser les performances du film cooling et ainsi permettre la réduction de la consommation en carburant des turbines à gaz.

Mots-clés

Refroidissement par film (film cooling), transfert de chaleur, convection, photo-luminescence, PSP, concentration de gaz, expériences transitoires

Table of Contents

Abstract	i
Version Abrégée	iii
Table of Contents	v
List of Figures	ix
List of Tables	xiii
Nomenclature	xv
Chapter 1 Introduction.....	1
1.1 Motivation	1
1.1.1 Controlling the Energy Consumption.....	1
1.1.2 Gas Turbine Development	2
1.1.3 Turbine Cooling	4
1.2 Cooling Techniques for Turbines.....	4
1.2.1 Viscous Dissipation in Compressible Flow	5
1.2.2 Heat Transfer through Forced Convection.....	7
1.2.3 Internal Cooling	10
1.2.4 External Cooling	11
1.3 Challenges in Platform Film Cooling Design.....	13
1.3.1 Turbulence	15
1.3.2 Numerical Flow Modelling	17
1.3.3 Platform Cooling and 3D Effects	19
1.3.4 Experimental Validation	22
1.4 Conclusions of Chapter 1.....	26
Chapter 2 State of the Art	29
2.1 Measurement Techniques for Platforms	29
2.1.1 Adiabatic Wall Measurements	34
2.1.2 Wall Heat Transfer Measurements.....	39
2.1.3 Engine Similarity.....	42
2.2 Missing in the State of the Art.....	44
2.3 Objectives of Thesis.....	44

Table of Contents

2.3.1	Hypothesis.....	45
2.3.2	Major Steps.....	46
2.4	Conclusions of Chapter 2.....	48
Chapter 3	Experimental Methodology	50
3.1	Pressure and Temperature Sensitive Paint.....	50
3.1.1	Set-up for Photoluminescent Measurements	51
3.1.2	Calibration	52
3.2	Measuring Adiabatic Film Cooling Effectiveness.....	55
3.2.1	Heat and Mass Transfer Analogy.....	55
3.2.2	Gas Concentration Measurement Procedure.....	57
3.2.3	Adiabatic Film Effectiveness using CO ₂	59
3.3	Measuring Heat Transfer Coefficients	62
3.3.1	Transient Heating Experiments	62
3.3.2	Baseline Heat Transfer Coefficients	67
3.3.3	Film Cooled Heat Transfer Coefficients.....	68
3.4	Conclusions of Chapter 3.....	69
Chapter 4	Test Case: Platform Film Cooling	73
4.1	Test Facility	73
4.2	Aerodynamics	76
4.3	Film Cooling Configuration.....	79
4.4	Conclusions of Chapter 4.....	82
Chapter 5	Results	85
5.1	Platform Film Cooling.....	85
5.1.1	Adiabatic Film Cooling Effectiveness.....	85
5.1.2	Heat Transfer without Film Cooling (Baseline).....	87
5.1.3	Validation of PSP as Temperature Sensor.....	89
5.1.4	Heat Transfer with Film Cooling.....	91
5.1.5	Comparison with Numerical Predictions.....	94
5.2	Uncertainty Analysis	95
5.2.1	Adiabatic Film Cooling Effectiveness.....	96
5.2.2	Heat Transfer Coefficients.....	99
5.2.3	Heat Release.....	102

5.3	Future Work.....	102
5.4	Conclusions of Chapter 5.....	103
Chapter 6	Conclusions.....	105
6.1	Experimental Feasibility.....	106
6.2	Adiabatic film cooling effectiveness using CO ₂	107
6.3	Convective Heat Transfer Measurements.....	107
6.4	Final Note.....	108
	Bibliography.....	109
	Appendix A.....	117
	Derivation of Adiabatic Film Cooling Effectiveness.....	117
	Appendix B.....	119
	Heat Release Distribution.....	119
	Appendix C.....	121
	In-Situ Calibration Procedure.....	121
	Appendix D.....	123
	Boundary Layer Modelling (TexStan).....	123
	Appendix E.....	125
	Inlet Boundary Layer Characterization.....	125
	Appendix F.....	129
	CFD Modelling.....	129
	Appendix G.....	133
	Film Cooling Flow Parameters.....	133
	Acknowledgements.....	137
	Curriculum Vitae.....	139

List of Figures

Figure 1: Working principle of a gas turbine cycle from Wagner (2007).....	3
Figure 2: Evolution of turbine entry temperature (Rolls-Royce plc).....	3
Figure 3: Heat transfer model (1D) for wall cooling.....	5
Figure 4: Schematic of viscous dissipation over an adiabatic wall.....	6
Figure 5: Convective heat load on an airfoil from Lakshminarayana (1996)....	7
Figure 6: Definition of driving temperatures of the heat transfer coefficient....	8
Figure 7: Heat transfer for a wall with both internal and external cooling.....	11
Figure 8: Three-temperature problem of film cooling.....	12
Figure 9: Superposition of the considered phenomena.....	13
Figure 10: Jet in cross flow adopted from Fric and Roshko (1994).....	14
Figure 11: Film cooling jet visualization by Jovanovic et al. (2008).....	16
Figure 12: Computed gas injection through a shaped cooling hole.....	19
Figure 13: Temperature profiles of combustion chambers (Alstom ltd).....	20
Figure 14: Illustration of 3D flow features (left) by Takeishi et al. (1990) and shear visualization of the present platform (right).....	21
Figure 15: Working principle of photoluminescent paints.....	25
Figure 16: Excitation and emission spectra of present PSP system.....	25
Figure 17: Analogous energy and species concentration fields.....	36
Figure 18: Platform test case with passive slot geometry.....	45
Figure 19: Camera view (left) and optical system set-up (right).....	51
Figure 20: LED-array lamp from Rapp Opto-Electronic (left) and CCD camera from PCO-imaging (right).....	52
Figure 21: Oxygen pressure sensitivity of PSP at constant temperature.....	53
Figure 22: Temperature sensitivity of PSP at constant pressure.....	55

Table of Contents

Figure 23: Analogy between energy and gas concentration boundary layers...	56
Figure 24: PSP workflow to derive the adiabatic film cooling effectiveness ...	58
Figure 25: Flat plate measurements with different tracer gases	60
Figure 26: Relation between energetic (concentration) and temperature-based definition of the adiabatic film cooling effectiveness.....	61
Figure 27: Adiabatic wall (left) and transient heating situation (right).....	62
Figure 28: Transient evolution of heat flux terms ($h = 500 \text{ W/m}^2\text{K}$)	65
Figure 29: Transient wall temperature response of the analytical model	66
Figure 30: Measured wall temperature response using PSP	68
Figure 31: Linear cascade	73
Figure 32: Cross-section of test set-up with slot and platform modules	74
Figure 33: Heat release distribution.....	75
Figure 34: Isentropic Mach number on the platform surface.....	76
Figure 35: Hot-wire measurement of the inlet velocity profile.....	78
Figure 36: Calculated isentropic Ma and flow paths on the wall (left), Experimental flow visualization on the wall (right)	79
Figure 37: Cooling hole footprints on the platform	80
Figure 38: PSP coated platform model.....	80
Figure 39: Hole discharge coefficients	81
Figure 40: Blowing ratio.....	81
Figure 41: Momentum ratio.....	82
Figure 42: Density ratio.....	82
Figure 43: Adiabatic film cooling effectiveness on the platform	86
Figure 44: Averaged effectiveness with varying cooling feed pressures.....	87
Figure 45: Baseline heat release (left) and heat transfer coefficient (right).....	88
Figure 46: Validation with TLC results along an axial line.....	90

Figure 47: Validation with TLC results along a streampath.....	91
Figure 48: Heat transfer coefficients with varying cooling feed pressures.....	92
Figure 49: Averaged heat transfer coefficients.....	93
Figure 50: Comparison with theoretical models.....	94
Figure 51: Absolute transfer function of the measurement chain.....	96
Figure 52: Random uncertainty of the adiabatic film cooling effectiveness.....	97
Figure 53: Oxygen pressure sensitivity linearized at the reference condition.	98
Figure 54: Distribution of measurement pixels in a η -experiment.....	98
Figure 55: Sensitivity to pressure-calibration drift (left), example (right)	99
Figure 56: Temperature and time uncertainties in a transient experiment ...	100
Figure 57: Random spread in heat transfer coefficients along a streamline...	101
Figure 58: Heat release distribution in the heater foil	119
Figure 59: Measurement and in-situ calibration procedure	121
Figure 60: Comparison of wall boundary conditions using TexStan.....	123
Figure 61: Transient evolution of wall temperature	124
Figure 62: Hot-wire calibration.....	125
Figure 63: Inlet velocity profile on the endwall	126
Figure 64: CFD (3D-RANS) model and mesh of a platform test case.....	129
Figure 65: Predicted heat release (top), heat transfer coefficients (bottom) .	130
Figure 66: Impact of inlet boundary layer on heat transfer coefficients	131
Figure 67: Sensitivity to inlet boundary layer on convective heat transfer ...	131
Figure 68: Calculated adiabatic film cooling effectiveness.....	132
Figure 69: Numerical comparison of adiabatic film cooling effectiveness.....	132

List of Tables

Table 1: Experiments for adiabatic film cooling effectiveness with PSP	57
Table 2: Wall material properties	64
Table 3: Mean isentropic flow conditions of the cascade	77
Table 4: Global blowing conditions for one vane passage	81

Nomenclature

Roman

A	hole area	$[\text{mm}^2]$
Ar	Argon	
a	speed of sound	$[\text{m/s}]$
Bi	Biot number, $Bi = h\delta/k_w$	$[-]$
C_d	discharge coefficient	$[-]$
C_f	friction coefficient	$[-]$
$C_{0, 1, 2}$	pressure calibration constants	$[-]$
c	specific heat of solid	$[\text{J}/(\text{kgK})]$
c_p	specific heat at constant pressure	$[\text{J}/(\text{kgK})]$
D	temperature calibration constant	$[-]$
D	mass diffusivity of binary CO_2/air mixture	$[\text{m}^2/\text{s}]$
DR	coolant-to-gas density ratio, $DR = \rho_c / \rho_g$	$[-]$
d	hole diameter	$[\text{m}]$
$erfc$	complementary error function	
G	electric heating power gain	$[-]$
h	local heat transfer coefficient	$[\text{W}/(\text{m}^2\text{K})]$
I	intensity (PSP-measurements)	$[-]$
I	momentum flux ratio, $I = (\rho_c u_c^2)/(\rho_g u_{g, is}^2)$	$[-]$
Kr	Krypton	
k	thermal conductivity	$[\text{W}/(\text{mK})]$
L	chord length	$[\text{m}]$
Le	Lewis number, $Le = Pr / Sc$	$[-]$
M	blowing ratio, $M = (\rho_c u_c)/(\rho_g u_{g, is})$	$[-]$
Ma	Mach number, $Ma = u / \sqrt{\kappa RT}$	$[-]$
\dot{m}	mass flow rate	$[\text{kg/s}]$
\mathcal{M}	molar weight	$[\text{kg}/\text{kmol}]$
Nu	Nusselt number, $Nu = hs/k$	$[-]$
P	vane pitch	$[\text{m}]$
Pr	Prandtl number, $Pr = \nu / \alpha$	$[-]$
p	pressure	$[\text{Pa}]$
R	specific (ideal) gas constant	$[\text{J}/(\text{kgK})]$
q	heat flux	$[\text{W}/\text{m}^2]$
Sc	Schmidt number, $Sc = \nu / D$	$[-]$

Nomenclature

St	Stanton number, $St = h/\rho u_{is} c_p = Nu_s/(Re_s Pr)$	[-]
s	surface distance	[m]
T	temperature	[K]
Tu	turbulence intensity, $Tu = \sqrt{(u - \bar{u})^2}/\bar{u}$	[-]
t	time	[s]
u, v	velocity components	[m/s]
u_τ	shear velocity	[m/s]
u^+	non-dimensional velocity in wall coordinates	[-]
w	slot width	[m]
$x/P, y/P, s/P$	non-dimensional surface coordinates	[-]
y	normal wall coordinate for fluid	[m]
y^+	non-dimensional wall coordinate	[-]
z	normal wall coordinate for solid	[m]

Greek

α	thermal diffusivity $\alpha = k/(\rho c_p)$	[m ² /s]
β	thermal inertia of heater foil	[J/(m ² K)]
δ	wall thickness	[m]
ε	factor of heating power reduction	[-]
ζ	mass fraction	[-]
η	adiabatic film cooling effectiveness	[-]
θ	non-dimensional wall temperature	[-]
κ	isentropic coefficient	[-]
μ	dynamic viscosity	[kg/(ms)]
ν	kinematic viscosity $\nu = \mu / \rho$	[m ² /s]
ξ	mole fraction	[-]
ρ	density	[kg/m ³]
σ_T	standard deviation of temperature	[K]
σ_θ	standard deviation of non-dimensional temperature	[-]
τ	shear stress	[N/m ²]

Subscripts

$\hat{}$	non-dimensional quantity
$\bar{}$	averaged quantity
∞	free-stream
<i>Aero</i>	reference injection (with O ₂)
<i>a</i>	adiabatic

<i>avg</i>	<i>average</i>
<i>ax</i>	axial
<i>CO₂</i>	carbon dioxide
<i>c</i>	coolant gas
<i>g</i>	main stream gas
<i>h</i>	convection
<i>i</i>	initial
<i>is</i>	isentropic flow
<i>k</i>	conduction
<i>m</i>	metal
<i>N₂</i>	nitrogen
<i>O₂</i>	oxygen
<i>r</i>	recovery
<i>ref</i>	reference case
<i>Tracer</i>	injection experiment (without O ₂)
<i>t</i>	total conditions
<i>w</i>	wall

Abbreviations

CCD	Charged Couple Device (camera sensor)
CFD	Computational Fluid Dynamics
DNS	Direct Numerical Simulation
FEM	Finite Element Method
fps	frames per second
LES	Large Eddy Simulation
NGV	Nozzle Guide Vane
PSP	Pressure Sensitive Paint
TET	Turbine Entry Temperature
TLC	Thermochromic Liquid Crystals
TSP	Temperature Sensitive Paint

Chapter 1

Introduction

1.1 Motivation

The main motivation of this thesis is the need for improved understanding and performance of external film cooling schemes of gas turbines. This is particularly important in order to design for robust film cooling in complex flow environments found on turbine endwalls. Cooling performance can be determined with modern computer-based prediction methods with the capability to model the underlying physics. A common approach to predict film cooling performance is the use of simplified tools based on the combination of physical principles and empirical data. In both of these cases, experimental validation is an important building block. Image-based experimental methods are rapidly developing with the potential to provide high resolution measurements. This thesis aims at exploring the possibility to employ photoluminescent paints as surface sensor for film cooling performance assessments.

1.1.1 Controlling the Energy Consumption

The recently accepted environmental impact of carbon emissions from fossil based energy sources is motivating accelerated engineering efforts in several domains ranging from the energy supplier to the consumer (e.g. energy conversion technologies, transport systems, heating of buildings, etc.).

Ever since its birth one century ago, aviation has developed faster than other transportation systems. The contribution of the global CO₂-emissions from aircraft is expected to grow from the small fraction today. The argument is based on the need for high density energy to propel an aircraft making it more difficult to replace fossil fuel as energy carrier than in land-based vehicles. Although today's passenger airplanes look very similar to the first jet powered airliners that revolutionized air travel in the 1950's, there has been a remarkable development through optimization of all the involved systems. Due to economical and safety considerations among others, there is a great deal of conservatism in the field of aeronautics which also means that there is still a large improvement potential when all aspects of air travel are taken into

account (e.g. evolution of aircraft designs, propulsion systems and operating concepts). Reducing CO₂-emissions by minimizing the gross consumption of fossil fuels leads to other advantages in that it leads to an automatic reduction of other environmentally harmful emissions such as nitrogen oxides (NO_x), sulphur oxides (SO_x) and soot.

At the same time, the electric energy consumption is expected to increase significantly during the next decades due to increased standard of living and the trend to distribute energy in the form of electricity instead fossil fuels (e.g. electric vehicles). Thus, the demand for reliable and predictable production of electricity will increase. In parallel to the development of gas turbines for aircraft propulsion, the land-based counterpart has seen a great success in delivering electrical power. On many markets, converting energy from natural gas and other fuels to electricity using large-scale gas turbine power plants is the optimal solution. In particular considering that the response time of gas turbines is relatively short at start-up, allowing energy providers to manage peaks in the grid power consumption.

1.1.2 Gas Turbine Development

Air breathing gas turbines provide superior power density in aircraft engines by working at high rotational speeds. The continuous combustion allows for a significantly cleaner process compared to the highly unsteady combustion in reciprocal engines. The continuous compression and expansion also minimize vibrations which allows to manufacture many components out of lightweight materials in thin-walled structures with rotational symmetry.

Simply speaking, the compressor design is driven by aerodynamic efficiency while ensuring a safe margin with respect to stall caused by boundary layer separation due to the adverse pressure gradients. The combustion system converts chemical energy into heat in a stable manner while minimizing emissions. Finally, the role of the turbine is to convert the heat of the high pressure gas into mechanical power driving the shaft of the engine. In order to do this, the turbine must above all withstand the elevated gas temperatures at the inlet.

The working principle of the gas turbine is illustrated in a temperature-entropy diagram (Figure 1). Ever since the innovation of the gas turbine ca. 70 years ago, cycle performance has been improved substantially through increased compression ratio and turbine inlet temperature (see e.g. Eckardt and Rufli (2002)). Today, the achievable thermal efficiency of the gas turbine

cycle (Brayton cycle) is in the order of 40% which is similar to Diesel engines – again with much lower emissions due to very lean combustion allowed by the continuous working process. This makes gas turbines suitable for large-scale electrical power production plants.

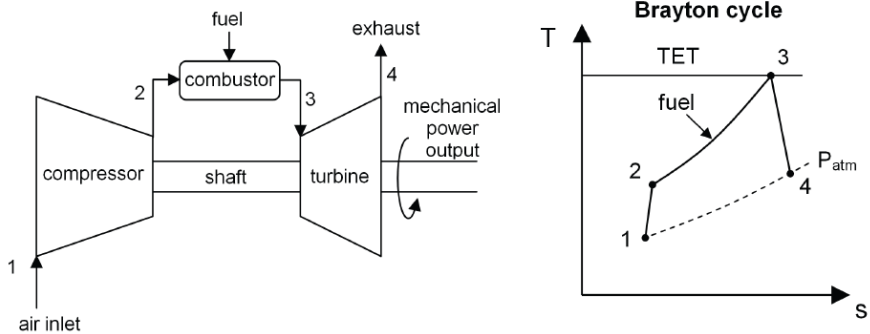


Figure 1: Working principle of a gas turbine cycle from Wagner (2007)

There are several ways of improving the thermal efficiency. Modern thermal power plants combine a heavy duty gas turbine with a boiler and steam turbine in order to recuperate a large portion of the substantial exhaust heat. Such combined cycle installations can reach a thermal efficiency in the order of 60%. A fundamental improvement of the gas turbine efficiency can be gained by increasing the Turbine Entry Temperature (TET). The tremendous increase in turbine inlet temperature shown in Figure 2 (from Saravanamuttoo et al. (2009)), depends heavily on the development of reliable cooling.

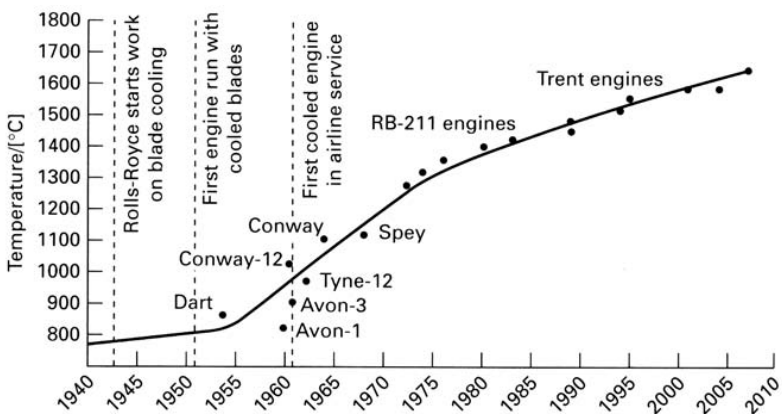


Figure 2: Evolution of turbine entry temperature (Rolls-Royce plc)

In fact, thermal management is one of the keys to improved engine performance and reliability of the hot section of the turbine. Thus, future improvements can be found in more efficient turbine cooling concepts, for example by reducing the cooling air consumption, or increasing the firing temperature further.

1.1.3 Turbine Cooling

High firing temperature requires reliable cooling schemes for high pressure turbines. Air is a suitable coolant for gas turbine components since high pressure air is available at the end of the compressor. Air cooling is relatively ‘soft’ compared to more intense techniques such as two-phase cooling. Still the convective heat transfer coefficients on the cold and hot sides of the wall are sufficiently high to produce significant temperature gradients in the metallic walls. In the hot section of gas turbines, the detailed distributions of adiabatic film cooling effectiveness and heat transfer coefficients on the surface are of interest since they dictate the temperature gradients that are sometimes critical for the mechanical integrity of the wall. The ideal design objective is isothermal surfaces in order to minimize thermal stresses inside the metallic blade walls. Therefore, controlling the cooling so as to avoid both hot and cold spots (caused by over-cooling) is part of the optimization exercise in turbine design.

1.2 Cooling Techniques for Turbines

The metal temperature is kept at acceptable levels by transferring heat from the hot side of the wall through a series of thermal resistances towards the heat sink provided by cool air flowing inside the blade. Thus the metal temperature will take a value in between the hot gas and coolant temperature according to the overall cooling *effectiveness*:

$$\Phi = \frac{T_m - T_g}{T_c - T_g} \quad (1)$$

Figure 3 shows a 1D representation of the heat transfer situation in turbine blade cooling. The heat flux depends on temperature difference and the total thermal resistance of the system. The thermal conductivity of the wall corresponds to typical blade materials such as nickel-based alloys. The objective to minimize the metal temperature is achieved by maximizing the convective cooling inside the blade while minimizing the external heat transfer coefficient. The latter objective can be achieved by applying insulating

materials on the hot-gas side of the wall in order to reduce the effective heat transfer coefficient, and the maximum temperature at the external surface of the metallic wall.

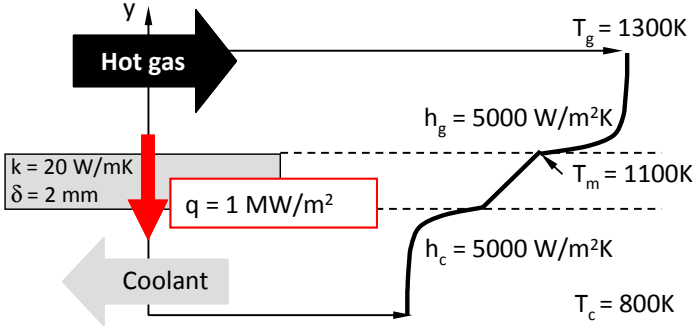


Figure 3: Heat transfer model (1D) for wall cooling

Optimum usage of the cooling air (cooling efficiency) often require complements to internal convective cooling schemes. Moreover, intensive internal cooling leads to large heat fluxes through the wall producing large temperature gradients in the wall-normal direction. Again, this leads to high thermal stresses in the metal and associated coating materials. Therefore, it is advantageous to reduce the effective gas temperature on the hot side by diluting it with cold air. This is referred to as external cooling and is typically realized with film cooling.

High levels of forced convection are present in high pressure turbines. The metal temperature of a cooled blade thus mainly depends on heat transfer due to gas convection and to conduction inside the wall. Heat transfer due to radiation is not considered in the present study.

1.2.1 Viscous Dissipation in Compressible Flow

In the Euler flow field outside of wall the boundary layers, the expansion from stagnation conditions to nearly sonic velocity leads to a significant reduction in the static temperature in a high pressure turbine. In the ambient temperature flow of the laboratory, this reduction is limited to approximately 40 K due to the lower speed of sound. Inside the boundary layers, the kinetic energy is converted into heat by viscous shearing until the velocity reaches zero at the wall (no-slip condition). According to Weigand (2010), this leads to the recovery temperature at an adiabatic wall:

$$T_r = T + r \frac{u^2}{2c_p} \quad (2)$$

Here the recovery factor for a turbulent boundary layer can be correlated to the Prandtl number according to:

$$r = Pr^{1/3} \quad (3)$$

The viscous heating leads to a static temperature gradient and a corresponding transfer of energy from the inner layers towards the free-stream. If Pr is unity, the transfer of kinetic and thermal energy are balanced, leading to a wall temperature equal to the total temperature of the free-stream. For turbomachinery flows, it is convenient to relate the recovery temperature to the total temperature:

$$T_r/T_t = \frac{1+r(\kappa-1)Ma^2/2}{1+(\kappa-1)Ma^2/2} \quad (4)$$

For fluids with $Pr < 1.0$ as in the present study, the rate of heat diffusion towards to the free-stream is larger than the rate of dissipation towards the wall leading to recovery temperatures that are a few Kelvin lower than the total temperature as sketched in Figure 4. The temperature gradient at the adiabatic wall is zero per definition.

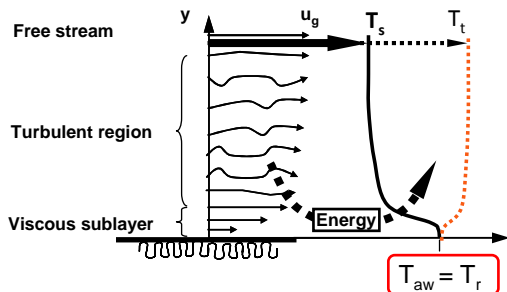


Figure 4: Schematic of viscous dissipation over an adiabatic wall

The viscous dissipation effects must be considered when selecting reference temperatures for the compressible flow test cases — in particular when small temperature differences are employed. Consistent inclusion of the recovery effect is necessary in the thermal definition of heat transfer coefficients and adiabatic film cooling effectiveness as described in the following.

1.2.2 Heat Transfer through Forced Convection

Heat conduction in one dimension depends on the driving temperature gradient and the thermal conductivity of the medium according to Fourier's law:

$$q = -k \left(\frac{\partial T}{\partial y} \right) \quad (5)$$

A constant thermal conductivity can be defined for solids as well as for fluids normal to the direction of any advective motion. This is the molecular conductivity of gas. The common feature of the convective heat transfer treated in this work is that the flow is bound to a wall. The no-slip condition at the wall generates frictional shearing forces inside the boundary layer of the fluid. The shear force maximum at the surface diminishes towards the outer edge of the boundary layer. As soon as there is relative motion between different gas layers, significantly larger amount of heat can be transported due to the continuous feed of un-affected gas in the next layer. In other words, the relative movement increases the effective heat capacity of the gas through advection. In addition, turbulent flow motions normal to the mean flow-direction lead to substantial increase the apparent thermal conductivity when Equation (5) is applied. Therefore, the transition from laminar to turbulent flow has a highly non-linear effect on heat transfer. Hence, in addition to flat-plate flow considerations, impinging, expanding and/or diffusing flows can lead to complex transition phenomena and strong variations in the convective heat transfer as illustrated on a blade airfoil in Figure 5.

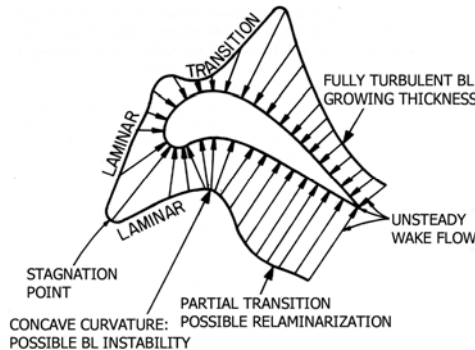


Figure 5: Convective heat load on an airfoil from Lakshminarayana (1996)

Figure 6 illustrates a wall boundary layer of a compressible flow (left). On the right, the wall is cooled down to a constant temperature and it can be seen

that the non-dimensional temperature boundary layer is similar to the velocity boundary layer according to the Reynolds analogy.

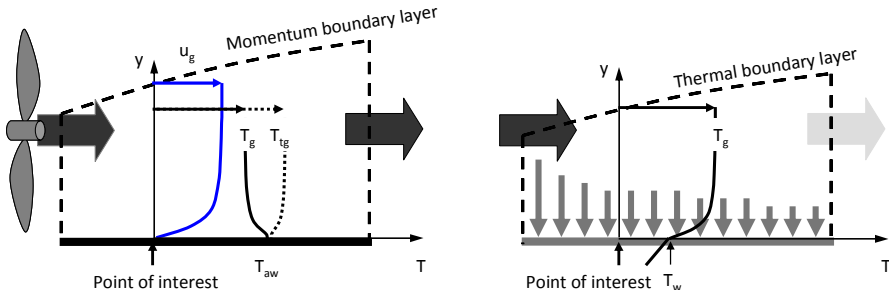


Figure 6: Definition of driving temperatures of the heat transfer coefficient

Convective heat flux is normalized by the difference in temperature according to the situations with and without heat transfer at the wall surface. Thus the local convective heat transfer coefficient of the boundary layer is defined by:

$$h = \frac{q_h}{T_w - T_{aw}} \quad (6)$$

By considering control volumes inside the boundary layer and performing a heat balance at several streamwise positions along the wall, it can be seen that each point on the surface is dependent on the heat transfer through the upstream, diabatic surface. Thus, the definition of the heat transfer coefficient makes it a particular measure of the boundary layer quality — for a given thermal wall-boundary condition upstream of the point of interest. Thus there are two drivers on the flow-side that dictate the convective heat flux:

- local boundary layer quality (e.g. turbulence and vorticity)
- particular thermal boundary layer approaching the point of interest.

Therefore, the *aerodynamic* footprint of the boundary layer on the wall is the most universal measure of the boundary layer quality. However, when the starting points of both velocity and thermal boundary layers coincide, the following Nusselt correlations developed for flat plates can be employed for laminar and turbulent boundary layers respectively:

$$Nu_s = 0.332 Re_s^{1/2} Pr^{1/3} \quad (7)$$

$$Nu_s = 0.0296 Re_s^{4/5} Pr^{1/3} \quad (8)$$

Effectively, many engineering applications such as turbine blades approach this situation. Further, numerous aerodynamic and heat transfer measurements on flat plates are available in terms of wall friction coefficients and Stanton numbers as function of free-stream Reynolds number. The friction coefficient corresponds to the Stanton number in heat transfer as long as the flow is incompressible, the wall temperature is constant and the Prandtl number is unity, there is a direct analogy between thermal and momentum boundary layers:

$$St \approx \frac{C_f}{2} \quad (9)$$

The friction coefficient is defined by the wall shear stress normalized by the dynamic head of the free-stream:

$$C_f = \frac{\tau_w}{\frac{1}{2} \rho u_{\infty}^2} \quad (10)$$

Correlating the heat transfer distribution from knowledge of the velocity boundary layer is convenient for simple thermal boundary conditions such as constant wall temperature. However, a significant influence on the resulting heat transfer can be expected where the wall heating is locally distributed (such as in the present film cooling configuration). In this case, the temperature boundary layer resulting from a particular thermal boundary condition requires a numerical iterative approach to derive heat transfer coefficients from knowledge of the velocity boundary layer. Moreover, when the starting points of the velocity and thermal boundary layers do not coincide, the so-called un-heated starting length must be taken into account.

The boundary layer solver *TexStan* (Kays et al. (2004)) has been used to estimate the impact of the thermal boundary conditions on the mid-span area airfoil suction-side. This is done by comparing resulting heat transfer coefficients obtained with constant wall temperature vs. constant heat flux at the wall. As shown in Appendix D, the difference can be significant in laminar and transitional areas that include steep streamwise gradients in the heat transfer coefficient. The influence is negligible in fully turbulent boundary layers as confirmed by Eckert (1992), “the upstream temperature or heat flux distribution has little effect on the local Stanton number in a turbulent boundary layer”. Typically, it is turbulent transport that dominates the transfer of heat between the wall and fluid in film cooling flows.

As a consequence of the above introduction, the distribution of the thermal boundary condition over the tested surface should be roughly similar in the experiment. The thermal boundary conditions are always particular although thermal stresses are reduced by aiming for isothermal surfaces ($T_w(x,y) = \text{constant}$) in cooling design. In addition, near-wall temperature alterations caused by e.g. wall heat flux can lead to significant gas property variation. This can be taken into account by evaluating the gas properties at a representative boundary layer temperature — e.g. the Eckert temperature.

1.2.3 Internal Cooling

The heat sink provided by internal cooling schemes is the driving cooling mechanism in most applications. Reduced metal temperatures are achieved by pulling heat through the outer to the inner side of the wall. Heat transfer coefficients are maximized on the cold side and minimized on the hot side of the wall. There are many methods to increase internal heat transfer coefficients as reviewed by Goldstein et al. (2006) and Bunker (2007). Further to the conventional air cooling designs, the following treatments are possible solutions:

- Convection is first of all driven by flow velocity. Ensuring sufficiently high internal flow velocity in the coolant flow path.
- Geometrical technologies allow for increased internal surface area and a higher degree of vortical flow structures as well as turbulence. Jet impingement schemes are extensively used by adding perforated plates inside the blade. Recent advances in casting techniques allows for complex geometries to be manufactured also inside rotating blades.
- Insulation by Ceramic Coatings. As long as a wall is cooled at the backside, it is possible to reduce the metal temperature by adding thermal insulation layer on the external surface of the wall. Since the 1980's, development of ceramic technology and Thermal Barrier Coatings (TBC) have allowed for further increased firing temperatures.
- Reducing the cooling air temperature by the use of external heat exchangers. This is becoming more and more important considering the trend of increasing compression ratios resulting in higher compressor-end temperatures.
- Increasing the heat capacity of the cooling air by mixing it with water vapour (steam). With steam available in combined cycle power plants,

closed-loop steam cooling concepts for further increase in thermal efficiency of the plant is a possibility. However, these concepts typically require complex feed systems to handle the steam.

However, there are limits in the attainable overall cooling effectiveness by increasing the heat transfer coefficients on the cold side. Therefore, it is often necessary to reduce the temperature on the hot side by the use of external cooling. With film cooling, an attractive overall cooling effectiveness can be reached already at low coolant mass flows as shown by Harasgama (1995).

1.2.4 External Cooling

The aim of external cooling is to reduce the hot side temperature by diluting the hot gas with coolant. This either means that less internal cooling is required to maintain sufficiently low metal temperatures. Alternatively, film cooling allows to increase the hot gas temperature as illustrated in Figure 7 (compare with Figure 3). Here, it was assumed that the adiabatic film cooling effectiveness is $\eta = 0.4$.

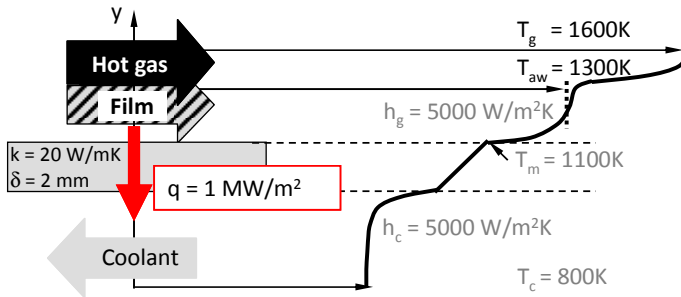


Figure 7: Heat transfer for a wall with both internal and external cooling

Two variants of external cooling are considered in this introduction. The first technique transpires cold air through a porous wall. A nearly homogenous distribution of cooling air injection makes this an ideal technique. Practical constraints however make it difficult to implement this technique in mechanically loaded blades. Therefore, the dominating solution to the problem is film cooling. Here, the cooling air is injected at discrete locations in order to generate films of diluted hot-gas near the wall. The significantly larger jets mean that the films of cooling air tend to occupy a large portion of the boundary layer in contrast to transpiration cooling.

Film Cooling

Film cooling consists of injecting cooling air through small holes, slots or similar geometries drilled through the wall. Fast, high precision machining of a large number of holes is typically done with electro-discharge machining or laser drilling. The diameter of the hole controls the cooling flow rate putting high demands on manufacturing quality. Minimizing the hole diameter allows to limit disturbances on the external boundary layers and aerodynamic losses, while maximizing the metering section limits surface degradation due to e.g. dirt deposit accumulating during engine operation.

Turbulent mixing of the coolant and main-flow produces a gas mixture on top of the wall. If the wall is perfectly insulated and flow velocities are low, the surface takes an adiabatic temperature in between the upstream temperatures of the two streams as sketched in Figure 8 (left). Therefore, film cooling coverage is defined by the adiabatic film cooling effectiveness:

$$\eta = \frac{T_{aw} - T_g}{T_c - T_g} = \frac{T_{aw, T_{tc} \neq T_{tg}} - T_{aw, T_{tc} = T_{tg}}}{T_{tc} - T_{tg}} \quad (11)$$

This definition is meant to indicate the adiabatic wall temperature due to a reduction in the coolant total temperature with respect to the main flow ($T_{tc} - T_{tg}$). This quantity is measured by comparing the above case with an isothermal injection case ($T_{tc} = T_{tg}$). Hence, the aerodynamic cooling effect (recovery temperature) is considered to be independent of the η -definition.

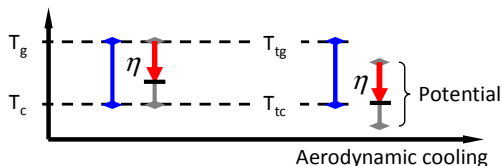


Figure 8: Three-temperature problem of film cooling

The same principle is applied in the wall heat transfer situation. In Equation (6) it is the temperature difference due to heat transfer to or from the wall that is employed as reference. Thus the recovery effect is handled consistently in the definition of adiabatic and diabatic wall temperatures.

As seen in the above introduction, there are several quantities to consider in the external cooling problem of this work. For example, the resulting convection is a result of the adiabatic wall temperature and the heat transfer coefficients. Those two quantities can be treated separately in order to

improve the understanding of the problem. According to Eckert (1992), superposition of the particular thermal solutions due to film mixing and wall convection can be done. This leads to the schematic total temperature distributions depicted in Figure 9.

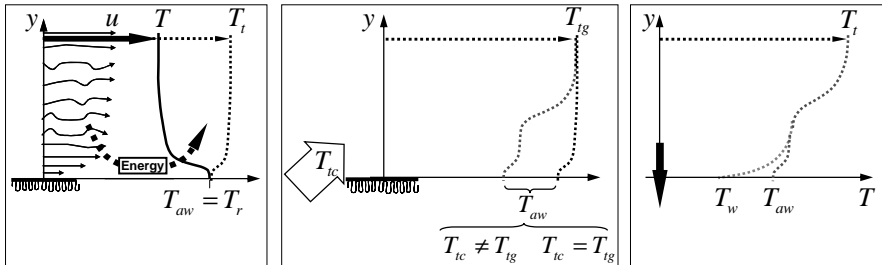


Figure 9: Superposition of the considered phenomena

Superposition assumes linearity of the energy equation and the thermal boundary conditions. In reality, there are significant non-linear effects due to e.g. gas property variations. Therefore, it is important to ensure similarity between experimental tests and engine conditions.

1.3 Challenges in Platform Film Cooling Design

Knowledge of the detailed distribution of convective heat transfer is needed for accurate life-time predictions of turbine blades and vanes. In order to design for safe and economically viable turbines with sufficiently long life-time, it is necessary to understand and predict the detailed convective action on the blade walls.

Film cooling protection depends on the turbulent mixing between the jets of cooling air and main-flow. There can be many different types of jet-mixing situations depending on the geometry and flow conditions. For example, the situation can be quite different at the leading edge (normal injection), pressure side (small injection angle), early suction side (steeper injection angle) and pressure side bleed at the trailing edge involving heavy vortex shedding due to the presence of a backward-facing step. On flat platforms, the situation is somewhere in between typical pressure and suction side injection.

The flow field resulting from injection through discrete holes approaches that of a jet in cross-flow involving intense vortical flow structures. Figure 10 shows an illustration of such vortex systems. These vortices enhance the mixing as well as the convective heat transfer onto the surface. Furthermore,

as the wall boundary layer is influenced by the injection, the total pressure loss tends to rise impeding on the thermodynamic efficiency of turbines. Therefore, the aero-thermal design task is a global problem.

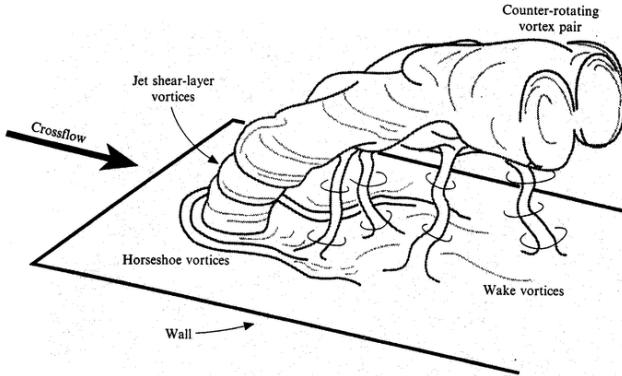


Figure 10: Jet in cross flow adopted from Fric and Roshko (1994)

Small-scale flow vortices makes it computationally expensive to accurately predict the mixing with numerical methods. Especially considering the large number of cooling holes typically distributed over the walls. Nevertheless, the most advanced numerical approaches with the least degree of empirical modelling are theoretically capable of predicting most of the phenomena occurring in the present test case.

There are many parameters influencing the film cooling performance. A remaining problem is that both experimental and numerical results depend on boundary conditions that are not straight forward to determine in an engine. For example:

- Inlet velocity distributions and boundary layer state
- Inlet free-stream turbulence characterization
- Inlet temperature distribution
- Thermal distribution on the surfaces
- Surface roughness
- Gas composition
- Unsteady effects

Although these conditions could be measured in laboratory environments, there is little hope of obtaining all of them in a real engine anytime soon. Therefore, engine experience is the prevailing approach using both numerical and experimental methods to determine the impact of design improvements with respect to a known baseline case. In this regard, experimental results can be used to develop correlations, establish design rules, validate numerical prediction methods and not least, to learn about the large number of boundary conditions required to solve such problems.

1.3.1 Turbulence

Most fluid flows exhibit some variation in time. In vehicle applications, time varying effects of large-scale are often minimized, e.g. by careful aerodynamic design. Therefore, the majority of theoretical analysis is restricted to time-averaged representations of the mean flow conditions. The assumption that the mean flow is steady is a convenient basis for theoretical analysis. However, most fluid flows exhibit some degree of unsteadiness that can be periodically ordered or highly random with a broad frequency spectrum as in the case of turbulence. Because turbulence is of particular importance in film cooling, a brief recapitulation of this vast topic is given.

Turbulence designates random flow motions caused by instability mechanisms. These depend on the ratio of inertial to frictional forces in the flow — the definition of the Reynolds number:

$$Re_L = \frac{\rho u L}{\mu}, \quad (12)$$

a very important parameter for convective heat transfer. In fact, heat transfer coefficients of turbulent wall-boundary layers depend nearly to the 1st order on the Reynolds number. On the contrary, adiabatic film cooling effectiveness is much less sensitive to the Reynolds number according to Jones (1999). This is due to the fact that the mixing between a jet and a cross-flow depends on relative velocity of the two streams. This is true within a limited range of Re within which the flow field does not vary significantly. For example due to highly non-linear effects such as transition, separation, impingement, etc.

Vortical flow structures (eddies) of a turbulent flow ‘cascade’ towards successively smaller scales of motion primarily due to inertial forces. Therefore, frictional forces become more and more dominating at the smaller eddy scales, leading to dissipation of the kinematic energy. As turbulent eddies

are advected downstream in a wall boundary layer, the average length scale increases and the turbulence intensity decays in the outer region. Although viscous forces have a damping action, it is also viscosity that initiates turbulence through shearing action due to relative motion of fluid layers. Hence turbulence can be found in free shear layers or wall bound shear layers. Figure 11 shows an example of a flow visualization adopted from Jovanovic et al. (2008). It is a snap-shot of a film cooling jet emanating from an inclined cylindrical hole visualized by laser induced fluorescence of seeded particles. A low-speed water-tunnel with large scale allows to capture the detailed flow features present at engine-realistic Reynolds numbers of cooling jets ($Re_d \approx 10^4$). A free shear layer can be observed on top of such a film cooling jet as it mixes with the main-flow. Wall shear is present throughout the turbulent wall boundary layer. As for most engineering applications, turbulence is an important driver for film cooling performance.

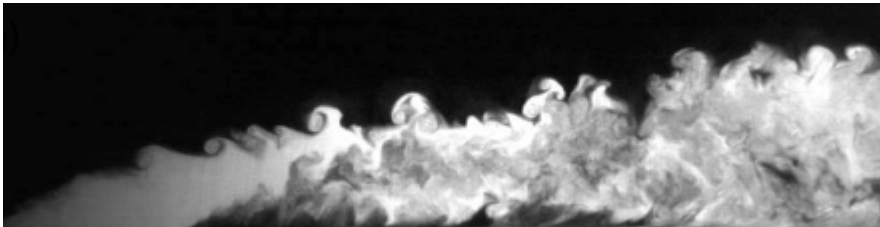


Figure 11: Film cooling jet visualization by Jovanovic et al. (2008)

Turbulence is present in the majority of practical applications. Boundary layers on airfoils typically start as laminar at the leading edge. Transition from laminar to turbulent flow occurs at some point downstream depending on the Reynolds number and many other parameters. By-pass transition is the typical mode in turbomachinery due to high free-stream turbulence levels, unsteady flow phenomena, rough surfaces and so on. Further, transition is often not an issue in film cooled high-pressure turbines due to the high Reynolds numbers and disturbing action of the cooling jets. On platforms, there are incoming turbulent boundary layers that are locally restarted depending on the inlet geometry. However, there are cases when the stabilizing effect of a wall is strong enough to partially damp the inertial effects of turbulence — this is the case when acceleration is sufficiently strong. The acceleration parameter gives an indication of whether such relaminarization will occur.

$$K = \left(\frac{v}{u^2}\right) \frac{du}{ds} \quad (13)$$

Values of $K > 3.5 \cdot 10^{-6}$ tend to relaminarise a boundary layer. Inversely, a laminar boundary layer will not transition under such conditions. This parameter takes the velocity derivative into account. One must consider the distance over which a certain acceleration is acting. For example, the boundary layer may go towards reverse transition (relaminarization) if a strong acceleration is maintained over a sufficiently long distance. This type of boundary layer has a relatively thick sub-layer as explained by Kays et al. (2004). The acceleration stretches the turbulent eddies leading to relatively lower transverse velocity components. However, the turbulent energy is still present and becomes important again if the acceleration decreases further downstream.

1.3.2 Numerical Flow Modelling

Free-stream aerodynamics is very well modelled by common software packages in the field of Computational Fluid Mechanics (CFD) – especially for high Reynolds number flows found in the blade passages in turbines. Here, the boundary layers are thin and the main-flow approaches the inviscid Euler solution. However, it is well known that the empirical basis of turbulence modelling leads to inherent application restrictions when it comes to predicting turbulent boundary layers and wakes dictating total pressure losses and heat transfer. Accurate prediction of the wall-perpendicular physics involved in wall heat transfer requires high resolution in the wall normal direction leading to demanding meshing and calculation tasks in 3D. Add to that the complex interaction between film cooling jets and mainflow that requires high mesh resolution also in the lateral direction. This leads to demanding calculation tasks that are today possibly applicable to final verification of a cooling design. In the early design phase, correlations and engine experience play a very important role. The following is a brief overview of the available numerical tools for simulating heat transfer problems and film cooling.

Integration of the full unsteady Navier-Stokes equations on very fine meshes using correspondingly very small time steps allows to resolve even the smallest scales of turbulence. Absence of empirical modelling of the turbulence is referred to Direct Numerical Simulation (DNS). This approach is mainly used to analyze limited academic problems in fundamental research due to the

heavy calculation task. In theory, a mesh independent DNS solution can be closer to the specified test case than experiments due to the possibility to accurately specify and control the boundary conditions. Experiments typically suffer from the difficulty to measure the exact test conditions everywhere which inevitably leads to uncertainties in the results. However, this is an idealized argument with little interest in the engineering world due to the extreme calculation cost.

Thus, a reasonable approach is to apply the knowledge of the relative importance of different turbulent length scales. The fact that the largest turbulent eddies dominate the turbulent transport of momentum, heat and mass species is one example. The turbulent eddies gradually decay through a cascade of dissipation into smaller scale eddies. As explained by von Kaenel (2003), the Navier Stokes equations can be transformed into the frequency domain allowing to filter out the smallest, computationally most expensive scales. Then it becomes less demanding to directly solve the remaining time-dependent turbulent scales. Only the filtered scales require modelling, which can be done in a more universal manner than the much more specialized Reynolds Averaged Navier-Stokes (RANS) models.

This is the classical method to avoid resolving the turbulent eddies in space and time – namely to consider time averaged flow quantities and model the additional stresses due to turbulence in various ways. The influence of turbulence is treated in analogy with molecular transport leading to significantly higher *effective* diffusivity than in the laminar case. This approach utilizes the RANS equations and is by far the most common CFD approach in industry today. An illustration of the phenomena of jet mixing and heat transfer at the wall is provided by a single hole calculation using RANS CFD. The model is based on the work by Charbonnier et al. (2008). Results are extracted in a plane positioned at the hole centreline (Figure 12). The flow development just downstream of this cooling hole reveals that the mixing between coolant and mainflow is most intense in the upper region of the jet. This is in contrast to wall heat transfer that takes place closer to the near-wall region of the boundary layer. At some distance away from the centreline, such a distinction is less evident. Nevertheless, this example shows clearly the two different types of phenomena that govern the adiabatic film cooling effectiveness and the heat transfer coefficient.

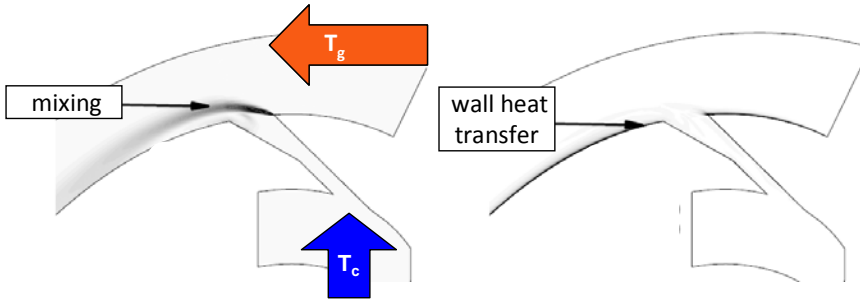


Figure 12: Computed gas injection through a shaped cooling hole

Turbulence models can also be implemented in boundary layer solvers allowing for accurate modelling of the steep gradients present in wall boundary layers. The code TexStan (see Kays et al. (2004)), solves the boundary layer equations using input from a pre-determined Euler flow field (free-stream velocity distribution). This type of solver is particularly convenient to apply on a cross section of an airfoil over which the flow is predominantly 2D. In the case of wall flows including 3D separation and impingement patterns, the free-stream can no longer be considered parallel to the wall everywhere. The vertical flow structures present near the endwalls of the present study motivate the use of a fully 3D flow solver. Nevertheless, it is possible to investigate the platform boundary layer locally along a wall flow-trace, as long as the flow is sufficiently two dimensional along a segment of that trace.

Boundary layer analysis of the endwall have been done on a smooth wall configuration (no cooling holes) by Zanker (2008). He implemented a series of TexStan datasets for the platform using the free-stream quantities along wall flow-traces predicted with a CFD model (cf. Charbonnier et al. (2009)). Despite the smooth wall, the complexity consists in a strongly accelerating flow, irregular heating boundary conditions, and a mature incoming boundary layer. The boundary layer code can take most of these parameters into account.

1.3.3 Platform Cooling and 3D Effects

It is the combustor that dictates the inlet conditions of the turbine as described by Boyce (2002). The first turbine stator vanes are facing very harsh conditions at their position directly downstream of the combustion chamber. Figure 13 attempts to illustrate that the nozzle guide vanes (NGV) of the high

pressure turbine might be considered as an integral part of the combustion system. Their task is to accelerate and align the hot-gas flow towards the rotor blades of the low-reaction turbine stage. Therefore, NGV's are designed using tools developed for turbine blades, with particular attention to the flow capacity determined by the minimum cross-sectional area (throat) of the nozzle. Figure 13 also illustrates the increasing inlet temperatures by the endwalls.

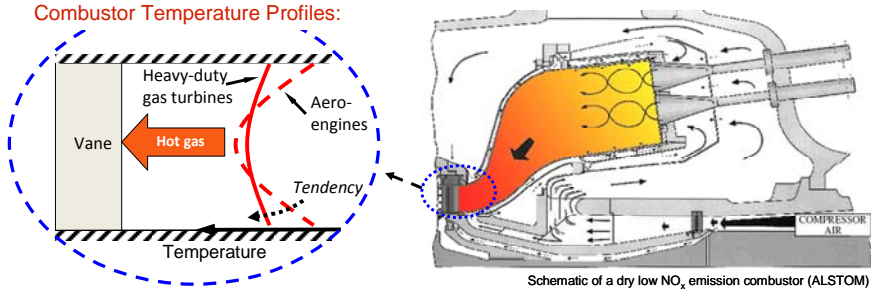


Figure 13: Temperature profiles of combustion chambers (Alstom Ltd)

As stated by Dunn (2001), the problem is that the upstream boundary conditions are difficult to measure with sufficient resolution and confidence due to the high gas temperatures. This is particularly the case close to the end-walls of the combustion chamber due to the incoming thermal boundary layer — with large temperature gradients. Therefore, in this work on film cooling of NGV platform surfaces, a flat temperature profile is employed. This allows to decouple the local flow features on top of the platforms from the inlet boundary conditions dictated by combustion chambers.

Just like for airfoil (mid-span) surfaces, endwall platforms are exposed to numerous, distinctly different, boundary layer types (accelerating, diffusing, separating and reattaching boundary layers, as well as local secondary-flow structures induced by cooling jets, etc.). In addition, platform cooling is associated with at least two additional drivers as compared with airfoil cooling:

- Firstly the local hot gas temperature. Modern combustion systems of stationary gas turbines are designed for highly lean combustion achieved by advanced pre-mixing of air and fuel. NO_x -emissions are reduced by minimizing the peak combustion temperature. The cycle performance is increased by further increasing the *average* hot-gas temperature by ensuring a more homogenous radial temperature distribution. However,

this leads to higher temperatures near the endwalls. Add to that the possibility to apply thick TBC-coatings on the combustor liners (low heat transfer coefficients and large wall radii) reducing the amount of film cooling flow upstream of the turbine increasing the adiabatic wall temperature further.

- Secondly the difficulty to predict film cooling on platforms due to the fact that endwall boundary layers exhibit various secondary (3D) flow features as illustrated in Figure 14. Thus the adiabatic wall temperature in this region is not only dependent on the free-stream flow but also on the local secondary flows requiring modern CFD calculations rather than classical design tools to be used. The over-turning of the end-wall flow is driven by the combination of blade-to-blade pressure gradients and the momentum deficit in the endwall boundary layer as explained by many authors e.g. Sieverding (1985) and reviewed by Langston (2001) and Rubensdörffer (2006). This produces a significant sensitivity to the physical size of the engine. For example, the over-turning is more severe in nozzles found in small aero engines. The reasons for this is twofold, first of all due to the fact that pressure gradients increase in magnitude at constant aerodynamic loading (Mach number) and, secondly due to a relative increase in the boundary layer thickness relative to the blade height.

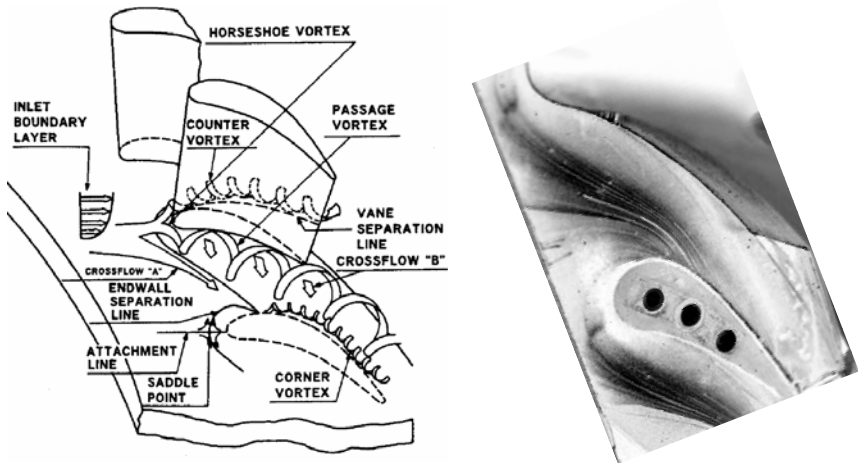


Figure 14: Illustration of 3D flow features (left) by Takeishi et al. (1990) and shear visualization of the present platform (right)

As a consequence, the application of film cooling is more complex on platforms than airfoils. 3D flow features must be considered by the designer in order to ensure that the cooling films stay clear from vortical flow features that might wash the colder gas away from the wall.

Due to the above mentioned complexities, and the relatively low temperature levels near the endwalls in aero engines, platform surfaces are traditionally not film cooled. Convective cooling on the backside of the platform is thus sufficient. However, future stricter environmental regulations are likely to change the prerequisites, motivating the application of film cooling on these parts.

1.3.4 Experimental Validation

It is clear that experimental heat transfer data from specific designs are highly valuable for the cooling design engineer since they show the result of the combination of several effects. Evolutionary design philosophies and real engine validation testing allows to manage the technical risks involved in turbine developments.

The following challenges in convective heat transfer and film cooling motivates experimental validation efforts in laboratory environment:

- Complex thermal boundary conditions found in film cooling applications motivates the use of *3D numerical modelling*. Empirical correlations are valid for specific geometries (pipes, flat plates, cylinders and specific airfoils) and situations where the momentum and thermal boundary layers develop simultaneously.
- Numerical methods require accurate *modelling of turbulence and transition*. This is still one of the main challenges in flow physics and computational modelling. Transitional flows are locally present in the present test case leading to large potential for uncertainty when it comes to transferring the results to engine situation as well as in reproducing the wall transport phenomena numerically.

Surface Sensors

Standard temperature measurement devices such as thermocouples are employed for point-wise measurements. However, surface temperature measurements in the steep gradients typically found in experimental heat transfer walls requires minimization of the sensor thickness. The following

techniques are commonly employed for turbomachinery research and development purposes:

- **Thin-film Gauges.** A classical method to obtain both heat flux and temperature simultaneously is the so-called hot film technique. Materials of which the electrical resistance is highly sensitive to temperature variations are used for this purpose. By making the probe very thin compared to the leads allows for measurement in a precise point. Variants of such thin film gauges are used extensively in blow-down facilities. The small thermal inertia of the probe allows for measurements of flow fluctuations with frequencies up to the order of 100 kHz. This outstanding frequency response allows to measure turbulence intensity with hot-wires based on the same principle.
- **Thermal Paints.** Engine validation tests are commonly done using so-called thermal paints. Those are also known as Temperature Indicating Paints as they provide a permanent visual record of the highest local temperature experienced during engine tests (120 – 1300°C). Such results allow for determination of the overall cooling performance of an engine part.
- **TLC Thermography.** Thermochromic (chiral-nematic) liquid crystal technologies have been reviewed by Ireland and Jones (2000). The narrow band type crystals have a colour spectrum that is visible within a 1 K-range which is suitable for accurate indication of a single calibrated temperature. Transient tests permit the narrow banded TLC's to indicate temperatures over the full surface as the indication contours travel along the surface. Very fast time response makes the TLC's suitable for transient measurements. The paint is applied using an airbrush. A matt black basecoat allows to render the TLC colours in order to record them in a video sequence. The image contrast can be maximized by aligning the illumination and camera parallel with each other at an angle away from the wall-normal in order to minimize reflected light. Once the TLC colour code has been calibrated, this technique has the advantage of a very well defined temperature determination. In fact, the precise colour indications limit the uncertainty to a narrow range that can be determined with high precision.
- **Infrared (IR) Thermography.** IR-techniques are commonly applied in qualitative and quantitative temperature measurements as long as the

signal sensitivity is well calibrated. Emissivity of the test surfaces and radiation from the surrounding is a concern. Therefore, this intensity based method depends on in-situ calibration procedures. In closed wind tunnels, the influence of the window should be taken into account. However, window absorption can be by-passed by the use of clever filtering.

- **Pressure Sensitive Paint.** The conventional application of Pressure Sensitive Paints (PSP) as a surface pressure sensor has been extensively studied in the domain of aeronautical research and development since the 1990's. The principle of the PSP technique is based on oxygen sensing property of luminescent molecules as explained by e.g. von Wolfersdorf et al. (2006).

Photoluminescent Paints

When the light sensitive molecules are excited to higher energy states through PSP sensor is illuminated with UV-light. This absorption of energy is followed by a reset to the initial state by the emission of visible, red-shifted light (fluorescence) as well as other types of energy transfer. One such transfer mechanism is oxygen quenching where the presence of oxygen molecules reduces the amount of emitted light. Thus with increased static air pressure (density) the number of oxygen molecules on the PSP sensor increases and the emitted light decreases. The competing actions of oxygen quenching and emission of light allows for optical full-surface measurements of the oxygen content on the surface.

Figure 15 shows the working principle of photoluminescent paint techniques. The distinct conversion of light between the far ends of the visible spectrum occurring in the fluorescence process allows for straight-forward filtering of unwanted illumination light (near-UV/blue) keeping only the emitted signal (red) by a combination of light filters. The excitation and emission spectra are depicted in Figure 16.

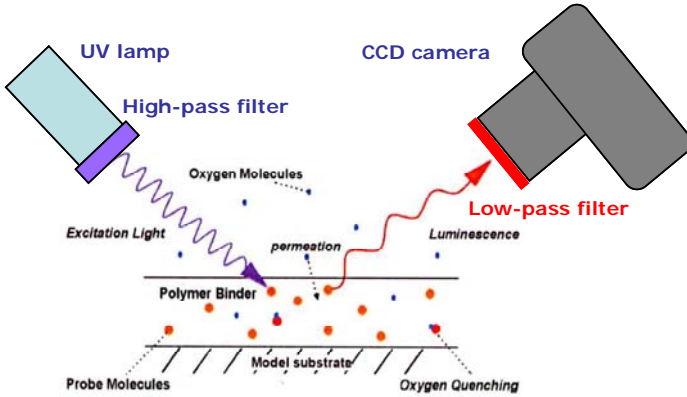


Figure 15: Working principle of photoluminescent paints

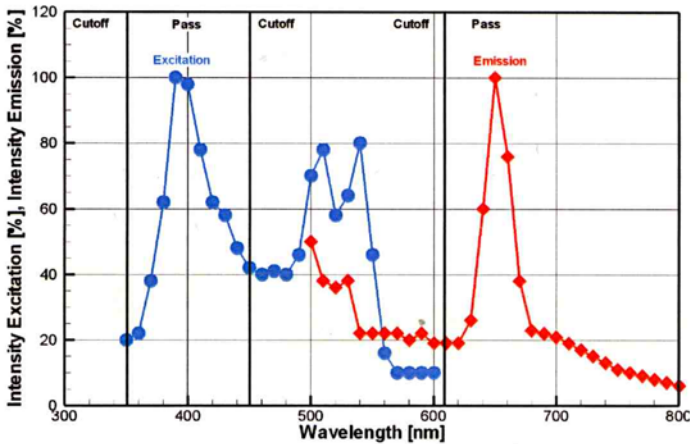


Figure 16: Excitation and emission spectra of present PSP system

The emitted light intensity of the PSP molecules depends not only on pressure but also on temperature. The temperature dependency originates from two main effects; firstly, due to the so-called ‘temperature quenching’ effect of the PSP luminophores and binder material as the material properties vary. Secondly due to the fact that the gas becomes less dense if the temperature is increased at constant pressure. Due to aerodynamic heating, most high speed pressure measurements using PSP struggle with the necessity to compensate for surface temperature variations and the influence this has on the PSP sensor. According to the introductory chapter in Tropea et al. (2007), a general description of temperature sensitivity of PSP is complex due to a combination of several mechanisms and the large number of possible PSP

systems. First of all, the dye sensitivity (luminophores). Secondly, and maybe most important are the characteristics of the binder material.

Here, the net temperature sensitivity will be considered without going into details of the different mechanisms. Simply speaking, temperature sensitive paint (TSP) is based on the same principle as PSP except that the oxygen sensitive molecules are completely sealed from the surroundings making them insensitive to oxygen pressure. TSP is integrated in the prevailing solution for aerodynamic pressure measurements of today, the so-called binary paint method. This technique uses a pressure independent probe (TSP) mixed with the oxygen sensor in order to obtain a reading of the sensor condition in each point (e.g. illumination intensity, temperature, etc.) independent of the oxygen pressure. Further, by calibrating the temperature sensitivity of the pressure and reference probes, the signal can be used to measure the wall temperature and thus correct the pressure measurements accordingly.

The linearity of non-intensified Charged Couple Device (CCD) cameras assure accurate measurement of the luminescent light signal. Complementary Metal Oxide Semiconductor (CMOS) sensors allow for much higher frame rates (up to 10 kHz) in high speed cameras. This comes at the cost of lower dynamic range and pixel dependent sensitivity.

An illumination source that is very stable and produces well-defined wavelengths became available with the blue LED's in 1995. Moreover, recent popularity and mass production have led to attractive pricing of LED arrays, even for the illumination of relatively large surfaces. This makes it suitable for photoluminescent measurements of the present type.

1.4 Conclusions of Chapter 1

It has been shown that there are several means of managing the life time and mechanical integrity issues caused by the hot-gas flow in the turbine. For a competitive design, technological complexity has to be balanced to the economical and environmental demands — ultimately in terms of competitiveness indicators such as Cost of Electricity (CoE), Specific Fuel Consumption (SFC) and quality/risk management.

One of the objectives with turbine cooling is to minimize the thermal stresses in blades and vanes. As the firing temperature of gas turbines increase, more accurate knowledge of the metal temperature distributions are required. Point-wise measurements and average temperature values might be sufficiently

accurate representation of the thermal status. Such simplified approaches are supported by the intrinsic smoothing of temperature fields inside the metallic walls due to heat conduction. This tendency is further supported by relatively smooth distributions of convective heat transfer as well as some degree of unsteadiness of fluid flows automatically tend to damp out locally excessive temperature levels. However, the physics is becoming less and less forgiving as designs advance to meet demands for improved performance and competitiveness. Therefore, it is motivated to provide engine realistic validation data with detailed surface resolution. There is a particular need for high resolution measurements on film cooling surfaces that are exposed to 3D flow features, e.g. endwall platforms.

The overall external cooling problem is split into two fundamentally different measures in order to separate the effects of external temperature reduction (adiabatic film cooling effectiveness) and a measure of the heat transmittance of the boundary layer (heat transfer coefficient). With those two parameters, the external cooling situation is defined, provided that the thermal boundary conditions at the surface are qualitatively similar. This motivates the use of engine realistic test configurations such as in the present work.

The fundamental drivers of the heat transfer process have been identified in order to analyse and optimize a cooling scheme. Further to the 1D example shown above, the coupling between solid and fluid can be important when it comes to characterizing the detailed heat transfer and cooling of a wall. At the end of the day, it is the heat flux under engine realistic boundary conditions that matters (see comments by Arts and Bourguignon (1990)). For example close to cooling holes due to the fact that the heat transfer situation is highly 3D when the convection inside the holes is added. This is particularly so in showerhead configurations at the leading edge due to the tightly spaced cooling holes. In fact, the internal heat exchanger provided by the cooling holes themselves are more important than the external temperature reduction due to film cooling as shown by Wagner (2007). This demonstrates that cooling design is a global, so-called conjugate, heat transfer problem.

It has been shown that engine realistic validation data with detailed surface resolution of the local performance measures is needed for further understanding and improvement of gas turbine performance. Despite the continuously growing capability of numerical simulation tools, convective heat transfer assessment is highly empirical. Maybe even more so when film cooling is involved.

Considering that the thermal boundary conditions in engines might be rather different at best and unknown at worst, a realistic approach is to consider technological improvements with respect to a known baseline case and compare relative results to numerical modelling or correlations as well as engine experience.

Absolute film cooling performance is tedious to predict numerically. However, simplified numerical methods serve well to improve the understanding of the flow physics. Although the more advanced methods mentioned above are becoming more and more common in research, the calculation time and the number of modelling parameters to control in e.g. LES modelling requires high quality guide lines and validation for the studied application. This summarizes an important challenge in the field of numerical modelling – namely the appropriate use of the powerful methods. Further, experimental benchmarks provide invaluable proof and confidence in numerical predictions. Therefore, well suited experimental measurement techniques are needed.

The large number of flow parameters presented in this introduction shows that it is important to isolate the effects that can be reproduced in the laboratory environment. This is done by comparing results to a reference case obtained in the same test facility using the same measurement techniques. Moreover, systematic measurement errors appearing in all tests tend to cancel and thus be minimized.

It has been shown that the use of CO₂ mimics the real engine situation with cold air injection.

Chapter 2

State of the Art

A large effort has been made in refining the understanding of external aerothermal problems. This is clearly illustrated by the nearly 500 references cited by Dunn (2001) in his review paper on convective heat transfer. Han et al. (2000) give an extensive overview of turbine cooling technologies including experimental techniques often used to assess the cooling performance in the beginning of the 21st century. While heat transfer of film cooled airfoils at mid-span is well documented and relatively well understood, there is a great need for experimental validation of edge-effects occurring near the hub and tip of the blades. Vane platforms exhibit several examples of such edge effects.

The limited work published on platform film cooling has been reviewed by Chyu (2001) as well as Simon and Piggush (2006). Even without film cooling, the main-flow field close to the endwall heat transfer distributions are already very complex due to flow acceleration, secondary flows and vortices. The main conclusion is that precise measurement techniques resolving the local heat transfer (h) and, in case of film cooling, the local film cooling effectiveness (η) distributions are required. Therefore, a literature survey specifically investigating platform measurements is provided in the following. The review focuses on appropriate sensors for platform measurements with reference to previous work on this topic. This leads to the motivation and objective of the present work as summarized in the last part of the chapter.

2.1 Measurement Techniques for Platforms

Many different types of test facilities have been used over the years. The optical access is important for full-surface measurements of the present kind. This makes linear cascade configurations a practical compromise between rotating rigs (require curved windows and auxiliary structures) and basic single passage tunnels. Moreover, periodicity is important in order to mimic geometric similarity of real engines especially for platform studies.

High Reynolds number flows over small-scaled turbine blades lead to thin boundary layers. This makes it difficult to perform direct measurements of the

boundary layer profiles. One method to overcome this resolution problem is to use large-scale models. Then, the Reynolds numbers are maintained by lowering the velocities towards the incompressible range. Such detailed flow temperature profiles using fine wire thermocouples have been measured by Piggush and Simon (2007) with the objective to obtain heat transfer coefficients from the slopes of the temperature profiles. They employed a heated aluminium wall using embedded heaters. With this technique, the knowledge of the surface heat flux is not needed in advance but can be determined from the temperature gradient at the wall. Therefore, this method could be applied to a configuration with complex heating distributions due to cooling holes. Adiabatic film cooling effectiveness results using the same technique were also obtained. The adiabatic wall temperature is less demanding to obtain with this technique due to the absence of a wall normal temperature gradient in adiabatic low speed situations. Obviously, performing a large number of hot-wire traverses inside the flow field can be a tedious task.

Therefore, it is preferable to observe the net thermal foot print on the surface. Knowing the free-stream flow conditions, this approach allows to deduce the state of a boundary layer by e.g. comparing with correlations or numerical models. Earlier endwall studies such as those by Blair (1974) and Graziani et al. (1980) used local wall thermocouples. Together with guard heaters or heated foils, they provided uniform thermal boundary conditions for the heat transfer measurements and to show the resulting complex heat transfer patterns. Blair (1974) also investigated the film cooling effectiveness for injection from an upstream slot.

As already shown in Section 1.2, there are several sources of temperature gradients present inside the boundary layers – in particular when viscous heating has to be considered. Therefore measurements of detailed temperature profiles inside the boundary layer are not trivial.

The aforementioned test facilities of large-scale and low velocity have been widely used in heat transfer research. As long as Reynolds similarity is fulfilled, this is considered to be sufficient since the properties of a wall boundary layer is to a large extent dictated by turbulent transport but only weakly influenced by compressibility. As the aerodynamic loading of turbines tends to increase for the reason of lower blade count and less weight, the Mach numbers increase towards transonic levels. This demonstrates the need for compressible flow facilities in addition to the traditional low-speed approach.

Compressibility is important when it comes to transition *length* similarity which is important for wall heat transfer in some areas, in particular for smooth surfaces without film cooling injection. Boyle and Simon (1999) demonstrated the impact numerically showing better agreement with experiments when the Mach number effects were taken into account in the transition modelling. The argument is based on the spreading angle of the turbulent spots and the Tollmien-Schlichting wave frequency governing the formation rate of turbulent spots. According to Hinze (1975), compressibility effects on turbulence may only become appreciable when the velocity fluctuations cause significant density fluctuations due to the associated pressure fluctuations. As the strength of the so induced turbulent sound waves increases, the turbulent dissipation rate increases as well, and must be taken into account in the closure modelling. The high subsonic Mach numbers encountered in the present work ($\overline{Ma} < 1.0$) imply that turbulent velocity components are only a fraction of the main velocity and can be considered incompressible. However, considering that transitional and relaminarising areas can be present locally also on film cooled turbine blades, the use of compressible test facilities is motivated.

With the progress of optical measurement techniques for full surface investigations of local heat transfer coefficient and adiabatic film cooling effectiveness distributions, several measurement methods have been developed. Most of them focus on the determination of either η or h .

Thermal measurement methods typically apply Infrared (IR)-thermography, Thermochromic Liquid Crystals (TLC) or thermocouples for surface or flow temperature measurements.

Full surface measurements with non-intrusive optical methods as high resolution IR-thermography have been used for η measurements by several authors. Combinations of cylindrical and fan-shaped hole rows and the effects of hole shapes were addressed by Colban and Thole (2006). Combined slot and hole injection was studied by Knost and Thole (2005) and Sundaram et al. (2008). Film cooling from an upstream slot without additional holes was investigated by Lynch and Thole (2007). Here, additionally endwall heat transfer measurements were taken applying a heat flux plate with discrete thin heating elements.

Steady state and transient TLC methods (see e.g. the review by Ireland and Jones (2000)) have been applied to both, h - and η -measurements in this context. Endwall h -distributions without film cooling have been obtained by Giel et al. (1998) in a transonic turbine blade cascade. Using a steady state technique with several thin heater foils at different electrical power levels and a mixture of two narrow-band TLC's, the authors were able to determine the local h -distributions in the case of strong variations as present at the endwall in a transonic turbine. A similar approach was used by Ames et al. (2003) for a vane cascade endwall. Wide-band TLC were used by Barigozzi et al. (2006) for detailed η -measurements using the thermal quasi-steady state after instantaneous injection of heated film cooling flows into a colder mainstream air. A steady state method with wide-band TLC was applied by Wu and Chang (2007) on a turbine vane endwall with streamwise and cross-stream film injection from holes to determine the adiabatic film cooling effectiveness. In this study the h -distribution was also measured using a transient method with time-wise increased flow temperatures at the start of the experiment in a single passage test rig. To eliminate the thermal effects of the coolant (η) both the mainstream flow and the coolant flows must achieve the same temperature rise and history during the experiment. The need for a significant temperature increase in the relatively large main-flow within a short time period hinders the application of this technique for cascade endwall investigations compared to the widespread use in simplified channel film cooling tests (see e.g. Ekkad and Han (2000)).

As indicated by this review, many studies have been carried out to investigate only one parameter (h or η) or the studies use separate tests with different thermal boundary conditions to acquire both quantities, especially for discrete hole configurations. To address this issue, Nicklas (2001) covered the endwall with meander-type heating foils wrapped around the individual holes to achieve known heat flux conditions in different steady-state tests. Several wall temperature distributions measured by IR-thermography were used together with the superposition approach to evaluate both h and η .

Another technique was introduced by Vogel et al. (2003) using TLC and heated foils tested in the present facility. Here a transient procedure with instantaneous film cooling flow injection and foil heating assuming one-dimensional conduction within a semi-infinite wall was applied. This method was employed in a vane cascade with contoured platforms and fan-shaped

holes. With this method all three parameters, h , η and the local heat release q , can be obtained simultaneously. Therefore the heat release in the foil is not required to be uniform and the foil can contain discrete holes for the film cooling configuration. This makes the method somewhat unique but also more complex compared to other techniques. As shown in Vogel et al. (2003) multiple experiments need to be performed and simultaneously analysed using nonlinear regression analysis to achieve acceptable experimental uncertainties of the measured parameters.

Vogel et al. (2002) also proposed a combination of TLC and PSP sensors. They also measured the static pressure distribution in order to derive velocity distributions as well as dump conditions for the cooling jets. Further, the potential to derive local recovery temperatures from the velocity results was put forward.

Pressure sensitive paints (PSP) for η measurements have been applied in a series of studies. The analogy between heat and mass transfer has been employed for this purpose. Zhang and Jaiswal (2001) investigated discrete cylindrical holes and slots. Wright et al. (2007) and Suryanarayanan et al. (2009) applied PSP on rotating platforms for blades with upstream slots and discrete film cooling holes respectively. A film cooling scheme with rows of fan-shaped holes for a vane passage endwall was investigated by Vogel (2002).

Another mass transfer technique for film cooled endwalls was applied by Friedrichs et al. (1996) using the Ammonia-Diazo method for discrete hole film cooling. Jabbari et al. (1996) among others used the naphthalene sublimation technique for such an application. Using the latter method, the local mass transfer distribution can also be determined and related to the heat transfer by the analogy between mass and heat transfer (e.g. Han and Goldstein (2008)) and applied for discrete hole film cooling as well.

TSP measurements have been carried out in a linear cascade by Narzary et al. (2009). They measured adiabatic film cooling effectiveness on platforms by injecting coolant with a different temperature compared to the main-flow. Kingsley-Rowe et al. (2003) have employed laser heating in combination with luminescent paint on wings in order to measure heat transfer coefficients through transient temperature response of the wall. Numerical modelling of laser-spot heating was employed in order to solve the 1D transient heat conduction problem.

2.1.1 Adiabatic Wall Measurements

Thermal smoothing due to heat conduction in metallic wall is considerable in gas turbines. As shown in a simplified 1D conduction model and order-of-magnitude analysis by Eckert (1992), the temperature equalization effect tend to diminish adiabatic wall temperature distributions towards less pronounced levels. Nevertheless, detailed measurements of film cooling are highly motivated when 3D effects are taken into account. Moreover, the smoothing phenomenon is already one of the mechanisms allowing for high combustion temperatures. Thus, it is preferable to know the detailed temperature distributions and average afterwards. This means that thermal equalizations must be minimized for external film cooling experiments.

Thermal Measurements

Measuring the adiabatic wall temperature as imposed by the flow can either be done using a wall with negligible conductivity or by modelling the conduction numerically in order to deduce the adiabatic condition with inverse methods. This can be done numerically but is relatively time consuming in 3D — especially when considering transient experiments. As shown by von Wolfersdorf (2007), the influence of lateral conduction can be locally significant in experiments of the type employed in temperature experiments. Because the highest lateral gradients are present close to the cooling holes, near-hole resolution can be impeded. However, the offset between 1D and 3D solutions to the heat conduction in the solid tends to diminish in laterally averaged results.

Mass Transfer Analogy

An alternative approach to obtain the adiabatic effectiveness is to utilize the analogy between heat and mass transfer and measure the impermeable effectiveness. The transport of scalar quantities such as heat and gas species (mass) depends on the velocity field as well as the driving difference of the considered quantity. Under certain conditions, the analogy between heat and mass transfer is sufficiently good to allow for quantitative conclusions of one of the quantities, based on a measure of the other one. Thus, for the purpose of adiabatic film cooling effectiveness measurements, the cooling gas can be marked with different gas species compared to the main-flow in order to derive the impermeable and adiabatic effectivenesses. In the following, it is shown that the field of normalized gas species concentration is analogous to the normalized enthalpy field ($i = c_p T$)

$$\hat{i} = \frac{i - i_g}{i_c - i_g} \quad (14)$$

$$\hat{\zeta}_{O_2} = \frac{\zeta_{O_2} - \zeta_{g,O_2}}{\zeta_{c,O_2} - \zeta_{g,O_2}} \quad (15)$$

The normalization effectively eliminates the driving potential so that the heat and mass transfer solutions can be compared. In incompressible gas flow with constant gas properties, the corresponding transport equations have the same form and analogous solutions can be found as long as the boundary conditions are equivalent according to Kays et al. (2004). This analogy between heat and mass transfer is illustrated in Figure 17.

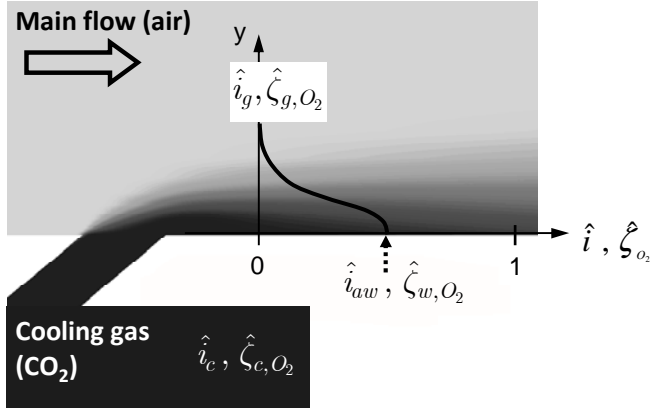


Figure 17: Analogous energy and species concentration fields

Quantitative analogy between the two transport phenomena exists as long as the Prandtl number of the heat transfer situation is equal to the Schmidt number of the mass transfer problem. This is the case when the molecular Lewis number is unity:

$$Le = \frac{Pr}{Sc} \quad (16)$$

As Eckert et al. (1976) summarized, the analogy is a good approximation as long as the Lewis number varies only little as a function of the composition of the gas mixture – in this case the CO_2/air mixture. According to Kays et al. (2004), this is indeed the case for the present gas combination since the Lewis number is very close to unity ($Le \approx 1.0$ for CO_2/air) over the complete range of gas compositions.

If this is not the case, analogy can still be found by the application of analogy functions according to the work by e.g. Häring (1996). In fact, molecular diffusion considered so far is the sole driver in a laminar flow – making it particularly important in wall transfer problems where the viscous sublayer plays an important role. On the other hand, mixing between film and main-flow is mainly driven by advective flow motions due to turbulence. The mixing is most intense in turbulent shear layers, caused by velocity gradients between the two streams, as well as turbulent boundary layers usually present near the walls. It has been shown that for most gases, the turbulent Lewis number is

very close to unity, even when the similarity constraint on molecular diffusion (Equation 16) is not met:

$$Le_t = \frac{Pr_t}{Sc_t} \approx 1 \quad (17)$$

Recall that the low velocity restriction mentioned above is not fulfilled everywhere in the present flow domain. The high subsonic velocities imply significant aerodynamic work which plays a 1st-order role in the energy equation but not in mass transport. For this case, the analogy becomes apparent by considering the total temperature (total enthalpy) according to Shadid and Eckert (1991). This can be observed in the total temperature profiles sketched in Section 1.2.

Further, the viscous dissipation effect must be taken into account for such flows (Figure 4). Again, the impact of viscous heating on the flow field (momentum) as well as the energy equation is significant in contrast to the mass diffusion equation. In the case $Pr = 1.0$, this effect is entirely covered by the above total-temperature argument. When it comes to gases with Prandtl numbers slightly different from unity, there might be significant differences between the non-dimensional heat and mass transfer solutions at the wall. However, as pointed out by Jones (1999), the mixing process of interest in film cooling is situated sufficiently far from the wall where viscous effects reduce in favour for inertial effects (turbulence). Consequently, the viscous dissipation effect can be decoupled – at least for the moderate Mach numbers encountered in the present study. When it comes to adiabatic wall measurements using thermal indication, the key is to separate the viscous heating effect from the thermal mixing problem. This is ensured by consistent handling of the adiabatic recovery temperatures through superposition as mentioned in Section 1.2.

Finally, many of the gas properties vary due to the injection of a highly concentrated foreign gas leading to large variations of the gas composition in the cooling films. According to Eckert et al. (1976) there is no *exact* analogy between heat and mass transfer for such flows. Nevertheless, they showed empirically that the analogy is a very good approximation for film mixing problems as long as the density ratios are the same in the flows compared. This argument relates to engine-laboratory similarity which can be carried over to the present application where the analogy aims at relating two scalar

quantities in the *same* flow (laboratory). Again, the main argument is that the mixing occurs in turbulent flow which is mainly governed by the turbulent motions that in turn depend heavily on momentum effects (ρ), but only weakly on Reynolds number effects. The local Reynolds number is also sensitive to variations of the remaining gas properties (c_p , μ , k and κ). Therefore, the heat and mass transfer analogy can be used with confidence for mixing processes that does not include transfer at the wall as summarized by Shadid and Eckert (1991). As a consequence, the adiabatic and impermeable effectiveness measurements with the present gas mixture are analogous without application of analogy functions.

Gas Concentration Measurements

Concentration measurements have been used extensively to study the mixing processes of film cooling. There are many methods available to measure gas concentrations; e.g. acoustic methods, hot-wire techniques, infrared spectroscopy, Schlieren techniques, laser induced fluorescence, Rayleigh scattering, Mie scattering, mechanical resonance sensors. Roback and Dring (1993) injected small amounts of tracer gas (0.1 % CO₂) in a hot-streak simulating the flow from combustion chambers. Adiabatic effectiveness data was obtained from gas samples drawn through static pressure taps on airfoil and endwalls. Another gas sampling probe for traversing the flow field at the vane exit plane of a rotating rig has been developed by Pomfret et al. (2002). They used a hot-wire to detect differences in the convective heat transfer due to gas concentration. Fast gas samples were achieved with an aspirated probe.

Adiabatic Film Cooling Effectiveness and PSP

The PSP technique has been employed successfully over the past 15 years in aerodynamic pressure measurements. As an oxygen sensor, PSP is a suitable technique to measure coolant gas concentrations as shown by e.g. Zhang and Jaiswal (2001) and Vogel et al. (2002). Ahn et al. (2007) performed PSP measurements on the leading edge of a rotor blades in a rotating test facility. Laser illumination and high speed camera allowed for integration times in the order to 15 μ s. Observe that this is not a fast response application of PSP in that the oxygen quenching is considered steady (time-averaged).

Influence of hole geometry imperfections on the adiabatic film cooling effectiveness can be considerable for cylindrical holes at high blowing ratios as

shown by Jovanovic et al. (2008). Independent of whether a real engine or experimental situation is considered, it is important to ensure high surface quality in the cooling holes. However, this is delicate to achieve as long as the cooling holes are small and full-surface sensors in the form of coatings are needed. One way to control variations between experiments is to ensure consistent surface quality between different tests.

Experiments with carbon dioxide as coolant in a main-flow of air implies a number of differences compared to the more common method of injecting nitrogen (N_2), in which case the gas properties of coolant and mainflow can be considered equal. **For this reason, the molecular mass correction is often left out in the theoretical analogy derivation for film cooling studies using N_2 -injection.** The gas properties of Nitrogen are similar to those of the main-flow since it is the dominating component of air. More specifically, the molecular mass.

CO_2 is a suitable gas to simulate the density ratios typical to engines with cold-air injection. **As observed by Ahn et al. (2005), the heavier molecular mass of CO_2 must be taken into account in the derivation of mass concentration from pressure data.**

Engler et al. (1992) documented the quenching of constituents in air other than oxygen. They concluded that the quenching due to CO_2 is at least two orders of magnitude smaller than O_2 . The only gas species present in air with noticeable influence are ozone and nitrogen oxides. However, the concentrations of those species are very small and can be neglected.

2.1.2 Wall Heat Transfer Measurements

The superposition approach is the basis for a classical method to determine both the adiabatic film cooling effectiveness and the heat transfer coefficient experimentally. The superposition method was first presented by Metzger et al. (1968) and Choe et al. (1974). It consists in performing two separate measurements using two different test plates, one that is nearly adiabatic and another with high heat conductivity. Generating continuous wall heat transfer requires particular hardware setup, e.g. internal heat transfer arrangements, electrically heated foils or coatings or radiation heated wall surface by the use of lamps or lasers. Wall temperatures result from several different heat transfer mechanisms. Separating the convective heat transfer and film cooling

effects from solid wall conduction requires some consideration on the wall material, even if numerical modelling of the heat transfer inside the wall can be applied to correct the result. The Biot number is defined as the ratio between convective and conductive resistance to heat transfer by including the thickness δ of the solid:

$$Bi = \frac{h \delta}{k} \quad (18)$$

The following drivers determine the choice of wall material for the parameters of interest:

- For adiabatic temperature measurements, wall conduction can be neglected if a material with low thermal conductivity ($Bi \gg 1$) is chosen. Any lateral conduction should be minimized (due to actual *diabatic* walls) in order to resolve lateral gradients without the result being laterally smoothed.
- For convection measurements, a Biot number in the order of unity (highly conductive wall material) is common in order to produce significant heat flux and temperature difference over the boundary layer. However, this can also complicated the analysis due to lateral conduction inside the wall — at least if there are steep lateral heat transfer gradients on the surfaces.

Transient Heat Transfer Experiment

Transient heat transfer methods can be used to overcome some of the experimental design and analysis problems associated with steady measurements as already pointed out. In the transient situation, the heat storage capacity of the wall is used to derive the convective heat transfer by measuring the time response to step changes of the flow temperature.

Experiments using rapid flow heating typically ensures a fast temperature step from an initially low to a higher temperature ($T_i \rightarrow T_g$). This can be done by rapidly inserting a simplified test model from a preconditioning chamber as e.g. Jonsson and Ott (2007). Alternatively, the entire main-flow can be heated using powerful heater meshes which is convenient for low speed flow found in internal cooling schemes, e.g. Gillespie et al. (1998). More powerful tube

heaters have been employed by Krueckels et al. (2009) for external heat transfer experiments.

If the duration of a transient experiment is short enough, temperature variations inside the wall due to a transient convective experiment only penetrate to small depths. Further, this leads to a heat flux that is predominantly normal to the surface — especially in the early phase of a transient experiment. This simplifies the thermal analysis of the solid, allowing for the use of 1D analytical modelling of the transient solid heat-conduction according to Carslaw and Jaeger (1992). Thus, the main motivation for using transient instead of steady-state experiments are the following:

- No need to implement a steady-state heating device in models with complex shapes (simplified design of experiment).
- Allows for using narrow band TLC-thermography as the single temperature indications travel over the surface.
- A complex heater foil shape does not overheat locally.

EPFL-LTT has a long proven experience with transient TLC methods for internal and external heat transfer measurements. The transient TLC method has been validated by Hoffs et al. (1997) by comparing transient results obtained with TLC-thermography and thin-film gauges. The same results compared well with steady heat transfer data obtained with the naphthalene measurement technique. The transient TLC technique has been applied for external heat transfer measurements in the present test facility by Drost and Bölcs (1999), Reiss (2000), Vogel (2002), Falcoz et al. (2006) as well as Jonsson and Ott (2007). The standard formulation of the analytical method assumes flat walls which is the case in the present work on platforms. A curvature correction method has been implemented by Wagner et al. (2007) particularly useful for leading edge geometries.

Insertion of a pre-cooled model is convenient for airfoil geometries. However, geometries that cannot be rapidly exposed to a warmer flow (e.g. platforms) require an alternative approach to realize transient temperature measurements. For this purpose, a variant of the heater foil technique of Vogel (2002) is employed. The inversed temperature difference between flow and wall can be used since the small difference is only used as a mean to mark the heat transfer at the wall.

2.1.3 Engine Similarity

Obviously, it is not possible to simulate all features present in an engine. The objective is to measure sensitivities to specific parameters and so it is envisaged to match as many similarity parameters as possible. Mach and Reynolds similarity have already been mentioned. The density ratio (DR) is known to be an important parameter in film cooling. As pointed out by Bogard and Thole (2006), similar density ratio allows to simultaneously match all of the parameters relevant to film cooling:

- Momentum ratio (J). Scales the dynamics of the interaction with the main stream indicating whether the jet will stay attached to the surface or lift off into the free-stream.
- Blowing ratio (M). Scales the thermal transport capacity of the coolant.
- Velocity ratio. Scales the shear layer between the coolant and mainflow and the turbulence production.

Simply speaking, the momentum ratio is important for the adiabatic effectiveness close to the cooling hole as long as the jet stays attached. This is the region where the boundary layer is mostly influenced making the momentum ratio a more important parameter for the turbulent flow field (also in terms of the heat transfer coefficient) as shown by Chana et al. (2005). The blowing ratio plays a more important role further downstream as predicted by heat balance analysis. Finally, the relative velocity dictates the amount of shearing between the flows.

As in several previous studies, CO_2 is used as coolant here in order to provide engine realistic coolant-to-main flow density ratios ($DR \approx 1.7$). Typical values with cold-air injection with respect to the hot gas of a gas turbine ranging between $DR = 1.5 - 2.0$. In addition, mass flow rates can be employed to characterize the absolute cooling potential of a film cooling scheme.

Thus, film cooling in real engines and the present test set-up include significant non-linear effects due to variable property flows. In many studies in the past, gas property variations have not been included in the experiments directly. Instead, scaling of the results using property ratios can be employed to transfer the measured result towards the engine situation.

Heat transfer experiments with ambient temperatures have the advantage of producing temperature differences in the order of only 10% allowing for the use of temperature-invariant properties. Then gas property variations can be neglected allowing for the linearized heat transfer coefficient employed in the present study. Working with small temperature differences has several practical advantages:

- Coolant temperature is only moderately varied in order to trace the films — without drastically changing the properties.
- Thermally induced stresses in the test plates remain small which allows for the use of e.g. acrylic materials in complex shapes.
- Allows for the use of photoluminescent coatings (optimal performance close to room temperature).

Net Heat Transfer Reduction due to Film Cooling

The particular thermal boundary conditions generated by the heater foils are present in all experiments of each case. Therefore, the parameter of interest is the relative change in the heat transfer coefficient due to film cooling with respect to an un-cooled baseline case. By computing the relative heat transfer change due a technological modification, comparison of film cooling performance trends can be done reducing the impact of thermal boundary conditions, surface roughness, etc. The same principle is useful in numerical modelling as well. An alternative solution to obtain consistency with CFD comparisons is to impose the same type of heating distribution as boundary condition. At the end of the day, it is the global influence of film cooling that should be considered according to the net heat transfer reduction. The purpose of such a laboratory experiment is to ensure a certain degree of similarity in the film cooling flows between laboratory and engine conditions (thermodynamic property ratios).

2.2 Missing in the State of the Art

Based on the experience available in the literature presented in this chapter it is clear that all measurement techniques have advantages and disadvantages. Most of the experimental methods available in the literature focus on one of the two quantities of interest in film cooling — the adiabatic film cooling effectiveness or the heat transfer coefficient. **Thus it is motivated to search for methods that can characterize the complete film cooling performance with a minimum of inconsistencies between test surfaces and models.**

Thermal equalization due to lateral condition in adiabatic wall measurement was mentioned in Section 1.1.3. This smoothing is advantageous in design since it gives some margin for uncertainties. At the same time, smoothing introduces uncertainty in experimental measurements aiming at providing detailed traces of a flow field — for example on surfaces as in the present work. Therefore, it is advantageous to minimize the solid conduction in experiments. Or by looking into the alternative methods in the field of mass transfer.

Highly concentrated tracer gases in mixing studies leads to a large range of light intensity signals that can be readily detected with a PSP system. This method is promising for film cooling studies since the noise levels typically associated with PSP in static pressure measurements diminish substantially for adiabatic film cooling effectiveness measurements. Therefore, it is motivated to use PSP in near-ambient temperature experiments where temperature uncertainties can be significant.

2.3 Objectives of Thesis

Considering the tendency of increased hot gas temperature and complex aerodynamics near the endwalls described in Section 1.3.3, there is a need for improved understanding and quantification of film cooling performance on platforms. The objective is to obtain high resolution measurements of film cooling coverage on advanced platform film cooling configurations as the one shown in Figure 18.

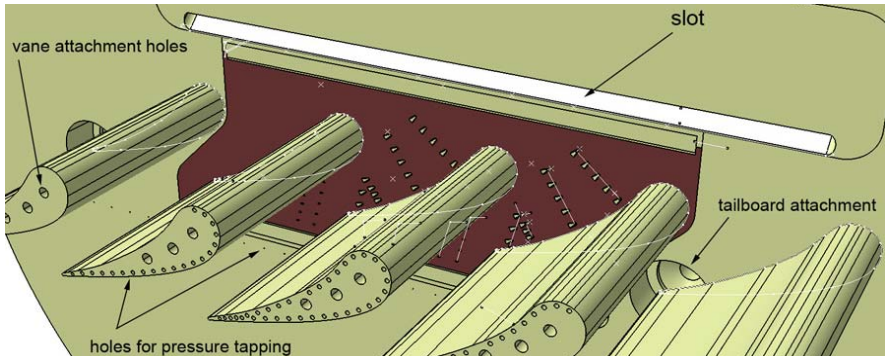


Figure 18: Platform test case with passive slot geometry

It has been shown that steady-state temperature conditions of the coolant are important for test cases with large number of cooling holes and multiple plenum chambers. Multiple transient temperature evolutions might result from the different plenum chambers due to different flow rates. Therefore, no unique coolant temperature can be defined. One way to overcome this problem is to experimentally decouple the measurement of adiabatic film cooling effectiveness and the measurement of heat transfer coefficients.

Furthermore, an accurate determination of the adiabatic (recovery) temperature is required due to the small temperature differences generated during the present experiments. **Alternatively, it would be advantageous to measure the temperature difference due to heat transfer directly.**

Based on the above arguments, it is motivated to **establish a suitable measurement procedure** given the need for experimental data on endwalls with complex film cooling schemes exposed to engine realistic Mach and Reynolds numbers. As such, the present thesis focuses on measurements of the external cooling problem without consideration of internal cooling aspects.

2.3.1 Hypothesis

The hypothesis is that a PSP-oxygen sensor is sufficient to provide the full external film cooling information without the need to repaint the test model with another sensor coating. More specifically:

- Can the PSP technique be applied to measure adiabatic film cooling effectiveness using CO_2 as tracer gas for engine realistic density ratios?

- Is it possible to utilize the temperature sensitivity of the PSP-sensor for transient HTC measurements? E.g. using ‘off-the-shelf’ PSP (single sensor) as both oxygen pressure and temperature sensor in combined concentration and heat transfer measurements?

There are a couple of advantages of doing it this way. As stated in Section 2.1.1, consistent surface quality is important. Therefore, a method is sought that can use the same surface coating for all experiments (adiabatic film cooling effectiveness and heat transfer coefficients).

- Single sensor coating for the complete film cooling characterization. This leads to consistent surface roughness and cooling hole imperfections (e.g. due to paints and dirt deposits) between tests.
- Combining thermal and concentration measurements (decoupling).
- Full time history of the temperature evolutions including the initial (adiabatic) wall temperature.
- High image resolution and full surface coverage.

Such a heat transfer method would be somewhat similar to that of Kingsley-Rowe et al. (2003). However, in the present work more realistic thermal boundary conditions can be achieved using a heated foil instead of local laser spot heating.

2.3.2 Major Steps

Introductory assessments of airfoil film cooling have been performed at mid-span of a nozzle guide vane (Jonsson and Ott (2007)). The 2D flow field is an excellent situation to isolate the fundamental parameters and physics of film cooling.

Experiments on the platform (Jonsson et al. (2008)) demonstrated experimental difficulties due to complex test conditions. It has been confirmed that transient heat transfer measurements performed with narrow banded liquid crystal thermography is not optimal for the present set-up due to the following reasons:

- Aerodynamic heating makes the temperature difference associated with wall heat transfer uncertain when small temperature differences are employed.

- Highly varying temperature raise over the surface is due to a wide range of heat transfer coefficients combined with the heated wall concept.
- The high accuracy of a single temperature indication lacks a similarly accurate measurement of the initial temperature of the wall.
- Complex heater foil geometry with a large number of holes. Local over-heating effectively limits the allowable heating power.

It is also identified that the material properties of Perspex approach the limit with respect to the large values of external heat transfer coefficients in the present flows. This leads to short response times and a camera system for faster image acquisition has been set-up by Zanker (2008) in order to improve the TLC measurements.

However, the above listed issues make it difficult and lengthy to achieve consistent measurements, e.g. cooling injection rate variations. These problems lead to partial surface coverage and relatively large uncertainties in each test. Moreover, a nearly wall-normal viewing angle is required for the present platform measurements. This is not a trivial set-up for TLC measurements since the image contrast suffers from reflected light in dark areas (poor rendering of black). Therefore, several attempts to overcome the technical limitations have been implemented

One way to improve the applicability of narrow band TLC's in this context have been tested by adding a second TLC indication temperature in order to obtain more information in each test (Jonsson et al. (2008)). Nevertheless, the root cause for the problem in the present application is the single indication temperature of narrow banded TLC's. Thus there is a need to determine the complete time history of the wall temperature in order to measure the sought temperature difference with the same sensor.

Later on, it was shown that FEM-modelling can be employed to determine the heat release from the heater foil in order to eliminate one of the unknowns. Jonsson and Ott (2009) presented heat transfer results using transient wall temperature experiments and narrow band TLC on the same test case as employed in this thesis. Again, detailed full surface measurements can be complex to perform but that the use of narrow band TLC thermography gives reliable results — although locally. Thus, this type of test case turned out to

be too time-consuming to obtain accurate full surface measurements for a complete test matrix employing this technique.

After exploring experimental challenges and possibilities in more detail, e.g. film cooling concentration measurements (Wunderlin (2006)), measurement of inlet boundary layers and secondary flows (Erber (2007)) and wall heat transfer using heated foils (Zanker (2008)), a combination of well adapted techniques could be set up. The development includes the application of a common surface sensor (PSP) for gas concentration and heat transfer measurements. The potential of a standard PSP technology is explored. The paint is chosen based on existing in-house experience of Steiner (2000) and Vogel et al. (2002).

2.4 Conclusions of Chapter 2

The difficulty to establish accurate turbulence closure models is one of the main motivations for film cooling experiments. If the objective of experiments is to validate turbulence modelling of numerical simulations tools only, then the test set-up must not necessarily be similar to the real application in all aspects. For example, gas mixing and wall heat transfer phenomena are primarily dictated by turbulence. Compressibility (Mach number) is more important in terms of achieving exact similarity in the flow structure, e.g. shape of cooling jet and of course shocks if present. Therefore, if a detailed database of heat transfer data is to be generated for design purposes, it is advantageous to include a more global similarity to the engine situation, including compressibility.

The most important gas properties dictating similarity with film cooling in engines can be simulated by the use of foreign gas injection. It has been shown that CO_2 is suitable to simulate cold coolant injection leading to similar tendency as in gas turbine engines. The choice of CO_2 as coolant opens up the possibility to measure the adiabatic film cooling effectiveness via gas concentration measurements using PSP. This relatively new technique in the field of turbomachinery has shown promising results in cold flow test facilities such as the present. The analogy between heat and mass transfer can be employed to determine the adiabatic film cooling effectiveness as long as consistent temperature definitions are employed in the definition of this mixing parameter.

There is clearly no standard solution in this field of research and development. Acquired experience is typically built upon considering the practical complexity of such measurements.

Temperature Sensitive Paints (TSP) have potential applications in heat transfer measurements. The TSP technique is based on similar detection principles as PSP. In fact, PSP is also temperature sensitive, a feature one can benefit from.

One of the objectives is to **show that CO₂ can be used as coolant in PSP concentration measurements** despite the difference in gas properties with respect to the main air flow. Further, there is a need for a heat transfer measurement technique that allows for fast and consistent thermal measurements. **It is proposed to employ the same PSP sensor for this purpose taking advantage of the temperature sensitivity of this technology.** In this thesis, the proposed methods are explained and illustrated with example results followed by an uncertainty analysis.

Chapter 3

Experimental Methodology

This chapter lists developments of the application of PSP-sensors. First, for the measurement of adiabatic film cooling effectiveness using CO_2 as coolant. Second, it is shown that the temperature sensitivity of PSP can be utilized for heat transfer measurements. Several advantages exist and are presented.

3.1 Pressure and Temperature Sensitive Paint

The present application of PSP combines classical oxygen quenching measurement methods but is also going further since it applies multiple oxygen pressure measurement in order to:

- Derive the adiabatic film cooling effectiveness using tracer gas concentration measurements on a surface. In fact, PSP is a highly suitable technique for gas concentration measurements since, in this application, the sensitivity to calibration uncertainties, typically present in absolute pressure measurements with PSP, becomes less important. This is due to the linearity of the pressure sensitivity reducing the importance of the calibration in relative PSP-results. Each set of measurements is performed with the same coating under equal optical conditions. Therefore, deviations in one point are present in the ensemble of PSP images.
- Derive the heat transfer coefficients using the same PSP sensor. In fact, photoluminescent coatings are inherently sensitive to temperature. This effect can be exploited for heat transfer measurements. Because heat transfer coefficients depend on the driving temperature difference, several PSP readings provide the relative time evolution of the wall temperature during the transient heating experiments to derive the heat transfer coefficients.

3.1.1 Set-up for Photoluminescent Measurements

Based on existing in-house experience by Steiner (2000) and Vogel et al. (2002), the commercially available PSP-paint *Uni-FIB*¹ is employed in the present study. It consists of PtTFPP² probe-molecules and TiO₂ scatterers suspended in a polymer binder (FIB³). The paint has been applied in approximately 10 layers using a standard airbrush. A ventilated hood is employed while spraying PSP considering the health and safety recommendations for this type of paint. Figure 19 shows a schematic of the experimental set-up for in-situ measurements. Nearly the entire platform surface is covered with a single camera view allowing for an excellent overview and fast data reduction of the area of interest.

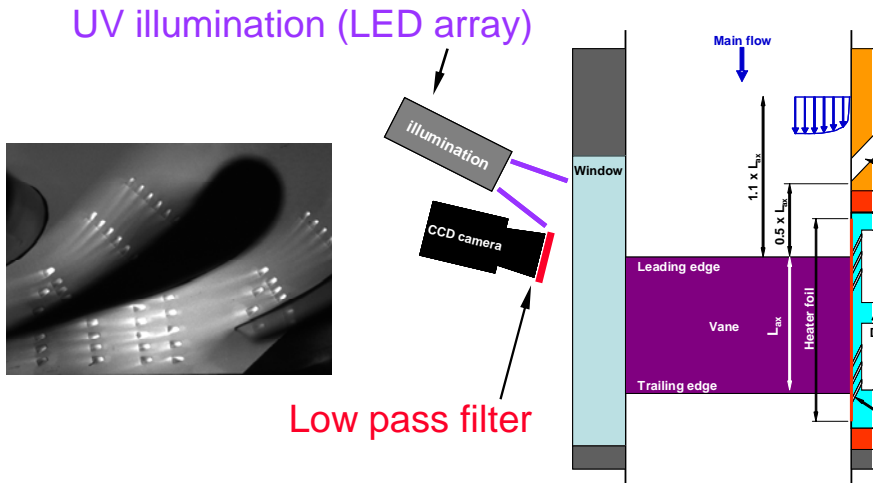


Figure 19: Camera view (left) and optical system set-up (right)

¹ Provided by ISSI, Dayton, OH, USA

² Pt(II) meso-tetra (Pentafluorophenyl) porphine

³ fluoro-isopropyl-butyl

Employing non-intensified CCD cameras ensures linear sensitivity to received light intensity. In this work, two different setups are employed for the η - and h -measurements respectively:

- For steady adiabatic film cooling effectiveness (gas concentration) measurements, the UV-illumination is provided with a Xenon flash lamp running at 20 Hz. The excitation light is distributed over the test surface with two light guides. The emitted light is recorded with a 16 bit CCD-camera from Princeton Instruments using a shutter time of 5 s. This integration of emitted light provides automatic time averaging of the measurement.
- For transient heat transfer measurements, a more powerful LED lamp from Rapp Opto-Electronic allowing for continuous illumination is employed. A more sensitive and faster CCD-camera from PCO-imaging is used to record the PSP signals. This comes at the expense of lower dynamic range (14 bit) than the original camera. The key point is that this optical combination (Figure 20) allows to resolve the wall temperature evolution by acquiring approximately 15 fps during the total transient acquisition time (12 s).

Both light sources provide cold illumination so that radiation heating of the wall can be neglected. This makes them suitable for measurements of convective heat transfer — indicated by small temperature differences in the present work.



Figure 20: LED-array lamp from Rapp Opto-Electronic (left) and CCD camera from PCO-imaging (right)

3.1.2 Calibration

Both pressure and temperature sensitivity depends on the local properties of the photoluminescent coating. Therefore, it is advantageous to perform a so-called pixel-by-pixel calibration by varying the calibration pressure in-situ.

Omitting this is typically visible as a spatial noise in *absolute* pressure measurements with PSP. However, it is often not possible to perform a pixel-by-pixel calibration due to the practical difficulty to seal a wind tunnel for pressure variations. Fortunately, this is not a major concern for concentration measurements as long as the ratio is taken between two consistent pressure measurements. Therefore, the pressure sensitivity is obtained by using a calibration chamber.

The calibration curve for oxygen quenching is given by the so-called Stern-Volmer plot in Figure 21. It shows the nearly linear sensitivity to oxygen pressure. The large range of pressure leads to a large dynamic range of the PSP sensor. This data is obtained as an average over a small region on a calibration specimen painted at the same time as the platform model. The calibration is performed in a sealed chamber with optical access. Air pressure is varied throughout the range of partial oxygen pressures present in the flow experiments. The calibration specimen is maintained at constant temperature by attaching it on top of an electronically controlled Peltier device as described by Steiner (2000).

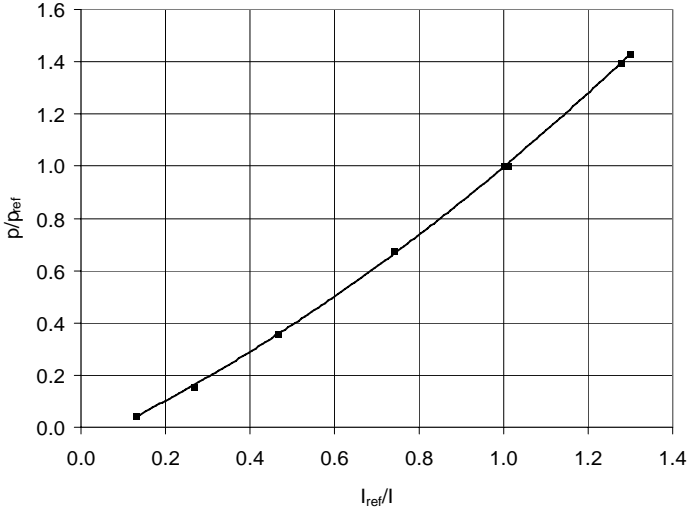


Figure 21: Oxygen pressure sensitivity of PSP at constant temperature

The net temperature sensitivity will be considered without going into details of the different mechanisms. The temperature dependency of the present PSP

can be linearized within the narrow temperature range employed in the current study ($0.9 < T/T_{ref} < 1.1$). This allows for scaling the measured intensities by a single temperature calibration-constant D . This is motivated by the fact that the PSP formulation employed in the present work has so-called ideal paint properties according to the concept introduced by Puklin et al. (2000). This means that the temperature and pressure dependencies can be considered decoupled. In other words, the temperature sensitivity is constant over a large span of pressure. Further, the calibration constants of oxygen quenching (C_0, C_1, C_2) can be considered independent of temperature.

In order to eliminate differences between the calibration chamber and the test facility in terms of illumination, reflexions, camera setup, window quality, viewing angle etc., reference measurements under known conditions are employed in order to normalize the results obtained in the two situations respectively:

$$\frac{p_{O_2}}{(p_{O_2})_{ref}} = C_0 + C_1 \frac{I_{ref}}{I} + C_2 \left(\frac{I_{ref}}{I} \right)^2 \quad (19)$$

Here I is a corrected intensity based on the difference between local recovery temperature and the reference temperature of the experiment:

$$\frac{I_{ref}}{I} = [1 - D(T_r - T_{ref})] \frac{I_{ref}}{I_{T_r}} \quad (20)$$

where I_{T_r} is the intensity measured in-situ. For the flow tests, this corresponds to the recovery temperature as described in Chapter 1. Being a light intensity method, it is advantageous to eliminate the influence of possible background illumination (stray light) and dark currents of the camera sensor. This is done by subtracting a non-excited (dark) image obtained without any UV-illumination. This linearization of each intensity measurement is referred to as flat-field correction:

$$I = I_{illuminated} - I_{dark} \quad (21)$$

Figure 22 depicts the light intensity-sensitivity to temperature of a single pixel. It shows that the sensitivity is linear within the temperature range employed in the experiments, confirming the use of a constant scaling parameter D . The temperature sensitivity calibration is done in-situ, e.g. after a test series during the slow cool-down of the test facility. In principle, this

allows for the derivation of independent calibration curves for each pixel. However, it is sufficient to conclude that the temperature sensitivity can be linearized since the measurements performed in this thesis is based on temperature differences. Due to the difficulty to include an accurate pixel-by-pixel calibration, a surface averaged value of D is derived for each test series.

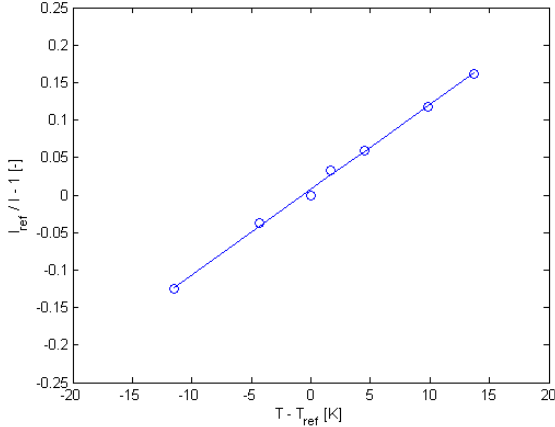


Figure 22: Temperature sensitivity of PSP at constant pressure

3.2 Measuring Adiabatic Film Cooling Effectiveness

Pressure Sensitive Paint (PSP) is employed to measure the adiabatic film cooling effectiveness. For this purpose, a tracer gas with different oxygen content compared to that of the main-flow is taken within a short time interval. Since CO_2 contains no free oxygen, this leads to low oxygen concentration where the film cooling effectiveness is high. Analogy between heat and mass transport is the basis for this indirect measurement technique. The technique allows for precise simulation of adiabatic conditions since the wall is impermeable. The technique offers high signal-to-noise ratio. In the first instance, due to the large span of oxygen concentration (injection of 100% CO_2), but also due to the fact that concentration is derived from the ratio of two consistent measurements.

3.2.1 Heat and Mass Transfer Analogy

The adiabatic film cooling effectiveness is a measure of the mixing between hot gas and cooling flows. Figure 23 illustrates that the mixing rate can be

measured with different indicators. For example enthalpy and concentration of a gas species.

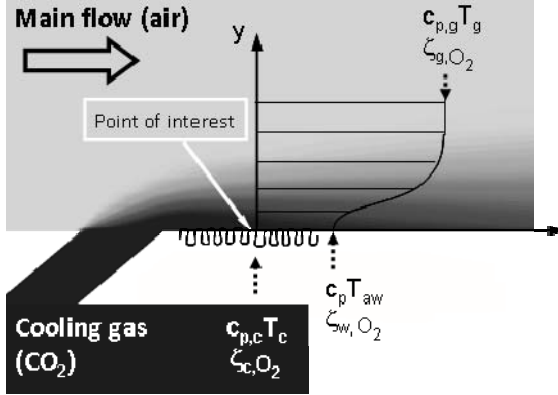


Figure 23: Analogy between energy and gas concentration boundary layers

The validity of the heat and mass transfer analogy in high velocity flows has been demonstrated in Chapter 2.1.1. Having ensured analogy between heat and mass transfer, it is straightforward to replace the energetic definition of film cooling effectiveness by mass fractions of oxygen. For the adiabatic wall, the analogy implies that the energetic film cooling effectiveness is equal to the impermeable wall effectiveness:

$$\eta_{energetic} \equiv \hat{i}_{aw} = \frac{c_p T_{aw} - c_{p,g} T_g}{c_{p,c} T_c - c_{p,g} T_g} = \frac{\zeta_{w,O_2} - \zeta_{g,O_2}}{\zeta_{c,O_2} - \zeta_{g,O_2}} \quad (22)$$

The coolant term is eliminated since CO_2 contains per definition no free oxygen:

$$\eta_{energetic} = \frac{\zeta_{w,O_2} - \zeta_{g,O_2}}{\zeta_{c,O_2} - \zeta_{g,O_2}} = \frac{\zeta_{g,O_2} - \zeta_{w,O_2}}{\zeta_{g,O_2}} \quad (23)$$

In the event CO_2 can be measured directly and for CFD models that include foreign gas injection, Equation 23 reduces to:

$$\eta_{energetic} = \zeta_{w,CO_2} \quad (24)$$

3.2.2 Gas Concentration Measurement Procedure

Analogous to the thermal problem, the adiabatic film cooling effectiveness is obtained from mass transfer by measuring the oxygen pressure on the surface. An expression that accounts for foreign gases with molecular mass different from air has been documented by Wunderlin (2006). The derivation is presented in Appendix A for completeness. Expressing Equation 23 in terms of partial pressures of oxygen, including the molecular mass of coolant and main-flow gas respectively, leads to:

$$\eta_{energetic} = 1 - \frac{1}{\left[\left(\frac{p_{O_2, Aero}}{p_{O_2, Tracer}} \right)_w - 1 \right] \frac{\mathcal{M}_c}{\mathcal{M}_g} + 1} \quad (25)$$

The mass fractions of oxygen are then determined using partial pressure measurements. More precisely, the measurement consists of two separate experiments as listed in Table 1. First, a so called *Aero* experiment where a gas with the same oxygen content as the main fluid (air) is injected. The purpose of the *Aero* test is to reproduce the same static pressure and recovery temperature on the wall as for the *Tracer* experiment. Second, the *Tracer* gas measurement allows the PSP sensor to determine the partial pressure of oxygen in order to derive the film cooling effectiveness. In fact, partial pressures of oxygen are measured in both experiments.

Experiment	Pressure	Coolant Gas Injection
Aero injection	$p_{O_2, Aero}$	equal oxygen content as main-flow (air)
Tracer injection	$p_{O_2, Tracer}$	no free oxygen (CO ₂)

Table 1: Experiments for adiabatic film cooling effectiveness with PSP

Figure 24 shows the emitted intensity as measured by the PSP camera (time averaged). Illumination effects such as shadows and reflections from surrounding surfaces are nearly identical in the above experiments and cancel out in the relative effectiveness result.

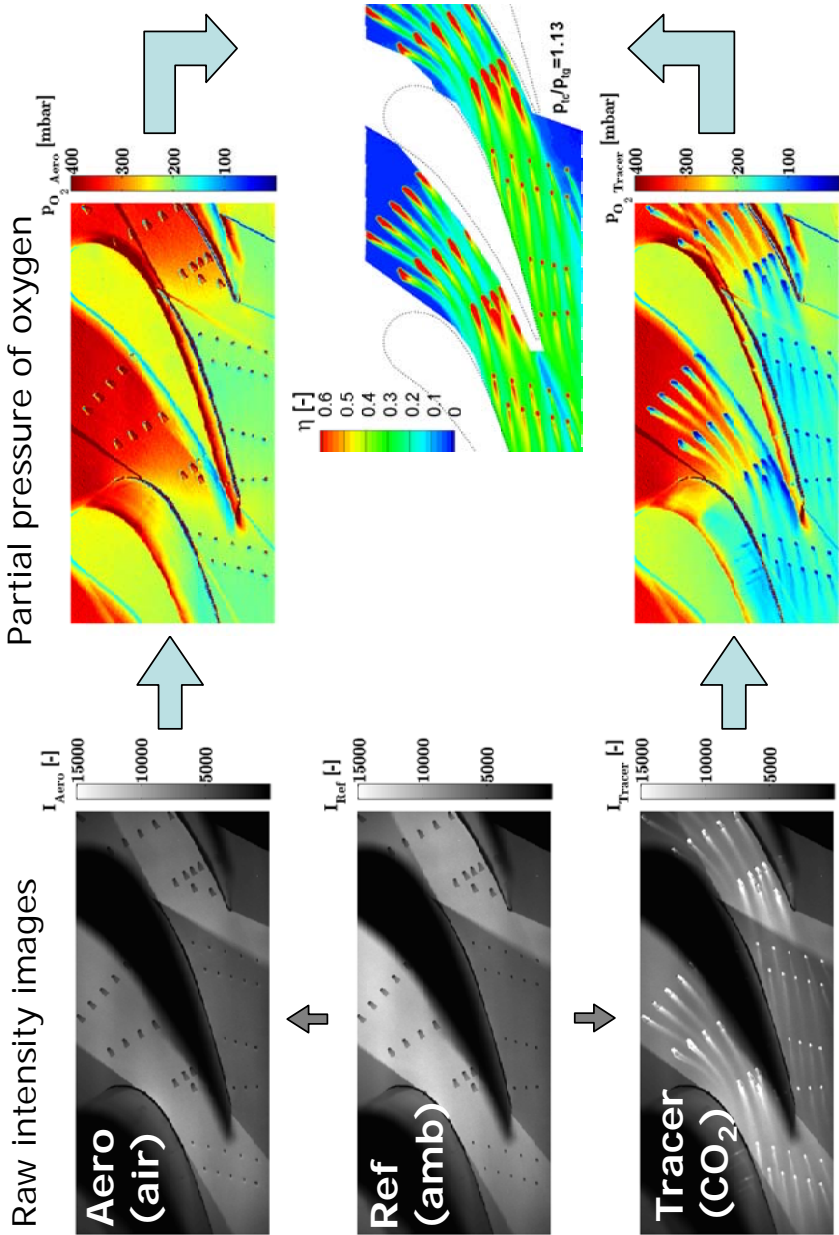


Figure 24: PSP workflow to derive the adiabatic film cooling effectiveness

Partial pressure implies that the gas components have the same temperature per definition. Therefore, the two PSP tests must be performed at the same temperature. This is achieved using iso-thermal blowing ($T_{tc} = T_{tg}$) and injecting air in the *Aero* experiment in order to produce similar recovery temperatures. As mentioned above, the locally varying recovery factor in the transonic flow regions may be significant. So as for the temperature tracing method, the mass concentration method requires consistent wall temperature distributions for the *Tracer* and *Aero* experiments. The temperature offset between the two participating experiments depends on the recovery temperatures of boundary layers with air and CO₂ injection respectively. This uncertainty is estimated to be smaller than $\Delta T < \pm 1$ K immediately downstream of the cooling holes assuming a worst case of $\eta \approx 1.0$. The uncertainty of the coolant temperature regulation (controlling for iso-thermal) is in the same range. These temperature uncertainties decay as a function of the adiabatic film cooling effectiveness further downstream of the injection. With the temperature sensitivity of the *Uni-FIB* paint employed in the present study, this leads to a negligible bias error. This is an obvious advantage to direct temperature measurement of the adiabatic film cooling effectiveness. Thus, the sensitivity to any temperature inconsistencies during such a mass concentration measurement is much smaller than for classical temperature measurement methods.

3.2.3 Adiabatic Film Effectiveness using CO₂

The applicability of CO₂ as coolant in PSP measurements has been verified by Wunderlin (2006). For this purpose, a low-speed facility and a two-dimensional slot configuration have been employed. Slots present a less complex situation compared to discrete film cooling holes. Therefore, the validation could be done by comparing the present method with film cooling correlations developed for similar slots. In particular, a correlation presented by Goldstein (1971) including the effect of injection angle with respect to the mainflow (30°) is include here for comparison.

Further, the adiabatic film cooling effectiveness due to injection of CO₂ was compared with the injection of a heavy gas-mixture of Argon and Krypton. The density of the gas mixture (90.9% Ar and 9.1% Kr) was matched to that of CO₂. Nearly identical effectiveness results can be observed in Figure 25. Thus it has been verified that CO₂ behaves like an oxygen-free gas on the

oxygen sensitive coating. By this it is proven that CO_2 can be employed as coolant for film cooling studies.

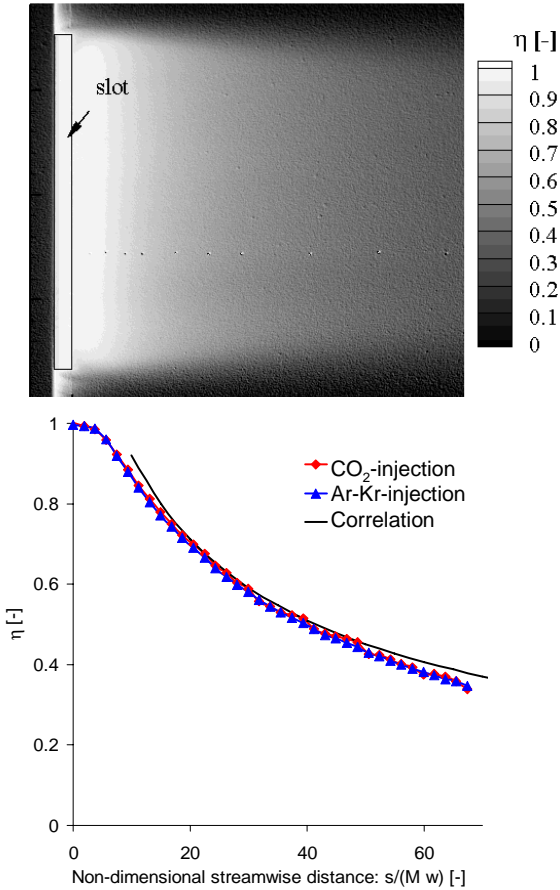


Figure 25: Flat plate measurements with different tracer gases

The energetic definition of eta is converted into the temperature-based definition of adiabatic film cooling effectiveness. Using the method documented by Jones (1999), the conversion between the two definitions can be done according to:

$$\eta = \frac{T_{aw} - T_g}{T_c - T_g} = \frac{c_{p,c}\eta_{energetic}}{c_{p,g}(1 - \eta_{energetic}) + c_{p,c}\eta_{energetic}} \quad (26)$$

The offset and conversion between the enthalpy and temperature definitions for CO₂/air leads to a moderate correction for the present gas mixture as shown in Figure 26.

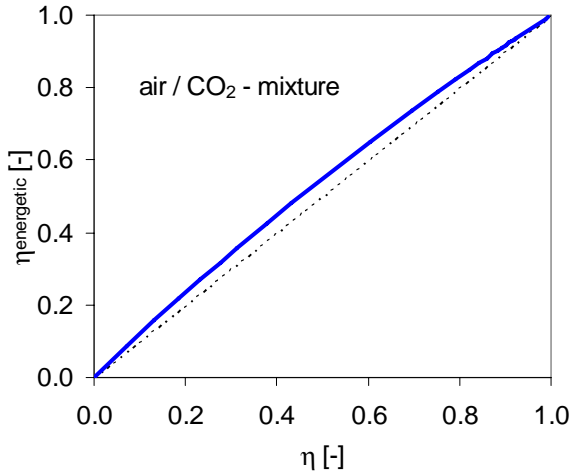


Figure 26: Relation between energetic (concentration) and temperature-based definition of the adiabatic film cooling effectiveness

3.3 Measuring Heat Transfer Coefficients

In this section, the transient heat transfer analysis for heater foil experiments is first described. This is followed by a description of the use of the temperature sensitivity of PSP for heat transfer measurements in transonic flows. Finally, a description of the particular procedure to obtain consistent temperature and heat flux measurements for the situations with and without film cooling is presented.

3.3.1 Transient Heating Experiments

The principle of the transient heater foil technique is to observe the time response of the surface temperature when a heating step is generated with an electrically heated foil. The foil, made of stainless steel is glued onto the wall surface using a thin double sided scotch tape with high bonding properties (3M VHB®).

Before performing a transient test, the cascade is exposed to airflow until thermal equilibrium is reached. It is then assumed that each position of the wall takes the local recovery temperature neglecting any lateral conduction effects in the Perspex wall. This pre-conditioning sets the local initial temperature according to the recovery temperature as sketched in Figure 27.

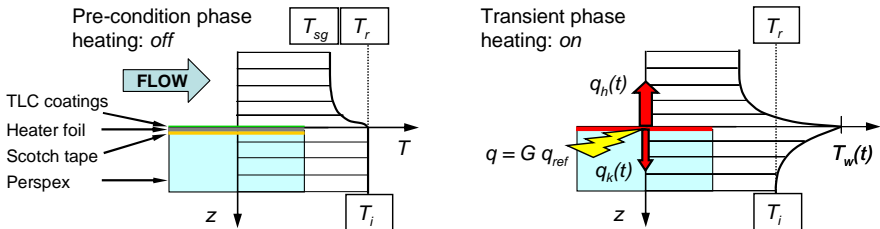


Figure 27: Adiabatic wall (left) and transient heating situation (right)

When coolant is injected, the mixture of a steady main-flow temperature and quasi-steady cooling flow temperature dictates the initial temperature of the wall, now according to the local recovery temperature of the mixture of coolant and main-flow in the film ($T_i = T_{aw} = T_r$) for each test case. Heating the wall surface allows for the determination of a convective heat transfer coefficient. Again, the convective heat flux at the wall is normalized by the driving temperature difference defined as the difference between wall surface temperature at heated and adiabatic states. In contrast to the heat transfer

situation in steady-state, heat flux and wall temperature are now time dependent:

$$h = \frac{q_h(t)}{T_w(t) - T_{aw}} \quad (27)$$

Thus, h is assumed to remain constant in time during the transient experiment. This is a good approximation for this class of convection problems as shown in Section 2.1.2. In order to determine the heat transfer coefficients from the measured time-temperature pairs, a one-dimensional analytical conduction model for the semi-infinite wall is applied. The governing equation is:

$$\frac{\partial T}{\partial t} = \left(\frac{k}{\rho c} \right)_{Perspex} \frac{\partial^2 T}{\partial z^2} \quad \text{for } 0 \leq z < \infty \quad (28)$$

With the initial condition:

$$T(z, t = 0) = T_i, \quad (29)$$

the semi-infinite boundary condition

$$T(z \rightarrow \infty, t) = T_i \quad (30)$$

and the boundary condition for the heat flux at $z = 0$ as determined from an energy balance including the thermal inertia of the heater foil

$$q = -k \frac{\partial T}{\partial z} \Big|_{z=0} + h(T_w(t) - T_{aw}) + \beta \frac{dT_w}{dt}, \quad (31)$$

gives the following solution for the non-dimensional wall temperature according to von Wolfersdorf et al. (1993)

$$\begin{aligned} \theta(t) &= h \frac{T_w(t) - T_{aw}}{G(t)q_{ref}} \\ &= 1 + h \left(\frac{e^{A^2 t} \operatorname{erfc}(A\sqrt{t})}{\beta A(A-B)} - \frac{e^{B^2 t} \operatorname{erfc}(B\sqrt{t})}{\beta B(A-B)} \right) \end{aligned} \quad (32)$$

where

$$A = \frac{\sqrt{(\rho ck)_{Perspex}}}{2\beta} \left(1 + \sqrt{1 - \frac{4h\beta}{(\rho ck)_{Perspex}}} \right) \quad (33)$$

$$B = \frac{\sqrt{(\rho ck)_{Perspex}}}{2\beta} \left(1 - \sqrt{1 - \frac{4h\beta}{(\rho ck)_{Perspex}}} \right)$$

and the heat storage capacity of the heater foil is taken into account in the boundary condition. It is treated as a scalar constant (lumped model) as follows:

$$\beta = (\rho c)_{steel} \delta_{foil} \quad (34)$$

Thus, the time response of the wall temperature is to the first instance dependent on the product of the heat storage capacity and the thermal conductivity of Perspex wall (ρck) , with respect to the square of the convective heat transfer coefficient. The material properties of the wall employed in the heat transfer analysis are listed in Table 2. When it comes to material properties of the glue, measurements revealed that the thermal conductivity is very close to that of Perspex. The heat storage capacity, an important parameter for transient experiments, is assumed to be the same as for Perspex considering the small thickness of the glue. Therefore, the glue is treated as an integral part of the wall. With the given thermal properties of the wall, the root terms in Equation (33) become negative as soon as $h > 958 \text{ W/m}^2\text{K}$. Therefore, Equation (32) is computed with the complex error function as implemented in Matlab® by Weideman (1994). This enables measuring higher heat transfer coefficients.

Material	k [W/(mK)]	ρ [kg/m ³]	c [J/(kgK)]
Perspex (acrylic wall)	0.19	1180	1450
Stainless steel (foil)	(not used)	7800	435

Table 2: Wall material properties

Time evolutions of the heat flux components of Equation 33 are depicted in Figure 28. The convective heat flux starts from zero due to the initial absence of driving temperature difference. A gradual increase of the convective heat flux approaching the steady state solution takes place. The heat absorbed by the Perspex wall through conduction is dominating in the beginning of a

transient test. The importance of the heat storage of the foil can be appreciated during approximately one second after switching to power. This is due to the large time derivative of the wall temperature in the very beginning of the heating step.

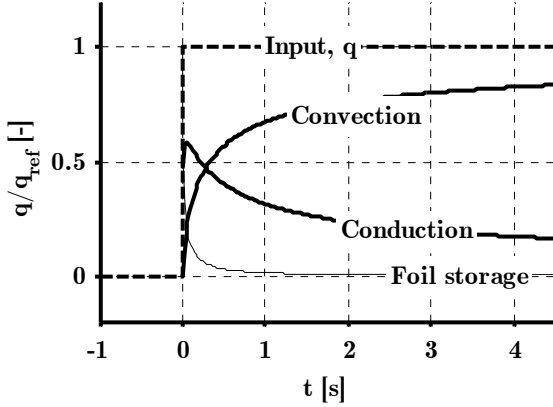


Figure 28: Transient evolution of heat flux terms ($h = 500 \text{ W/m}^2\text{K}$)

The local area-specific heat release $q(x,y)$ depends only on the heater foil and produces the same distribution in each experiment with a given foil set-up. Thus the distribution of heating is independent of the global power setting. In case of multiple experiments with different power settings, q is scaled with a global gain factor G with respect to a reference case (experiment with the lowest power setting). In fact, a single maximum power setting ($G = 1.0$) is used in the present version of the measurement procedure:

$$G(t) = \frac{q(x,y,t)}{q_{ref}(x,y)} \quad (35)$$

By adding a second heating phase over which the power is reduced to a fraction of the initial input ($\varepsilon = q_2/q_1$), the effect of the heat transfer coefficient emerges even more clearly. This effect can be seen in the relative temperature change during the 2nd phase (Figure 29). The solution for the non-dimensional wall temperature evolution for the 2nd heating phase is:

$$\begin{aligned}
 \theta(t) &= h \frac{T_w(t) - T_{aw}}{G(t)q_{ref}} \\
 &= \varepsilon + h \left(\frac{e^{A^2 t} \operatorname{erfc}(A\sqrt{t})}{\beta A(A-B)} - \frac{e^{B^2 t} \operatorname{erfc}(B\sqrt{t})}{\beta B(A-B)} \right) \\
 &\quad + (\varepsilon - 1) h \left(\frac{e^{A^2(t-t_s)} \operatorname{erfc}(A\sqrt{(t-t_s)})}{\beta A(A-B)} \right. \\
 &\quad \left. - \frac{e^{B^2(t-t_s)} \operatorname{erfc}(B\sqrt{(t-t_s)})}{\beta B(A-B)} \right) \quad t > t_s
 \end{aligned} \tag{36}$$

In fact, such a sequential procedure allows for the determination of the non-dimensional temperature rise (θ), which is the ratio of the a-priori unknown heat release (q) and heat transfer coefficient (h). The history of the time derivative (shape of the curve) allows to identify h which in turn quantifies the heat release. However, the latter requires low noise levels and well calibrated sensors which are not always achievable. Moreover, it is not necessary to solve the initial temperature T_{aw} since relative temperature changes caused by heat transfer are measured directly in order to determine the searched heat transfer coefficient (h).

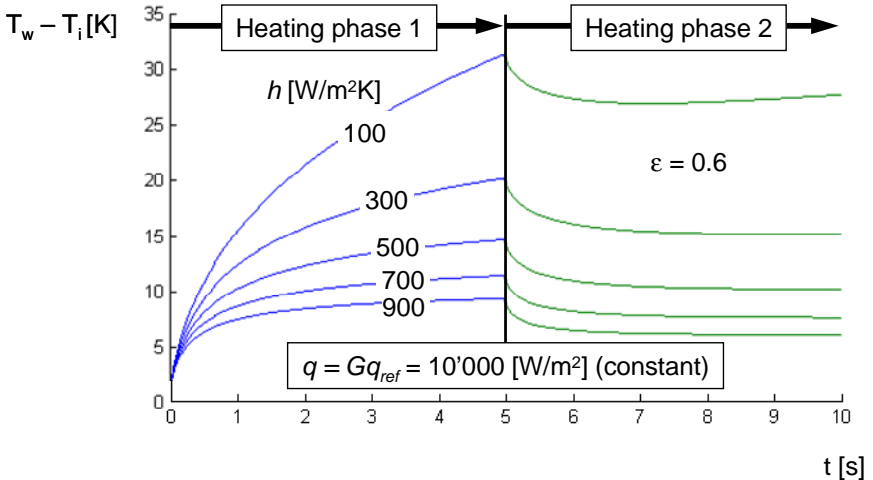


Figure 29: Transient wall temperature response of the analytical model

A novel thermography technique is introduced in the following. Related measurements have previously been carried out by Kingsley-Rowe et al.

(2003). Employing the linearized, first-order temperature sensitivity (D) of the PSP sensor (see Section 3.1.2) gives a measure of the temperature difference between the initial (adiabatic) and a time instance during the heating phase:

$$(T_w(t) - T_i)_{PSP} = \frac{I_i/I(t) - 1}{D} \quad (37)$$

The corresponding temperature change of the analytical model is given by Equations (32) and (36) for the first and second heating phases respectively. The following expression is valid for any of the heating phases:

$$(T_w(t) - T_i)_{1D\text{-model}} = \frac{q}{h} \theta(h, t) \quad (38)$$

3.3.2 Baseline Heat Transfer Coefficients

With the two unknowns h and q , and a large number of data points N from the transient experiment, the problem is over-defined and a solution that satisfies Equation (37) and Equation (38) in an optimum way is sought. For this purpose, a regression analysis similar to that of Vogel et al. (2003) is employed. Because the original method also solved for the adiabatic film cooling effectiveness as a 3rd parameter, a simplified version is used for the present situation. Thus the decoupling of the adiabatic film cooling effectiveness (concentration measurements) from the heat transfer measurements is one of the advantages of PSP.

The two unknowns can be combined by expressing the heat release as a function of the heat transfer coefficient $q(h)$. Thus, the difference between measured and theoretical temperature changes is minimized in each pixel by solving for the heat transfer coefficient that produces the optimal match to all data of the transient experiment. Practically this is done by performing a least square fit of the analytical 1D model to the measured temperature history (200 points) using vector notation. The remaining error is stated as the standard deviation calculated with vector notation according to:

$$\sigma_{T_w} = \sqrt{\frac{\left\| \left(\frac{I_i/\vec{I}(t) - 1}{D} - \frac{q(h)}{h} \vec{\theta}(h, t) \right) \right\|^2}{N}} \quad (39)$$

In order to derive the absolute heating input (q) from the PSP thermography experiments, an accurate pixel-by-pixel calibration of the temperature

sensitivity D is required. This should be done regularly since it is known that the PSP molecules undergo some curing and ageing depending on the temperature history. Due to the difficulty to obtain accurate pixel-by-pixel calibrations of the temperature sensitivity, a globally averaged value of the temperature sensitivity D of the PSP is employed (cf. Section 3.1.2). As a consequence, the resulting heat release distribution is based on the averaged constant temperature sensitivity. Thus with the heat release,

$$q(h) = \frac{(T_w(t) - T_i)_{PSP} \cdot \left(\frac{\theta(h, t)}{h} \right)}{\left\| \frac{\theta(h, t)}{h} \right\|^2}, \quad (40)$$

the agreement in terms of the absolute evolution of the wall temperature can be verified by observing single pixels as shown Figure 30.

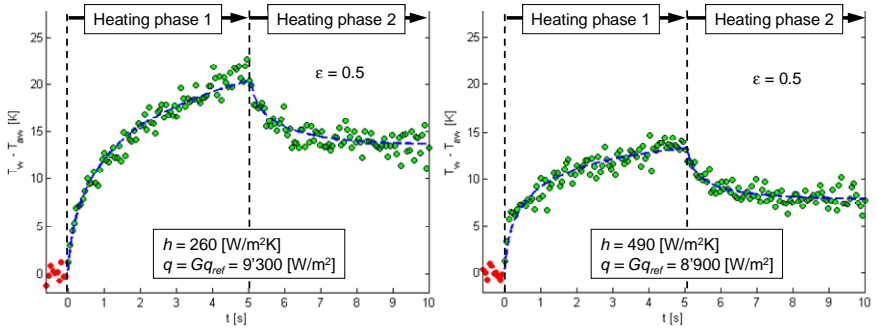


Figure 30: Measured wall temperature response using PSP

Because the convection measurements are based on relative temperature changes (evolution of the time derivative of the wall temperature), the temperature sensitivity D determines q . Hence, only the time information must be dimensional whereas the temperature readings can be non-dimensional to determine the heat transfer coefficient h . It should be stated that with the present wall material properties, values of $h > 1000 \text{ W/m}^2\text{K}$ are outside of the optimum range leading to relatively low transient sensitivity.

3.3.3 Film Cooled Heat Transfer Coefficients

The novel use of PSP techniques for fast and consistent measurement of h and q as outlined in Section 3.3.2 works in principle also for the case with film cooling injection. The heat transfer coefficient as defined in this work is

independent of the adiabatic wall temperature. However, because of the nature of a PSP-sensor, it is necessary to consider the additional variable η during the heat transfer measurement. For example when a CO₂-rich coolant is injected or if there is a significant temperature difference between coolant and mainflow. In these three-temperature situations, the method works if the films are perfectly steady. Consider for a while the relatively weak sensitivity to temperature compared to oxygen pressure of PSP. Thus if the CO₂-rich films oscillate slightly, this will result in locally fluctuating oxygen pressure, potentially leading to a stochastic noise of high intensity making it difficult to identify the temperature signals. Obviously there exist time-varying signals locally on the film cooled platforms due to unsteady flow features of sufficiently low frequency to be detected by the PSP sensor. This over-laid noise level is locally high, making it difficult to apply the method. It has been confirmed in preliminary data reduction efforts that the minimization of Equation (39) does not work for this situation. However, an important feature of the present heat transfer procedure is that the heat release distribution inside the foil remains the same in all experiments of the same test campaign. In order to apply the method on film cooled cases, the following solution has been successfully implemented.

An un-cooled test case is always performed in the present film cooling campaigns. Moreover, it is fair to state that the actual heating distribution q is identical between the experiment of each test campaign, provided that all experiments are performed within a limited time interval. Thus a heating distribution q is already available from the un-disturbed baseline case (without oxygen pressure variation). Therefore, this solution to the distribution of q can be applied as a-priori known boundary condition for the film cooled cases. Further, this leads to consistency in q and ultimately h between the baseline and film cooled results. This consistency is independent of the calibration accuracy of D — an important for absolute q -measurements

3.4 Conclusions of Chapter 3

Methods to handle the intensity based measurements are given. In general, normalization of the intensity measurements using known reference conditions allows for the use of calibrated sensitivities obtained in a calibration chamber as well as inside the test facility. Therefore, parameters related to the optical

set-up can differ between the calibration and flow measurements without influencing the trends.

The distinction between the driving temperature T_{aw} or adiabatic film cooling effectiveness (η) and the heat transfer coefficient (h) of the boundary layer allows for separate measurements of those two quantities.

At the same time, the presented methods combine the same sensor for measuring both quantities with a maximum of consistency between the experiments. Although not tested here, it is in principle possible to perform the adiabatic film cooling effectiveness and heat transfer coefficient measurements simultaneously leading to faster measurements. Two applications of the same PSP-sensor have been described — both of which contain new developments.

Limitations of the PSP sensor consist in an upper temperature limit in the order of 100 °C. Therefore, the sensitivity to temperature of PSP can be utilized as long as the heat flux levels remain relatively low. Moreover, experiments must be performed within a controlled time-interval in order to minimize degradation of the paints. A proposed test procedure is given in Appendix C.

Adiabatic Film Cooling Effectiveness

The use of heat and mass transfer analogy to derive the adiabatic wall temperature eliminates the need to determine the heat transfer inside the wall as might be necessary in thermal experiments. Therefore, metallic wall materials can be employed. Consequently, the PSP technique has potential as an industrial certification technique applied on actual engine turbine parts (in cold flow experiments). This applies to η -measurements.

The molecular mass correction is normally left out in the derivation of the adiabatic film cooling effectiveness in studies that uses N₂-injection. Here it is shown that CO₂ can also be employed as tracer gas as long as the appropriate definition (Section 3.2.2) of the partial pressure including the molecular mass correction is included. The relative nature of a gas concentration measurement makes PSP highly suitable for film cooling studies.

Heat Transfer Coefficients

As shown in Section 3.3, convective heat transfer coefficients can be measured with the same PSP-sensor employed for gas concentration measurements. Thermography measurements are possible by taking advantage of the inherent temperature sensitivity of the PSP technology as well as recent developments in illumination and camera performance. This novel temperature sensing technique is herein denoted “PSP” despite the original meaning of this abbreviation.

One of the main advantages of this approach is that it identifies the temperature rise relative to the initial (adiabatic) temperature due to wall heat transfer. Thus it is not necessary to accurately determine the absolute thermal wall boundary conditions beforehand. As a consequence, the heat transfer coefficients can be obtained with relatively small temperature differences, even in the presence of significant recovery temperature variations. Further, iso-thermal cooling gas temperature ($T_{tc} = T_{tg}$) is not an absolute requirement as long as the temperature remains within the calibrated range.

The method to derive heat transfer coefficients is based on measurements of relative temperature evolutions in time. This can be applied for baseline cases without film cooling and the heat release distribution is determined from the absolute temperature differences. Assuming that q will not change due to the injection of film cooling and the solution can be carried over to the heat transfer analysis of the film cooled cases.

Chapter 4

Test Case: Platform Film Cooling

An engine realistic platform application is investigated in order to demonstrate the applicability of the proposed measurement techniques for film cooling assessment.

4.1 Test Facility

The linear cascade used for the present tests consists of 5 airfoils (4 passages) as shown in Figure 31. The prismatic airfoil geometry has previously been manufactured and tested by Reiss (2000). The profile is a representative mid-span section of the vane of a high pressure turbine. The dimensions of the inlet flow section are $340 \times 99 \text{ mm}^2$ with flat end-walls. There is a retractable total pressure probe 153 mm upstream and static pressure taps drilled in the end-wall 70 mm downstream of the leading edge plane. These measurements are used to determine the isentropic outlet Mach number. A continuously running compressor supplies main-flow air with the possibility to vary the inlet temperature between 25°C and 60°C . This temperature is monitored inside the settling chamber upstream of the linear cascade. It is ensured that the main-flow and wall temperatures reach steady-state prior to the transient experiments.

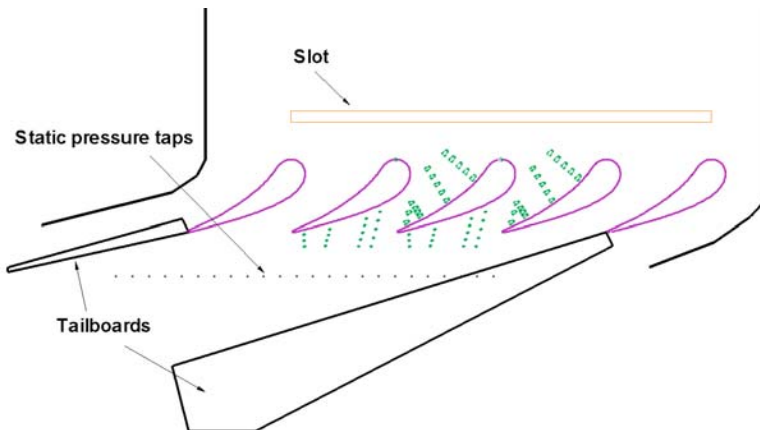


Figure 31: Linear cascade

Figure 32 shows a cross section of the test facility. One of the sidewalls is equipped with a large window for optical access to the platform. CO₂ is supplied from two gas bottles via a pressure regulator to a large intermediate tank. The tank pressure is held constant in order to achieve the desired flow rate that is determined by laminar flow elements. An electric tube heater is employed in order to obtain the temperature as measured inside the different plenum chambers using miniature ‘K-type’ thermocouples. The cooling gas is fed through separate cavities inside the platform module. Flow diffusers are employed in order to damp out any effects of high momentum jets inside the plenum chambers. There is a slot present upstream of the cascade with the possibility to inject cooling gas. This feature is not employed in the present study but the slot serves as an engine realistic reset of the incoming boundary layer on the endwall.

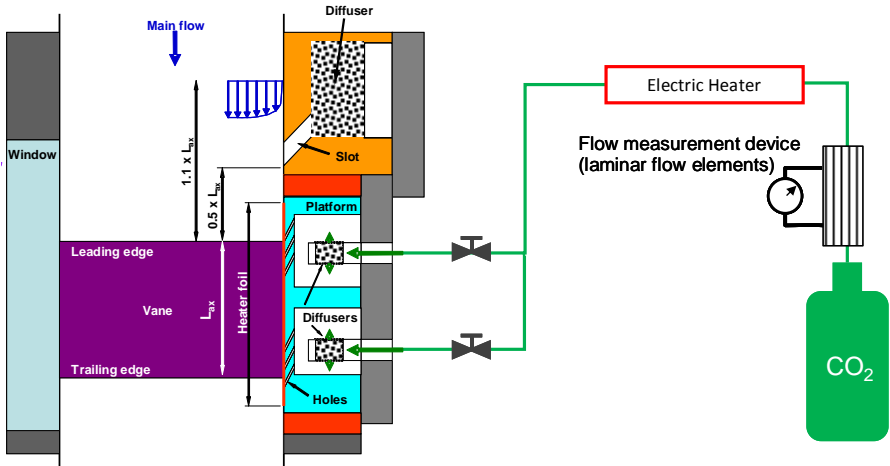


Figure 32: Cross-section of test set-up with slot and platform modules

The platform test model made of Perspex has a total thickness of 30 mm and minimum wall thickness is 3 mm at the locations of the plenum chambers. Figure 33 depicts the model covered with a stainless steel foil that is electrically heated for thermal measurements. Joule heating is induced by passing direct current between the upstream and downstream edges of the foil. The thickness of the foil is 25 μm . A thin double sided scotch tape with high bonding properties is used to attach the foil to the Perspex part. Several rows

of cooling holes and vane attachment holes have been drilled through the foil and the wall once the foil was glued to the wall.

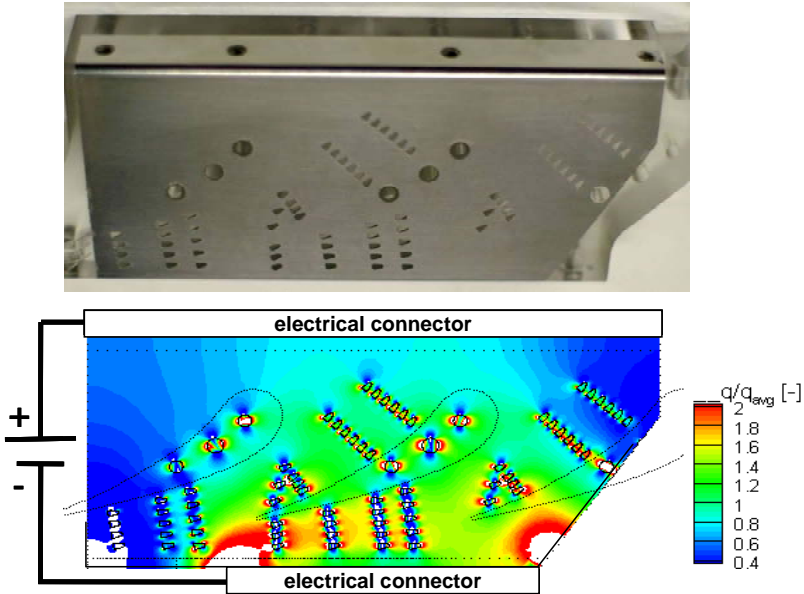


Figure 33: Heat release distribution

The finite element results in Figure 33 show that the heating is focused towards the downstream region by adjusting the width of the electrical connector downstream of the platform according to Jonsson et al. (2008). This is done since the highest heat transfer coefficients are expected in this region. Consequently higher heating levels are required in order to obtain sufficiently large temperature rise for the heat transfer measurements:

$$T_{w,t \rightarrow \infty} - T_{aw} = q/h \quad (41)$$

The thermal boundary conditions (q_{ref} and T_{aw}) are determined by the experimental method. A comparison of the FEM results versus experimental data is provided in Appendix B. In addition, the heat release from the foil has been determined using numerical modelling for design of the layout. The FEM result is also used as input for parameter studies (Appendix F) in order to verify the importance of the complex heating distribution according to the theory of Chapter 1.

4.2 Aerodynamics

The main-flow is held constant during the film cooling studies. The inlet flow is axial with a total pressure in the order of 150 kPa and total temperature of 312 K (39 °C). The static pressure measurements are done with pressure taps drilled in the wall as depicted in Figure 34. Since a static pressure measured at the wall can be considered constant through the boundary layer (due to the absence of flow curvature in the wall normal direction) the isentropic free-stream value is readily available. The ratio of the static pressures vs. the inlet total-pressure (span-wise averaged measurement) is used to calculate the local isentropic Mach number (Appendix G). Further in Figure 34, CFD results (without any cooling holes) are shown at the top and the results agree very well along the instrumented lines downstream (row I), inside the passage (row E) and upstream of the cascade (row A).

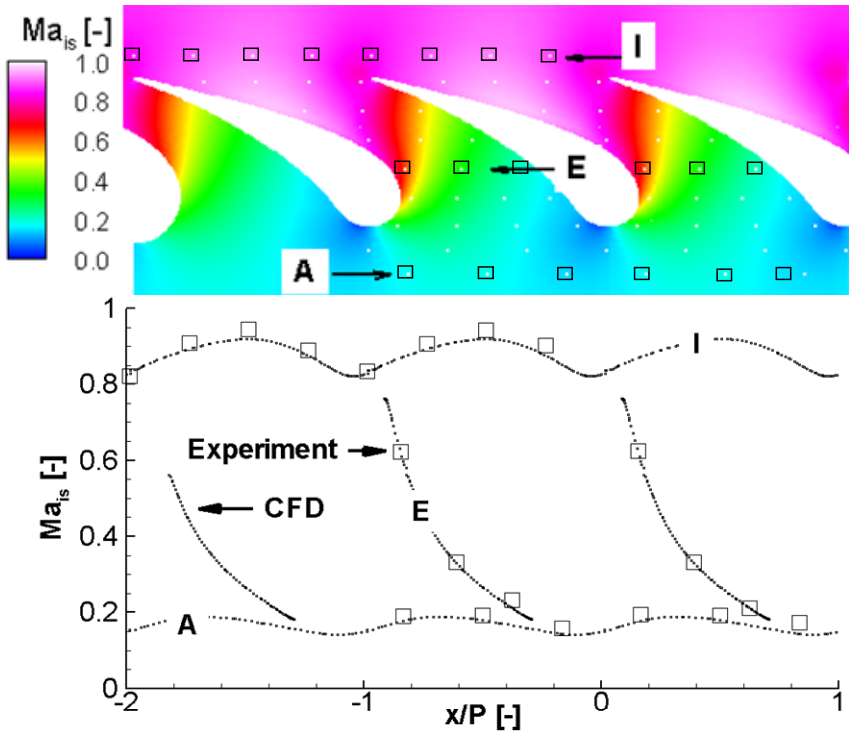


Figure 34: Isentropic Mach number on the platform surface

Tailboards are employed to regulate the vane-to-vane periodicity of the linear-cascade according to Ott et al. (1998). For the purpose of film cooling investigations around the centre vane, it can be seen that the aerodynamic flow conditions are periodic for the two central vane passages of interest. As listed in Table 3, Reynolds numbers are derived from the inlet and exit flow conditions with the chord length of the vane airfoil ($L = 80.43$ mm).

Quantity	Inlet	Exit
Mach number, Ma_{is} [-]	0.165	0.88
Reynolds number, Re_L [-]	$0.4 \cdot 10^6$	$1.7 \cdot 10^6$

Table 3: Mean isentropic flow conditions of the cascade

For endwall studies, it is important to quantify the incoming boundary layer quality. This is different from airfoil studies where the stagnation point ensures a well defined incoming flow. Contrary to engines, the thermal boundary layer at the inlet of the cascade is negligible due to the fact that the upstream walls of the test facility approach adiabatic conditions. This is ensured by running the main-flow for a sufficiently long time prior to the measurements in order to reach time-constant temperature and pressure fields. A single traverse with a hot-wire probe is done 70 mm upstream of the leading edge plane according to Figure 35. The measurements reveal a turbulent boundary layer with a displacement thickness of about 0.37 mm and a momentum loss thickness of 0.28 mm. The derivation of these parameters are provided in Appendix E.

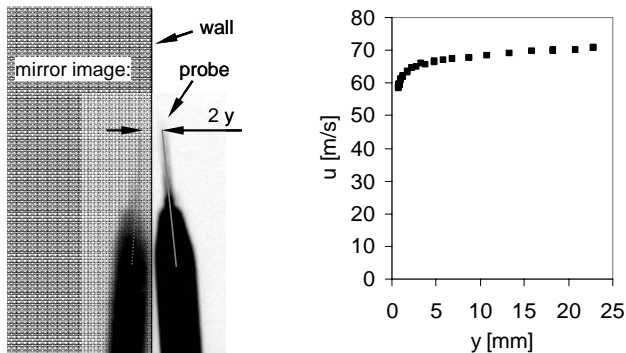


Figure 35: Hot-wire measurement of the inlet velocity profile

Further to the inlet velocity profile, turbulence intensity and integral length scale have been derived from the hot-wire data at mid span. The mean turbulence intensity measured in the free-stream is determined to $Tu = 10\%$ with an uncertainty of $\pm 3\%$. The corresponding mean length scale is in the order of 0.01 m.

A CFD-study revealed that the influence of the incoming velocity profile on the heat transfer is significant in the inlet region of the cascade. However, the development of new boundary layers downstream of the slot and cooling holes are dominating the near-wall flow behaviour in these regions. Therefore, the impact of the inlet velocity profile is small further downstream in the cascade. A conclusion of this study is the advantage to include a slot-geometry in experimental and numerical platform experiments in order to ensure a well-defined incoming flow field (even if no coolant is injected).

The flow direction at the wall is visualized in Figure 36. On the left, CFD results by Charbonnier et al. (2009) in terms of isentropic Mach number contours as well as particle traces integrated from the wall shear stress distribution are shown. The image on the right shows the result of a shear stress sensitive liquid crystal experiment. Both of these flow visualizations reveal an over-turning of the low-momentum boundary layer towards the suction side of the airfoil. In general, here is a relatively small amount of over-turning through the passage compared to small-scale rotor blades. The over-turning depends on the strength of pressure gradients with respect to the momentum deficit in the endwall boundary layer. The moderate secondary flow through such an NGV geometry is due to high Reynolds numbers,

relatively strongly accelerated flow in relation to the low amount of turning. Moreover, the slot (although un-blown) tends to diminish the momentum deficit which reduces the over-turning. It appears that the separation line emanating in the saddle point reaches the suction side close to the trailing edge. Also the saddle point, caused by the so-called horseshoe vortex system near the leading edge is clearly visible. The smeared appearance of the shear point visualization close to the saddle point confirms the unsteady nature of this separation phenomenon as visualized by Praisner and Smith (2006). The CFD calculation is performed with the assumption of steady flow.

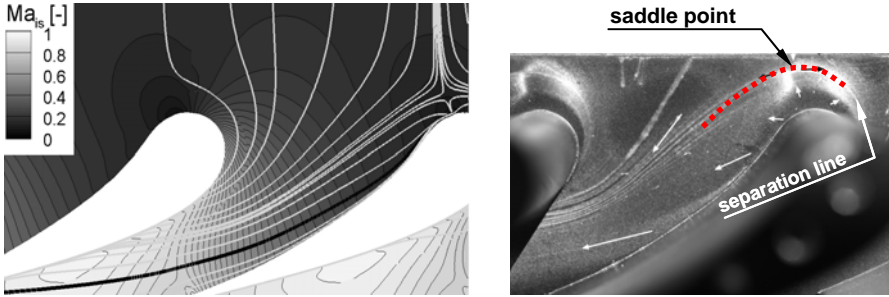


Figure 36: Calculated isentropic Ma and flow paths on the wall (left), Experimental flow visualization on the wall (right)

4.3 Film Cooling Configuration

The tested cooling hole configuration is shown in Figure 37. The holes are organized in multiple rows, each of which is roughly aligned with isobars in order to consider a common back-pressure for each row. Two mainflow channels are equipped with film cooling holes in order to achieve periodic cooling around the centre vane. All holes are equipped with shaped hole exits corresponding to advanced film cooling technology. Holes situated up- and downstream of the aerodynamic throat are fed separately through two different plenum chambers. This allows to regulate the upstream and downstream group of holes independently if desired. However in the present study, the feed pressure is set identical for all plenum chambers. This arrangement is repeated for both mainflow channels.

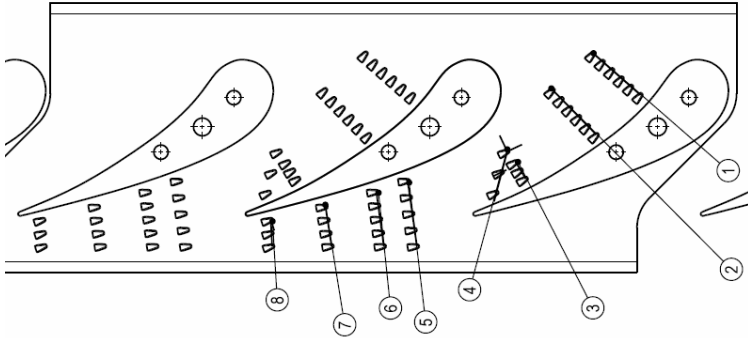


Figure 37: Cooling hole footprints on the platform

The cooling holes were drilled once the heater foil was already attached in order to ensure high-quality surface finish at the outlet of each hole. The Perspex platform model is covered with a thin stainless steel-foil having a thickness of $25\ \mu\text{m}$. It can be electrically heated for heat transfer measurements. A thin glue (3M VHB®) is employed to attach the heater foil to the Perspex wall. Figure 38 depicts the PSP-instrumented platform.

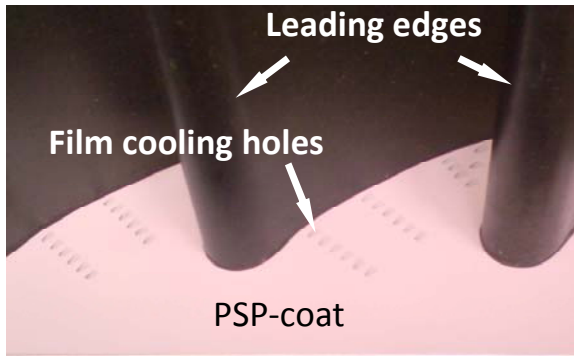


Figure 38: PSP coated platform model

The film cooling parameters are derived from flow conditions according to Appendix G. Figure 39 depicts the discharge coefficients as given by a measured flow characteristic. The corresponding blowing and momentum ratios vary mainly for the upstream rows due to the large variation in coolant Mach numbers as shown in Figure 40 and Figure 41. On the contrary, the density ratios vary mostly for the downstream holes since they are choked at

the highest blowing cases as shown in Figure 42. Table 4 summarizes the film cooling settings and the total flow rate (all holes in one vane passage).

p_{tc}/p_{tg} [-]	\dot{m}_c/\dot{m}_g [%]	\dot{m}_c [g/s]
1.410	0.68	4.2
1.156	0.52	3.2
1.030	0.42	2.5

Table 4: Global blowing conditions for one vane passage

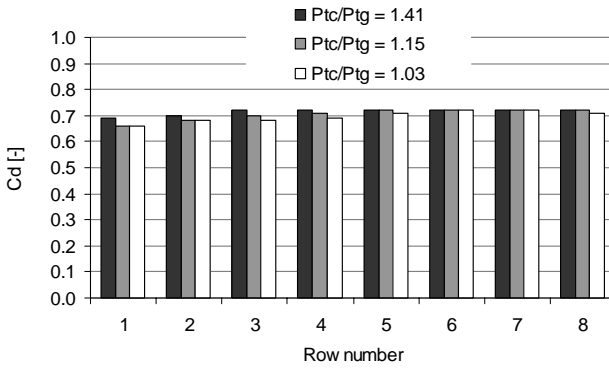


Figure 39: Hole discharge coefficients

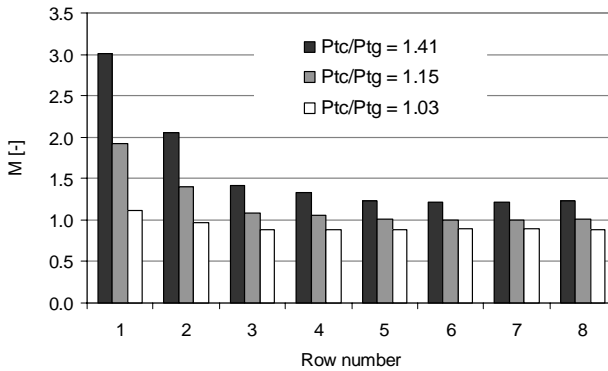


Figure 40: Blowing ratio

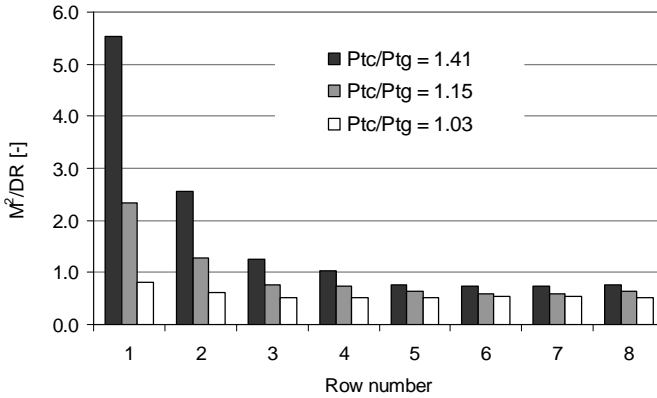


Figure 41: Momentum ratio

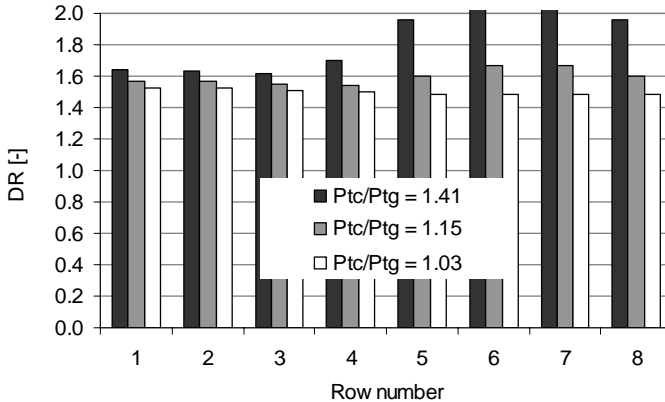


Figure 42: Density ratio

4.4 Conclusions of Chapter 4

The hardware and flow conditions of the test-case used to demonstrate and validate the method has been described. The main-flow aerodynamics simulate Mach and Reynolds numbers of real engines and the film cooling parameters are realistic due to the injection of a heavy foreign gas (CO_2) into air.

An analysis of the thermal boundary conditions important for heat transfer measurements has been provided. This leads to the recommendation to consider heat transfer results relative to a baseline case in order to transfer results to engine correlation databases.

CFD predictions indicate that the inlet velocity profile (measured) has an impact on the heat transfer coefficient results only in the upstream area of the platform. This leads to the conclusion that for this case, the upstream slot and the subsequent acceleration of the flow through the NGV passage have a dominating influence on heat transfer compared to the upstream velocity profile. Therefore, it is recommended to include engine-representative slot geometries for endwall experiments.

Chapter 5

Results

Example results obtained on the complex test case are presented and discussed. This is followed by an uncertainty analysis and comments on future possibilities related to the measurements technique.

5.1 Platform Film Cooling

Detailed result of adiabatic film cooling effectiveness, heat transfer coefficients and the corresponding heat release are presented and commented upon. This is followed by a brief analysis of the averaged film cooling performance on the platform.

5.1.1 Adiabatic Film Cooling Effectiveness

Figure 43 shows adiabatic film cooling effectiveness for varying feed pressure. Generally, there is a very good film cooling coverage over the areas that the scheme is intended to protect. The hole diffusers appear to perform well producing increasing effectiveness levels up to at least $P_{tc} / P_{tg} = 1.41$. A relatively weak secondary motion of the main-flow washes cooling gas towards the suction side. Notice the low effectiveness level below the wake of the trailing edge due to the presence of intense turbulent mixing.

The measurement technique is able to resolve the film cooling footprints very neatly due to the absence of lateral heat conduction in the measured data. Furthermore, the signal strength leads to low noise levels.

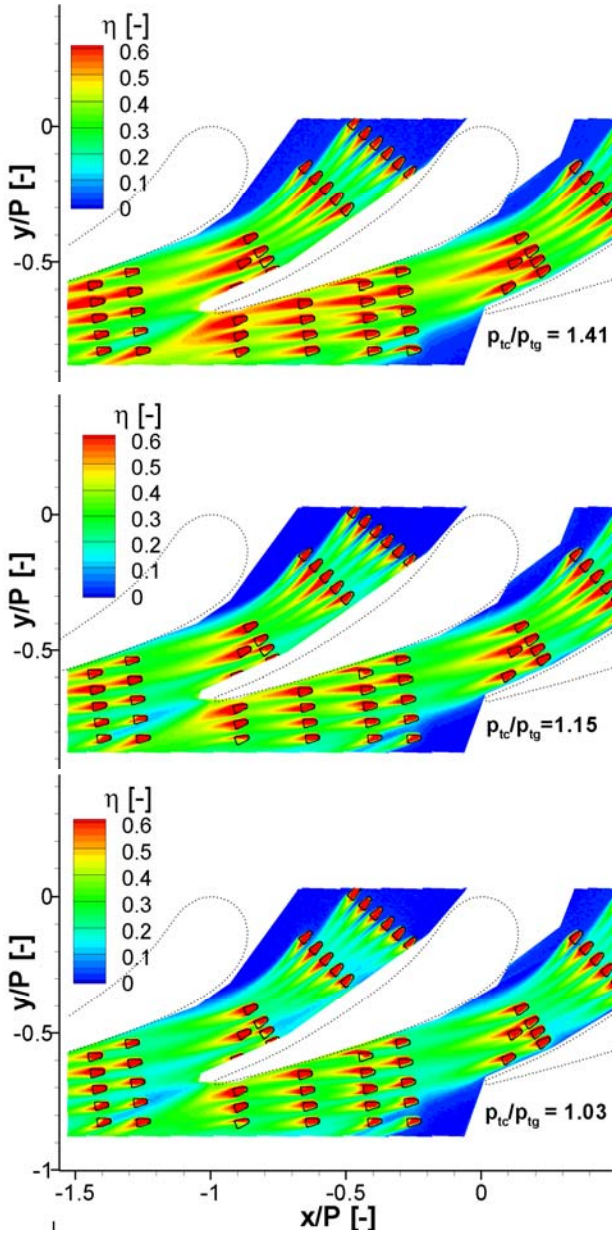


Figure 43: Adiabatic film cooling effectiveness on the platform

Figure 44 shows the averaged effectiveness results. The slot-like geometry of the shaped cooling holes produces local effectiveness levels of unity just downstream of the holes due to the attached cooling jet. Therefore, the effectiveness at the hole position is independent of the blowing ratio but merely a function of the hole geometry.

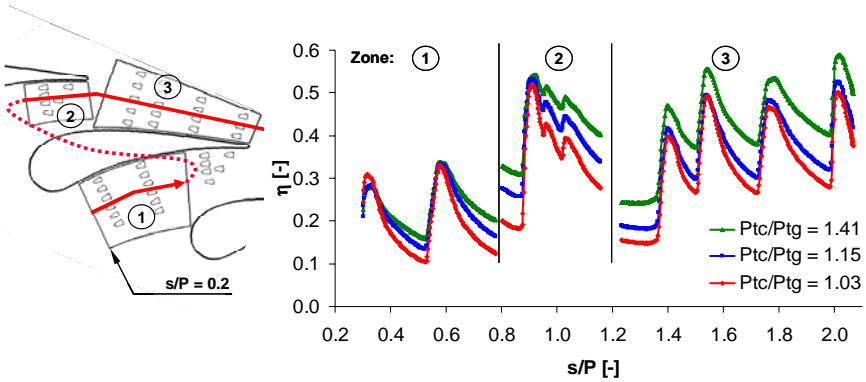


Figure 44: Averaged effectiveness with varying cooling feed pressures

5.1.2 Heat Transfer without Film Cooling (Baseline)

Transient heat transfer measurements are performed using the transient PSP thermography technique presented in Chapter 3. The baseline measurement is done on the same test model with open cooling holes but without any cooling gas injection. While there is no net injection of cooling gas from the supply system, there is some amount of main-flow ingestion into the upstream holes that is injected again through the downstream holes due to the external pressure distribution on the platform.

Figure 45 shows the two quantities involved in wall heat transfer. As intended, the heating distribution (q) has been successfully focused towards the downstream region by adjusting the electrical connectors. This was done since the highest values of h were expected in this region and, consequently larger amounts of heat flux were required to obtain optimal temperature differences for the measurements (Chapter 4). There is no noticeable cross influence of the heat transfer coefficient visible in the q -result. Recall that this baseline heat release serves as basis for the test with film cooling.

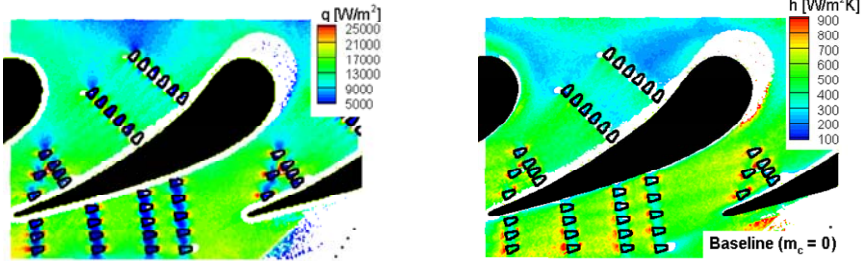


Figure 45: Baseline heat release (left) and heat transfer coefficient (right)

There is an increasing trend in the heat transfer coefficient (h) from inlet to outlet of the cascade due to the accelerating flow. In a constant velocity situation, a gradual decrease is expected due to boundary layer growth. Just upstream of the leading edge, locally high heat transfer coefficients can be observed at locations where the horseshoe vortex makes the flow impinge on the wall. The opposite effect is seen along the separation line where the convection is relatively weak. Thus, the distribution of heat transfer is heavily dependent on the 3D nature of the flow in this region. Downstream of the cooling holes, there is generally a sudden rise in heat transfer coefficient due to restarted boundary layers. Downstream of row 1, some degree of relaminarization is observed similarly to airfoil pressure sides. Downstream of row 2, the disturbances of the holes spread rapidly in the lateral direction affecting the complete area downstream. It is concluded that the flow is fully turbulent again from row 2 onwards based on the comparison with the boundary layer code TexStan (Appendix D).

Regions not captured by the camera have been blanked in the plots. Moreover, results with excessively high variation are filtered out according to the following criterion on the standard deviation of the wall temperature:

$$\sigma_{\theta_w} = \frac{\sigma_{T_w}}{q/h} > 0.2 [-] \quad (42)$$

Particular thermal boundary conditions obtained with the heated foil can lead to local extremes in heat transfer coefficients. This effect is visible in areas exposed to under- and over-heated incoming boundary layers leading to low and high heat transfer coefficients respectively. Locally high transient temperature rise close to some of the cooling holes may violate the linear

temperature dependence of PSP. Therefore, such results are blanked out from the surface plots also.

5.1.3 Validation of PSP as Temperature Sensor

As already explained in Chapter 2, the use of narrow banded TLC thermography turned out to be too time-consuming to obtain full surface measurements with this technique. Nevertheless, the TLC results are used for local validation of the proposed PSP technique in combination with the transient heater foil method. Equation (32) contains two unknowns (q_{ref} and h) when the present measurement technique is employed. This due to the fact that the **temperature difference** due to heat transfer is obtained directly. This is not the case when narrow band TLC thermography is employed leading to a third unknown ($T_j = T_{aw}$). Therefore, all three quantities have been determined separately by performing additional measurements with TLC in transient and steady-state heat transfer experiments as presented by Jonsson and Ott (2009).

The comparison between the two techniques is made on the baseline results (Figure 46). As far as the coverage of the TLC allows, good agreement can be seen between the PSP and TLC surface thermography methods when compared along an axially oriented line in the throat region.

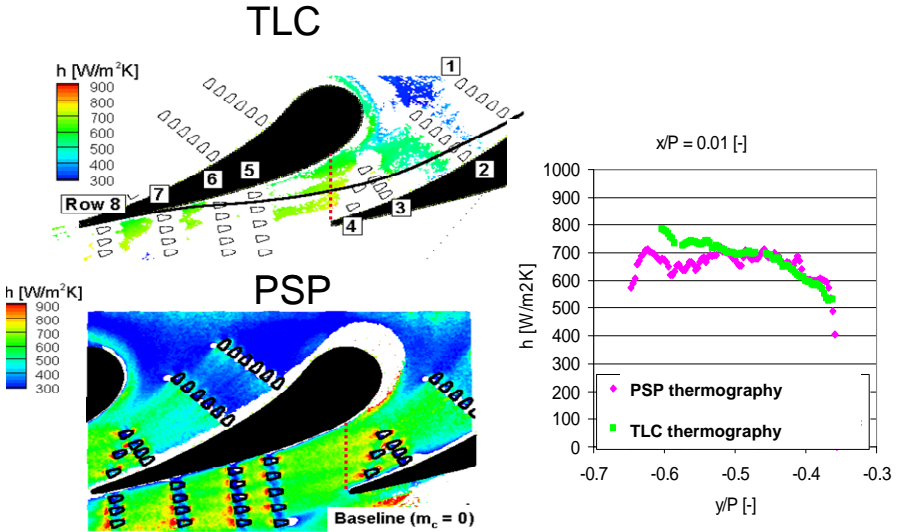


Figure 46: Validation with TLC results along an axial line

The complexity of the test case consists in 3D flow fields, strongly accelerating flow, complex film cooling hole configuration and irregular heating boundary conditions. The non-trivial flow conditions that develop downstream of the measured inlet velocity profile ultimately require three-dimensional modelling or measurements due to the presence of the leakage slot, horse-shoe vortex system and intersecting corner of the vane airfoil. The same consideration has to be made when it comes to presenting, comparing and validating the full-surface measurements. It helps to consider actual streampaths along which the boundary layer develops. Such a wall streampath that crosses the platform has been traced in the CFD model of Charbonnier et al. (2009) and validated with flow visualization measurements. Figure 47 shows a comparison along the streampath. There is good agreement despite the fact that the path passes through relatively steep lateral gradients.

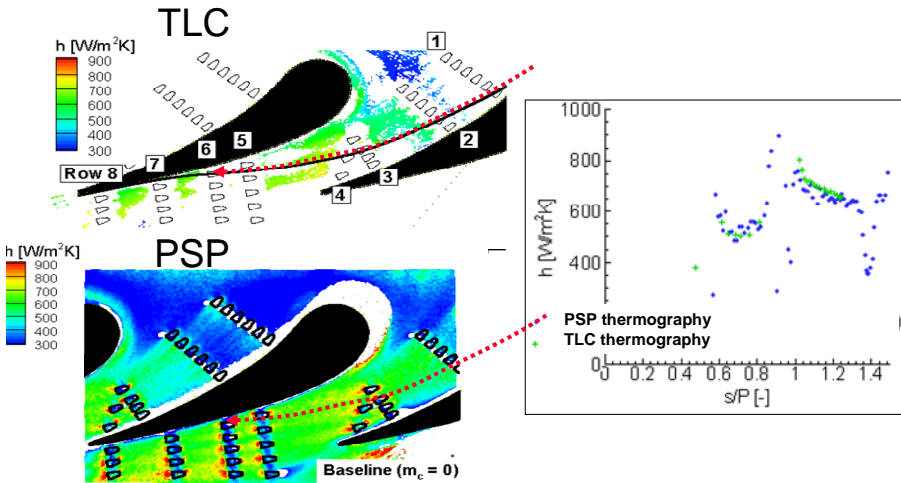


Figure 47: Validation with TLC results along a streampath

It is obviously visible that the covered area is substantially larger with the PSP method. The continuous monitoring of the wall temperature allows to measure the complete time-history in contrast to the narrow band TLC technique. This leads to excellent surface coverage during the transient experiment – both in the upstream region (low h) and the downstream region (high h).

5.1.4 Heat Transfer with Film Cooling

As explained in Section 3.3.3, the heat release distribution in the heater foil is taken from the baseline experiment (open cooling holes without injection). This process is illustrated in Figure 48 showing the resulting convective heat transfer coefficients of the film cooled cases.

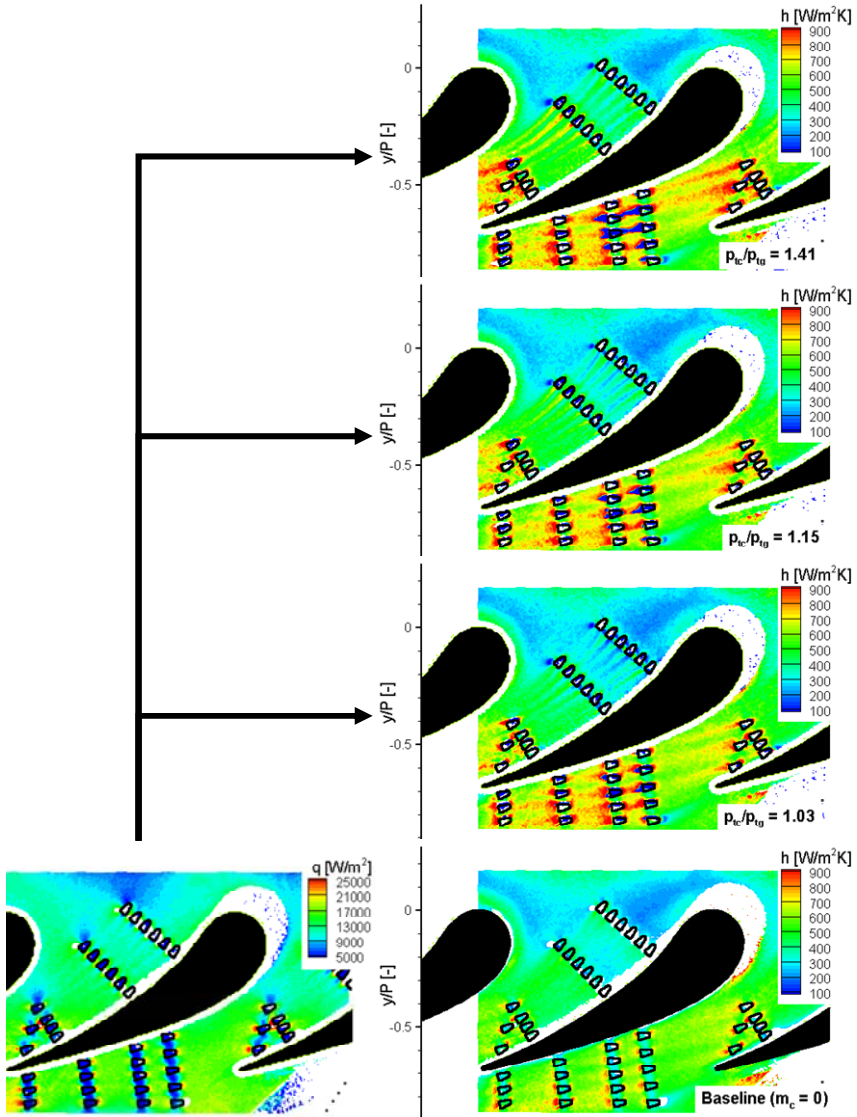


Figure 48: Heat transfer coefficients with varying cooling feed pressures

Laterally averaged heat transfer coefficients are shown in Figure 49. The upstream data ($s/P = 0.2$) indicates excellent repeatability between the experiments. The common heat release determined in the baseline experiment

helps to achieve consistency despite relatively high noise levels in the film cooled cases. Downstream of the film cooling holes, there are generally higher levels of heat transfer coefficients due to disturbances of the holes. Downstream of rows 1 and 2, the baseline case exhibits h -values that are locally higher than in the film cooled cases. An explanation to this is that there is main-flow ingestion into those holes due to the pressure distribution on the platform. This leads to locally impinging flow towards the upstream holes, restarted boundary layers and consequently higher heat transfer coefficients than with a small amount of injection. In the 2nd zone (rows 3 and 4), there is an increasing trend in h due to film cooling injection. However, downstream of the throat, it appears that h is independent of the varied feed pressure. There are two explanations to this observation. First of all due to a lower *relative* change in blowing ratio compared to the holes located in the low Mach number region. Second and maybe more important is the effect of varying coolant concentration in the boundary layers which tends to reduce h due to beneficial properties of CO₂. The gas property influence on convection can be partially compensated by computing Stanton numbers based on effective film properties according to Lutum et al. (2001). The adiabatic film cooling effectiveness can be employed to estimate the gas properties. Although outside of the scope of this thesis, the combination of the same sensor in the presented methods provide a potential for gas property corrections if required.

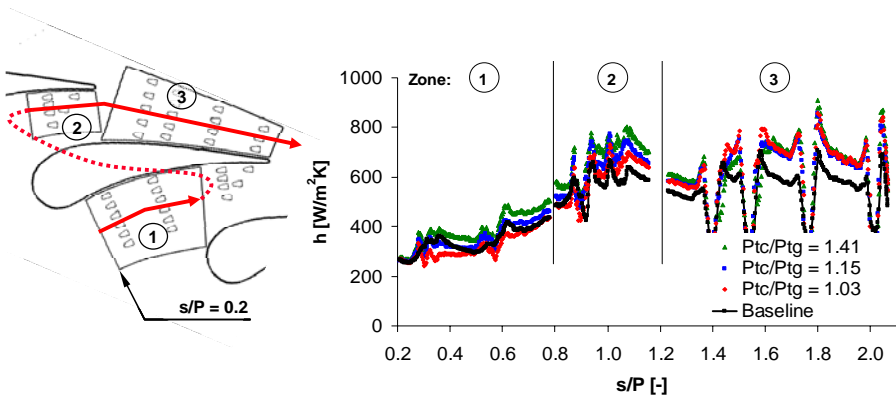


Figure 49: Averaged heat transfer coefficients

5.1.5 Comparison with Numerical Predictions

This work utilizes the numerical results to support the set-up of experiments and the assessment of measured results and uncertainties. The objective is not to judge the correctness of the numerical models.

A comparison with correlations and boundary layer calculations has been done. For 1D analysis with correlations and boundary layer solvers, the incoming boundary layers can be considered as partially unknown. Therefore, 3D modelling is recommended to assess such test cases. On the other hand, the asymptotic behaviour of boundary layers typically makes the solution approach the simplified 1D situation sufficiently downstream of any complex inlet effects. In any case, these simplified methods give an indication of the correctness of measured and predicted results.

The free-stream flow quantities are applied as input for the boundary layer code TexStan as set-up by Zanker (2008). This 1D modelling of the wall convection includes the effect of acceleration along the streampath and allows to interpret the boundary layer quality and identify the dominating input boundary conditions. Figure 50 shows results along the streampath considered previously, starting close to the leading edge corner.

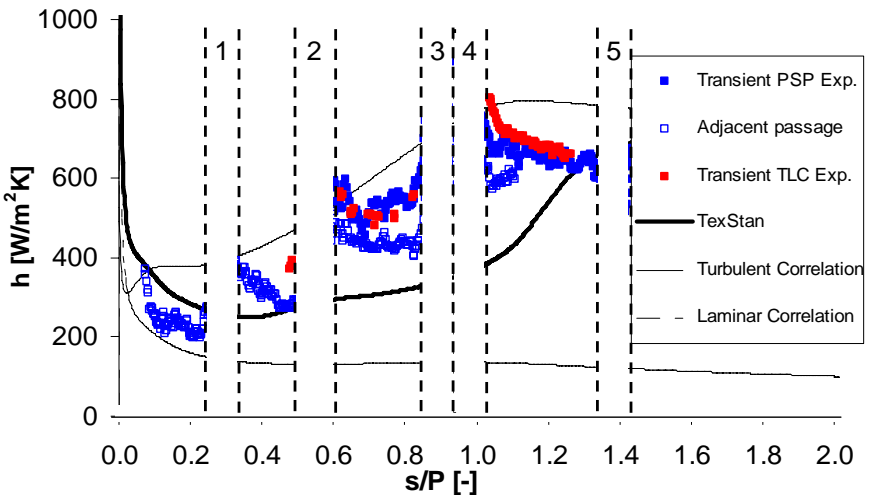


Figure 50: Comparison with theoretical models

It appears that the experimental result is closer to the fully turbulent correlation (Equation 8) downstream of row 2. The boundary layer code does not predict the transition from laminar to turbulent until further downstream. It has been observed that the sensitivity to the free stream turbulence kinetic energy is high when it comes to predicting this type of by-pass transition. The periodicity between the two measured vane passages is fairly good as can be seen downstream of row 2. An explanation to the offset is the non-periodic heating distribution. This points towards the importance of the thermal boundary condition.

Further to the boundary layer analysis, a comparison with CFD (RANS) results obtained with the model presented in Appendix F. Measurements of the adiabatic film cooling effectiveness have been compared to computations using different codes and presented in a common paper by Charbonnier et al. (2009). The comparison between measured and computed adiabatic film cooling effectiveness shows promising agreement for the first two rows of holes. The comparison is based on tracer gas concentration data converted into the temperature-based definition of the adiabatic film cooling effectiveness (Equation 26). One of the conclusions is that further mesh-refinement would be beneficial. This leads to long calculation times for the present type of application since the plenums need to be included in the model. One approach to reduce the computational effort is to decouple the plenum and mixing zones in separate models as demonstrated by Charbonnier et al. (2008).

5.2 Uncertainty Analysis

PSP responds to excitation light depending on the oxygen content, temperature and several other factors, e.g. the light-path and the optical set-up as illustrated in Figure 51. In this case the intensity of electromagnetic light waves. Thus each component of the test set-up might potentially influence the intensity signal finally *measured* by the CCD camera. This is a typical complexity of intensity-based photoluminescent techniques. The following is an attempt to summarise error sources present in PSP-measurements:

- Calibration of photo-luminescence (sensor molecules, binder material)
- Light filter leakage (high-pass filter, low-pass filter)
- Quality of observation window, camera lens, CCD-chip, light reflections

- Drift due to light source
- Drift due to degradation of the coating (temperature hysteresis, photolysis, mechanical wear, dirt deposits, etc.)

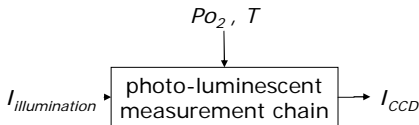


Figure 51: Absolute transfer function of the measurement chain

The impact of those uncertainties are significantly reduced when relative results are considered. As is the case for the derivation of adiabatic film cooling effectiveness and heat transfer coefficients. Many of the first order effects such as excitation light intensity cancel out by considering that calibrations and measurements are done relative to known reference cases with the same optical set-up and light excitation. Therefore, the uncertainty assessment is limited to the relative quantities of interest in this work.

5.2.1 Adiabatic Film Cooling Effectiveness

The adiabatic film cooling effectiveness is determined from time averaged signals integrated during 5 s. In order to estimate the uncertainties in these measurements, Wunderlin (2006) applied the method of Kline and McClintock (1953) for single sample experiments. The analysis is based on the propagation of errors in each of the measured quantity according to the respective exchange rate in η . (see e.g. Moffat (1982)). In this work, the underlying uncertainties are based on the confidence interval given by the standard deviation, i.e. the variation ($\pm \sigma$) about the mean value within which the odds of finding the true value is 68%. The underlying measurements are pressure and temperature readings employed in the calibration of the PSP-sensor, but also to establish the actual flow conditions. To this end, cooling flow rate and hardware tolerances are important for the adiabatic film cooling effectiveness. This is due to the first-order influence of coolant massflow on η . The analysis led to the conclusion that random uncertainties diminish with increased η as shown in Figure 52. Since effectiveness is already a relative quantity the errors are given as $\Delta\eta$.

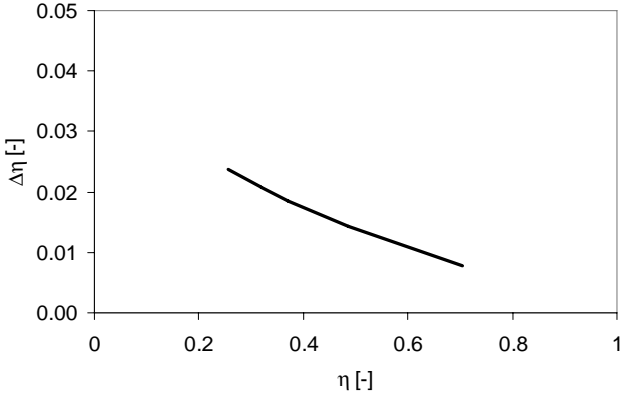


Figure 52: Random uncertainty of the adiabatic film cooling effectiveness

In addition to the random uncertainties, there are also potential sources of systematic bias errors. For example the assumption of 100% tracer gas purity, derivation of cooling flow rates based on different flow characteristics, etc. Obviously, the absolute values are never exact. But since most uncertainties are present in all measurement — trends with high quality can be derived. Similarly, drift in the global quantum yield of PSP due to e.g. photolysis is compensated by the reference measurement taken just before the flow measurements. The *Reference*, *Aerodynamic* and *Tracer* experiments are performed within a short time interval allowing to neglect this effect.

Recall that the oxygen pressure sensitivity is considered constant between the calibration and the flow experiments. However, any reduction of oxygen pressure sensitivity occurring between calibration and measurement would lead to an under-estimation of η . This effect might aggravate between experiments and should be included in the error analysis. The impact of such a bias error on η depends on the separation of the *Aero* and *Tracer* intensity signals, as well as the respective offset from the known reference. Therefore, drift is more important at high adiabatic film cooling effectiveness and high Mach number since these conditions are situated in the lower left corner of the calibration chart (Figure 53). Here, the Stern-Volmer plot is linearized around the reference condition — keeping only the first order term (C'_1) of the Taylor series (Equation 19) in order to simplify the analysis of drift errors. The histogram from a typical adiabatic film cooling effectiveness measurement

(Figure 54) illustrate to which part of the calibration curve the *Aero* and *Tracer* measurements correspond.

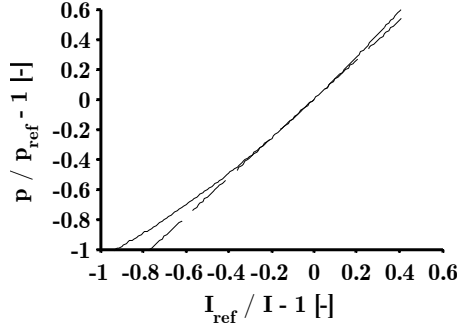


Figure 53: Oxygen pressure sensitivity linearized at the reference condition.

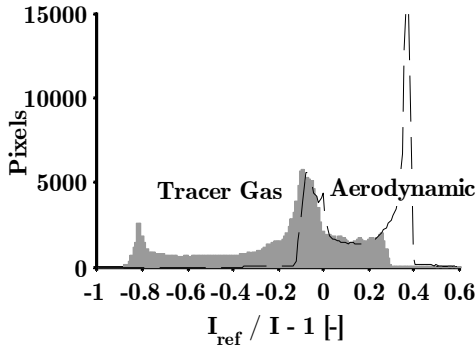


Figure 54: Distribution of measurement pixels in a η -experiment

Figure 55 shows the impact of any drift of oxygen pressure-sensitivity occurring between calibration and a flow experiment. This kind of bias error is proportional to the adiabatic film cooling effectiveness ($\Delta\eta/\eta = \text{const.}$) in contrast to the random uncertainties treated above. Therefore any drift in pressure sensitivity of PSP has the highest impact when η approaches unity. This is illustrated in Figure 55 (left) by introducing a hypothetical sensitivity drift of 5%. In discrete-hole film cooling, effectiveness values close to unity occurs only locally just downstream of a hole when incoming films are superposed. With slot injection however, film cooling effectiveness of unity is common just downstream of the slot. The amplification of such a drift error is nearly 1:1 as shown in Figure 55 (right) but also depends on the Mach number

to some extent. This is because it dictates the absolute offset between the *Aero* and *Tracer* intensities. Since the majority of the η -measurements presented in this work are measured at moderate η and Ma , the measurements of a test series are relatively insensitive to drift — in contrast to absolute pressure measurements with PSP.

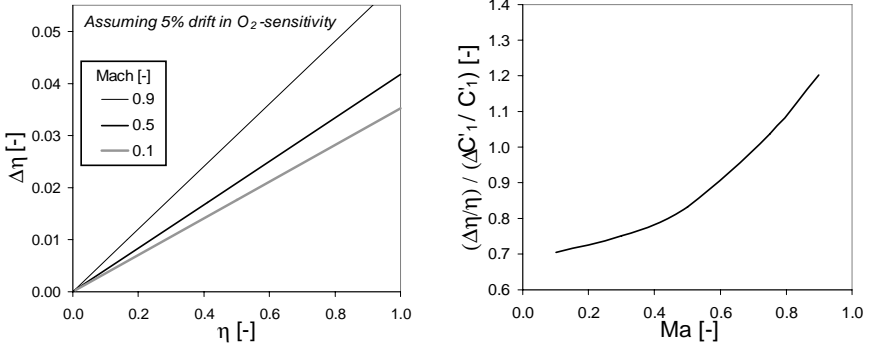


Figure 55: Sensitivity to pressure-calibration drift (left), example (right)

Thus, for increased effectiveness, random uncertainties diminish whereas the bias errors considered here become more important. Finally, there are potentially error sources of constant nature (independent of η) present in the measurement chain — notably the assumption of invariant illumination energy. With the flash lamp system of the present work, this uncertainty is quantified to $\Delta\eta = \pm 0.02$ based on repeatability observations. As a consequence, an average uncertainty of the adiabatic film cooling effectiveness is most representative. It is estimated to $\Delta\eta = \pm 0.03$ ($\pm 3\%$).

5.2.2 Heat Transfer Coefficients

Uncertainties in the time sampling must be considered for the transient heat transfer experiments. Figure 56 shows the increasing importance of accurate time measurements for high values of heat transfer coefficient (fast time-response of the wall). However, for the present test set-up, time measurement errors are generally smaller than those of the temperature measurement. This is due to the dedicated PSP paint leading to low signal strength with respect to the noise level. Therefore, the analysis focuses on the dominating temperature uncertainty.

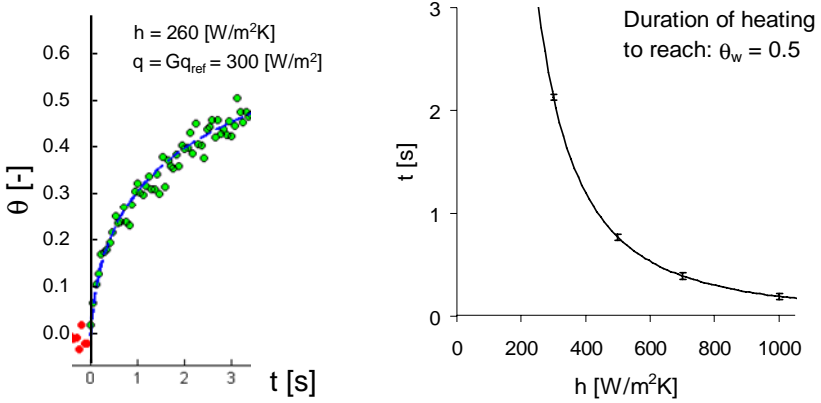


Figure 56: Temperature and time uncertainties in a transient experiment

The uncertainty assessment of the heat transfer coefficients is based on random variation of the measured temperature differences. As for η , the statistical uncertainty is quantified according to the standard deviation. Information of temporal variation due to noise is directly available from the regression analysis (Equation 39). The relative uncertainty in h is considered proportional to the temperature uncertainty according to:

$$\frac{\Delta h}{h} \approx \sigma_{\theta_w} \quad (43)$$

Based on statistical evaluation of 200 time samples in each pixel, Figure 57 depicts the estimated uncertainty along the streamline employed in Section 5.1. A nearly constant uncertainty along the platform is a result of the optimized heat release distribution of the heater foil.

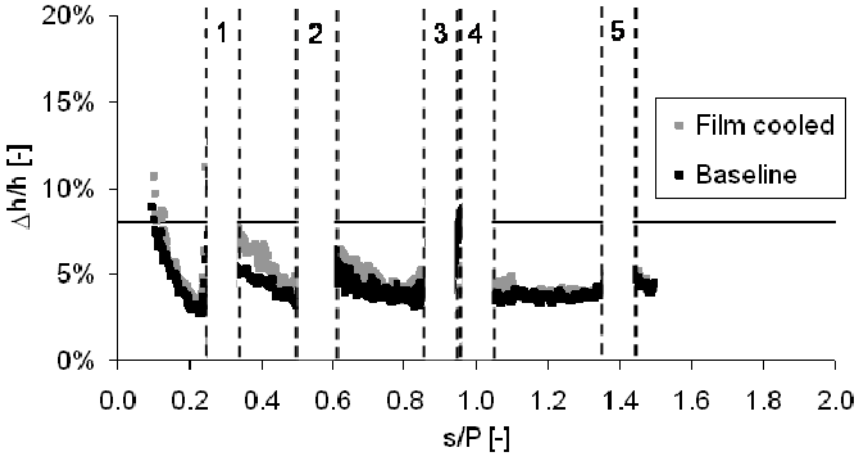


Figure 57: Random spread in heat transfer coefficients along a streampath

A comparison of the heat transfer coefficients obtained upstream of the first row of holes (Section 5.1.4) indicate excellent repeatability. This leads to the conclusion that temperature sensitivity drifts occurring during a test campaign are smaller than the random uncertainty. Hence the uncertainty of the measured heat transfer coefficients is estimated to be within $\Delta h/h = \pm 8\%$. This is in good agreement with the pixel-to-pixel variation that can be seen in Section 5.1.3.

The relatively large level of uncertainty is mainly due to the low temperature sensitivity of the investigated PSP-sensor. At the same time, it is known that global errors in heat transfer experiments are associated with relatively large uncertainties due to the inherently delicate nature of this quantity. While the **precision** in the h -measurements with PSP is lower than with narrow band TLC, the **accuracy** is higher for the present type of high-speed experiments. This is due to the fact that the **temperature change** induced by heat transfer at the wall is obtained directly in the measurement.

In terms of improvement potential of the present heat transfer method, the following possibilities are identified:

- Take adjacent pixel information into account by spatial smoothing. This involves trade-off between resolution and noise minimization.
- Employ a photoluminescent paint with higher temperature sensitivity.

5.2.3 Heat Release

Recall that the heat release (q) is an auxiliary quantity based on the average temperature sensitivity of the PSP paint. Therefore, the q -results are considered qualitative rather than quantitative. Nevertheless, the method provides a sufficiently accurate distribution of the heat release when it comes to the influence on the heat transfer coefficient as explained in Section 1.2.2.

5.3 Future Work

- The PSP and TLC techniques are established techniques at EPFL-LTT and thus logical choices to be employed for the present studies. Recent advances in luminescent paint chemistry and micro structures are interesting topics for future application in the field of film cooling.
- During the present heat transfer measurements, it was observed that high temperature exposure leads to irreversible increase in the PSP-signal intensity. Without going into detail of the photochemistry and photophysics, the paint producer has observed such thermal curing reduces the temperature sensitivity of pressure sensors. Therefore, it is suggested to investigate the degree of hysteresis during the presented type of heat transfer measurements.
- Explore recent advances in PSP-technology such as TSP, binary paints (separate PSP and TSP sensing molecules), PSP surface technologies for faster time-response, etc.
- Experimental uncertainty due to injected coolant massflow can be reduced by increasing the size of the holes using larger test models. Perfect periodicity might not be required if the objective is to compare the relative impact due to technological changes with e.g. CFD-predictions.
- The present experiments involve high levels of foreign gas concentration in the film cooling flows. Therefore, it is suggested to assess the gas property impact on the convective heat transfer using e.g. property-ratio scaling methods.
- The present work was focused on the platforms making the optical access for PSP straight-forward. In particular, wall-normal orientation of both illumination and camera is made possible since reflected light is eliminated by the optical filters. The results obtained in this work on the platforms

lead to the conclusion that the airfoil surfaces can also be measured with PSP despite more shallow viewing angles. Alternatively, the continuous miniaturization of digital camera technology can be utilized to mount several low-cost cameras closer to the flow in order to monitor the entire surface of the tested object.

5.4 Conclusions of Chapter 5

Excellent resolution and repeatability of the PSP technique for adiabatic film cooling effectiveness measurements have been demonstrated.

The measurement of the full time history of wall temperature in the transient experiments allows to solve the heat transfer problems in each point of the surface. Doing this in a single experiment allows to speed up the measurement process and increase the accuracy compared to using multiple transient experiments. Applying the well-established TLC technique locally has allowed to validate the PSP thermography technique.

Despite the locally high noise levels, the large amount of data points in combination with the a-priori known heating distribution q , lead to a well-posed problem for the determination of the film cooled h even for the case of CO_2 injection. Moreover, any locally biased uncertainty in the calibration of the temperature sensitivity (D) cancels since the same heat release (q) is present in each experiment. This is an interesting feature when it comes to isolating changes in heat transfer due to film cooling.

Chapter 6

Conclusions

Film cooling can theoretically be predicted by numerical methods of today as long as accurate boundary conditions, extremely fine calculation meshes and sufficient computational resources are available. However, practically it is very time consuming to accurately simulate the flows due to the large number of discrete cooling holes. With simplified modelling approaches, it is difficult to control all parameters influencing the film cooling performance. It is primarily due to the complex physics and the range of influencing parameters. Therefore, it is necessary to combine experimental tests with advanced measurement techniques and numerical methods in order to understand the flow fields where measured data is missing. Combining the academic understanding of individual mechanisms with engine experience allows for reliable design methodologies.

There are a number of experimental approaches to obtain film cooling performance measurements on turbine models. Given the difficulty to obtain accurate full-surface results of film cooling performance for the present application using existing methods, a new development is needed.

The goal of the research is to improve the cooling performance of gas turbines. The goal of this thesis is to develop efficient and accurate methods for experimental film cooling assessment.

Photoluminescent techniques offer attractive solutions for such a complex experimental test case. The methodology is based on the analogy between heat and mass transfer to obtain the adiabatic film cooling effectiveness and transient wall conduction analysis to obtain the convective heat transfer. The presented PSP-techniques allow for engine representative tests in terms of Reynolds and Mach numbers. The latter leading to significant aerodynamic heating/cooling effects.

In the present thesis, suitable experimental techniques have been developed, validated and applied. The combination of the oxygen pressure sensitivity and temperature sensitivity has led to a new development that allows for

measurements of the entire external film cooling performance. Although two separate optical set-ups have been employed here, there is great potential to be found by the use of the more modern system. This means that excellent consistency can be obtained and much less time required to perform the measurements and the data reduction.

6.1 Experimental Feasibility

Starting at the steady-state thermal problem of gas turbines, two physical dimensions are considered in order to obtain measurements of the film cooling quality. The adiabatic film cooling effectiveness and heat transfer coefficient are measured nearly simultaneously, using independent indication methods for different physical mechanisms, namely that of mass and heat transfer measurements. This greatly helps to isolate the influence of each quantity and to increase the confidence in the measurement.

Small temperature variations allow for the approximation of quasi-constant gas and wall material properties. Thus temperature is merely used as in indicator to measure the convective heat transfer resistance of the boundary layers. Furthermore, the independence of temperature means that wall heat flux can be applied in any direction without significantly influencing the resulting heat transfer coefficients.

The importance of considering *relative* trends obtained in the laboratory has been emphasized. Both the adiabatic film cooling effectiveness and the **ratio** of heat transfer coefficients with respect to a baseline are relative measurements that can be used to compare with numerical models and used to establish empirical correlations to model real turbines.

Developments of photoluminescent measurement techniques for film cooling assessment has been done. It is concluded that a single surface coating greatly simplifies the challenge to obtain quantitative measurements:

- Full-surface coverage.
- Surface consistency, e.g. geometrical tolerance and optical set-up during test campaigns.
- Minimal problem with light reflections in the test facility due to the colour filters.

Limitations of the PSP sensor consist in:

- Upper temperature limit in the order of 100 °C for the present paint.
- Experiments must be performed within a controlled time-interval (hours) in order to minimize degradation of the paints between tests and calibration.

6.2 Adiabatic film cooling effectiveness using CO₂

The PSP technique is traditionally employed for absolute pressure measurement in wind tunnels. Strengths of the PSP technique when applied in adiabatic film cooling effectiveness (gas concentration) measurements are:

- High signal to noise ratio obtained with substantial amount of tracer gas injection.
- Relative measurements cancels out many calibration uncertainties.
- By sensing the oxygen concentration remaining from the air flow, PSP offers flexibility on the choice of foreign gas (e.g. other than CO₂).
- Perfectly adiabatic conditions even on metallic walls. It is motivated to minimize or control the lateral heat conduction and monitor lateral oscillations of films.

It has been shown that CO₂ can also be employed as tracer gas as long as the appropriate definition (Section 3.2.2) of the partial pressure including the molecular mass correction is included. The relative nature of a gas concentration measurement makes PSP highly suitable for film cooling studies.

6.3 Convective Heat Transfer Measurements

The PSP thermography is faster and allows for more accurate analysis of heat transfer measurements than narrow-band TLC thermography. The latter is more precise, but typically lacks in providing a consistent measure of the adiabatic wall temperature. This is an important quality in compressible flow experiments with limited heat flux.

To the author's knowledge, it is the first time that the same PSP sensor is also applied for wall heat transfer measurements. This thesis shows that the new method allows for assessing the performance of film cooling schemes in the laboratory environment. Results obtained on a complex film cooled

platform test case are used to demonstrate the capability of the techniques. A validation of the thermography method is done by comparing with the well-established TLC method.

6.4 Final Note

The objective to find a suitable method for film cooling assessment has been attained. It has been demonstrated that the applicability of PSP-paints in experimental film cooling assessment is a competitive alternative for this field of research and development.

Bibliography

- Ahn, J., Schobeiri, M. T., Han, J. C. and Moon, H. K.** (2005), *Film Cooling Effectiveness on the Leading Edge of a Rotating Film-Cooled Blade using Pressure Sensitive Paint*, ASME Turbo Expo 2005, Reno-Tahoe, Nevada, USA, ASME.
- Ahn, J., Schobeiri, M. T., Han, J. C. and Moon, H. K.** (2007), *Effect of rotation on leading edge region film cooling of a gas turbine blade with three rows of film cooling holes*, Int. J. Heat and Mass Transfer **50**, pp: 15-25.
- Ames, F. E., Barbot, P. A. and Wang, C.** (2003), *Effects of Aeroderivative Combustor Turbulence on Endwall Heat Transfer Distributions Acquired in a Linear Vane Cascade*, J. Turbomachinery **125**, pp: 210-220.
- Arts, T. and Bourguignon, A. E.** (1990), *Behaviour of a Coolant Film with Two Rows of Holes along the Pressure side of a High-Pressure Nozzle Vane*, J. Turbomachinery **112**, pp: 512-521.
- Barigozzi, G., Benzoni, G., Franchini, G. and Perdichizzi, A.** (2006), *Fan-shaped hole effects on the aero-thermal performance of a film-cooled endwall*, J. Turbomachinery **128**, (1), pp: 43-52.
- Blair, M. F.** (1974), *An Experimental Study of Heat Transfer and Film Cooling on Large-Scale Turbine Endwalls*, J. of Heat Transfer **96**, p: 524-529.
- Bogard, D. G. and Thole, K. A.** (2006), *Gas turbine film cooling*, J. Propulsion and Power **22**, (2), pp: 249-270.
- Boyce, M. P.** (2002), *Handbook for cogeneration and combined cycle power plants*, ASME Press.
- Boyle, R. J. and Simon, F. F.** (1999), *Mach Number Effects on Turbine Blade Transition Length Prediction*, J. Turbomachinery **121**, (4), p: 694.
- Bruun, H. H.** (1995), *Hot-wire Anemometry; Principles and Signal Analysis*, Oxford science publications.
- Bunker, R. S.** (2007), *Gas Turbine Heat Transfer: Ten Remaining Hot Gas Path Challenges*, J. Turbomachinery **129**, (2), pp: 193-201.
- Carslaw, H. S. and Jaeger, J. C.** (1992), *Conduction of Heat in Solids*, 2nd Ed., Oxford, UK.
- Chana, K. S., Hilditch, M. A. and Anderson, J.** (2005), *An Investigation of the Effects of Film Cooling in a High-Pressure Aeroengine Turbine Stage*, ASME Conference Proceedings **2005**, (47306), p: 591.

- Charbonnier, D., Jonsson, M. and Ott, P.** (2008), *Numerical Analysis of Adiabatic Film-cooling Effectiveness around an HP-Turbine Airfoil - Decomposed Computation of Internal - External Flows*, 12th ISROMAC Conference, Honolulu.
- Charbonnier, D., Jonsson, M., Ott, P., Köbke, T. and Cottier, F.** (2009), *Experimental and Numerical Study of the Thermal Performance of a Film Cooled Turbine Platform*, ASME Turbo Expo 2009, Orlando, FL, USA, GT2008-50623.
- Choe, H., Kays, W. M. and Moffat, R. J.** (1974), *The superposition approach to film cooling*, Bd. 74-WA HT-27, ASME.
- Chyu, M. K.** (2001), *Heat Transfer near Turbine Nozzle Endwall*, Annals of the New York Academy of Sciences **934**, pp: 27-36.
- Colban, W. F. and Thole, K. A.** (2006), *A Comparison of Cylindrical and Fan-Shaped Film-Cooling Holes on a Vane Endwall at Low and High Freestream Turbulence Levels*, ASME Turbo Expo.
- Drost, U. and Böls, A.** (1999), *Performance of a Turbine Airfoil with Multiple Film Cooling Stations Part 1: Heat Transfer and Film Cooling Effectiveness*, International Gas Turbine & Aeroengine Congress & Exhibition, Indianapolis, Indiana, 99-GT-171.
- Dunn, M. G.** (2001), *Convective Heat Transfer and Aerodynamics in Axial Flow Turbines*, J. Turbomachinery **123**, (October 2001), pp: 637-686.
- Eckardt, D. and Ruffli, P.** (2002), *Advanced Gas Turbine Technology: ABB/BCC Historical Firsts*, J. Engineering for Gas Turbines and Power **124**, (3), pp: 542-549.
- Eckert, E. R. G., Ernst, R. G. and Goldstein, R. J.** (1976), *Measurements in Heat Transfer*, 2nd Ed., Hemisphere Publishing Corp., Wash.
- Eckert, E. R. G.** (1992), *Similarity Analysis of Model Experiments For Film Cooling in Gas Turbines*, Wärme- und Stoffübertragung **27**, pp: 217-233.
- Ekkad, S. V. and Han, J. C.** (2000), *A transient liquid crystal thermography technique for gas turbine heat transfer measurements*, Measurement Science and Technology **11**, (7), p: 957.
- Engler, R. H., Hartmann, K., Troyanovski, I. and Vollan, A.** (1992). *Description and assessment of a new optical pressure measurement system demonstrated in the high speed wind tunnel of DLR in Göttingen*. Göttingen, DLR.
- Erber, A.** (2007), *Hot-wire Anemometry Measurements of the Main Flow Properties Downstream of a Slot for the Investigation of Secondary Flows*, Semester Project EPFL, Lausanne

-
- Falcoz, C., Weigand, B. and Ott, P.** (2006), *Experimental Investigations on Showerhead Cooling on a Blunt body*, Int. J. Heat and Mass Transfer **49**, pp: 1287-1298.
- Fric, T. F. and Roshko, A.** (1994), *Vortical Structure in the Wake of a Transverse Jet*, J. Fluid Mech. **276**, pp: 1-47.
- Friedrichs, S., Hodson, H. P. and Dawes, W. N.** (1996), *Distribution of Film Cooling Effectiveness on a Turbine Endwall Measured Using the Ammonia and Diazo Technique*, ASME J. Turbomachinery **118**, pp: 613-621.
- Giel, P. W., Thurman, D. R., Van Fossen, G. J., Hippensteele, S. A. and Boyle, R. J.** (1998), *Endwall Heat Transfer Measurements in a Transonic Turbine Cascade*, J. Turbomachinery Vol. **120**, (April 1998), pp: 305-313.
- Gillespie, D. R. H., Wang, Z., Ireland, P. T. and Kohler, S. T.** (1998), *Full Surface Local Heat Transfer Coefficient Measurements in a Model of an Integrally Cast Impingement Cooling Geometry*, J. Turbomachinery **120**, (January 1998), pp: 92-99.
- Goldstein, R. J.** (1971), *Film cooling*, Advances in Heat Transfer, pp: 321-379.
- Goldstein, R. J., Ibele, W. E., Patankar, S. V., Simon, T. W., Kuehn, T. H., Strykowski, P. J., Tamma, K. K., Heberlein, J. V. R., Davidson, J. H., Bischof, J., Kulacki, F. A., Kortshagen, U., Garrick, S. and Srinivasan, V.** (2006), *Heat transfer--A review of 2003 literature*, Int. J. Heat and Mass Transfer **49**, (3-4), p: 451.
- Graziani, R. A., Blair, M. F., Taylor, J. R. and Mayle, R. E.** (1980), *An Experimental Study of Endwall and Airfoil Surface Heat Transfer in a Large Scale Turbine Blade Cascade*, J. of Engineering for Power **102**, pp: 257-267.
- Gritsch, M., Saumweber, C., Schultz, A., Wittig, S. and Sharp, E.** (2000), *Effect of Internal Coolant Crossflow Orientation on the Discharge Coefficient of Shaped Film-Cooling Holes*, J. Turbomachinery **122**, (No. 1), pp: 146-152.
- Han, J. C., Dutta, S. and Ekkad, S. V.** (2000), *Gas Turbine Heat Transfer and Cooling Technology*, Taylor and Francis, New York.
- Han, S. and Goldstein, R. J.** (2008), *The heat/mass transfer analogy for a simulated turbine endwall*, Int. J. Heat and Mass Transfer **51**, pp: 3227-3244.
- Harasgama, P.** (1995), *Heat Transfer and Cooling in Gas Turbines*, VKI.
- Häring, M.** (1996), *Experimentelle Untersuchung der örtlichen Wärmeübergangszahl an Gasturbinenschaufeln anhand der Sublimationstechnik im kompressiblen Strömungsbereich*, 1291, EPFL, Lausanne
- Hinze, J. O.** (1975), *Turbulence*, 2nd Ed., McGraw-Hill, New-York.

- Hoffs, A., Bölcs, A. and Harasgama, P.** (1997), *Transient heat transfer experiments in a linear cascade via an insertion mechanism using the liquid crystal technique*, J. Turbomachinery **119**, (Jan. 1997), pp: 9-13.
- Ireland, P. T. and Jones, T. V.** (2000), *Liquid Crystal Measurements of Heat Transfer and Surface Shear Stress*, Meas. Sci. Technology **11**, pp: 969-986.
- Jabbari, M. Y., Marston, K. C., Eckert, E. R. G. and Goldstein, R. J.** (1996), *Film cooling of the gas turbine endwall by discrete hole injection*, ASME J. Turbomachinery **118**, (April), pp: 278-284.
- Jones, T. V.** (1999), *Theory for the use of foreign gas in simulating film cooling*, Int. J. Heat and Fluid Flow, (20), pp: 349-354.
- Jonsson, M. and Ott, P.** (2007), *Heat Transfer Experiments on a Heavily Film Cooled Nozzle Guide Vane*, 7th European Turbomachinery Conference, Athens, Greece, pp: 1011-1020.
- Jonsson, M., Charbonnier, D., Ott, P. and von Wolfersdorf, J.** (2008), *Application of the Transient Heater Foil Technique for Heat Transfer and Film Cooling Effectiveness Measurements on a Turbine Vane Endwall*, ASME Turbo Expo 2008, Berlin, GT2008-50451.
- Jonsson, M. and Ott, P.** (2009), *Data Analysis of Endwall Heat Transfer Measurements in Transonic Cascade-flow using Transient Heater Foil Techniques*, 8th European Turbomachinery Conference, Graz, Austria.
- Jovanovic, M. B., de Lange, H. C. and van Steenhoven, A. A.** (2008), *Effect of hole imperfection on adiabatic film cooling effectiveness*, Int. J. Heat and Fluid Flow **29**, (2), p: 377.
- Kays, W. M., Crawford, M. E. and Weigand, B.** (2004), *Convective Heat and Mass Transfer*, 4th Ed., McGraw Hill, New York.
- Kingsley-Rowe, J. R., Lock, G. D. and Davies, A. G.** (2003), *Aerospace Applications of Luminescent Paint Heat Transfer Measurement*, Royal Aeronautical Journal **107**, pp: 1-21.
- Kline, S. J. and McClintock, F. A.** (1953), *Describing Uncertainties in Single-Sample Experiments*, J. Mech. Eng., pp: 3-8.
- Knost, D. G. and Thole, K. A.** (2005), *Adiabatic Effectiveness Measurements of Endwall Film-Cooling for a First-Stage Vane*, ASME J. Turbomachinery **127**, (April), pp: 297-305.
- Krueckels, J., Gritsch, M. and Schnieder, M.** (2009), *Design Considerations and Validation of Trailing Edge Pressure Side Bleed Cooling*, Turbo Expo 2009, Orlando, FL, USA, ASME, GT2009-59161.

-
- Lakshminarayana, B.** (1996), *Fluid dynamics and heat transfer of turbomachinery*, John Wiley & Sons Inc.
- Langston, L. S.** (2001), *Secondary Flows in Axial Turbines - A Review*, Annals of the New York Academy of Sciences **934**, (HEAT TRANSFER IN GAS TURBINE SYSTEMS), pp: 11-26.
- Lutum, E., von Wolfersdorf, J., Semmler, K., Dittmar, J. and Weigand, B.** (2001), *An Experimental Investigation of Film Cooling on a Convex Surface subjected to Favourable Pressure Gradient Flow*, Int. J. Heat and Mass Transfer **44**, pp: 939-951.
- Lynch, S. P. and Thole, K. A.** (2007), *The Effect of Combustor-Turbine Interface Gap Leakage on the Endwall Heat Transfer for a Nozzle Guide Vane*, Turbo Expo, GT2007-27867.
- Metzger, D. E., Carper, H. J. and Swank, L. R.** (1968), *Heat transfer with film cooling near non-tangential injection slots*, J. Eng. Gas Turbines Power **90**, pp: 157-163.
- Moffat, R. J.** (1982), *Contributions to the Theory of Single-Sample Uncertainty Analysis*, J. Fluids Engineering Vol: **104**, (June), pp: 250-260.
- Narzary, D. P., Liu, K. C. and Han, J. C.** (2009), *Influence of Coolant Density on Turbine Blade Platform Film-cooling*, Turbo Expo, ASME, GT2009-59342.
- Nicklas, M.** (2001), *Film-Cooled Turbine Endwall in a Transonic Flow Field: Part II - Heat Transfer and Film-Cooling Effectiveness*, ASME **123**, pp: 720-729.
- Ott, P., Norryd, M. and Bölc, A.** (1998), *The Influence of Tailboards on Unsteady Measurements in a Linear Cascade*, Gas Turbine and Aeroengine Congress, Stockholm, ASME, 98-GT-572.
- Piggush, J. D. and Simon, T. W.** (2007), *Heat Transfer Measurements in a First-Stage Nozzle Cascade Having Endwall Contouring: Misalignment and Leakage Studies*, J. Turbomachinery **129**, (4), p: 782.
- Pomfret, J. R., Guo, S. M., Oldfield, M. L. G. and Rawlinson, A. J.** (2002), *A high-speed concentration probe for the study of gas turbine vane film cooling*, Measurement Science and Technology **13**, (12), p: 1966.
- Praisner, T. J. and Smith, C. R.** (2006), *The Dynamics of the Horseshoe Vortex and Associated Endwall Heat Transfer - Part I: Temporal Behaviour*, J. Turbomachinery **128**, (October), pp: 747-754.
- Puklin, E., Carlson, B., Gouin, S., Costin, C., Geen, E., Ponomarev, S., Tanji, H. and Gouterman, M.** (2000), *Ideality of pressure-sensitive paint. I. Platinum tetra(pentafluorophenyl)porphine in fluoroacrylic polymer*, J. Applied Polymer Science **77**, (13), pp: 2795-2804.

- Reiss, H.** (2000), *Experimental Study on Film Cooling of Gas Turbine Airfoils using Shaped Holes*, Ph.D. Thesis 2209, EPFL, Lausanne
- Roback, R. J. and Dring, R. P.** (1993), *Hot Streaks and Phantom Cooling in a Turbine Rotor Passage: Part 1 - Separate Effects*, J. Turbomachinery **115**, (4), p: 657.
- Rubensdörffer, F. G.** (2006), *Numerical and Experimental Investigations of Design Parameters Defining Gas Turbine Nozzle Guide Vane Endwall Heat Transfer*, KTH, Stockholm
- Saravanamuttoo, H. I. H., Rogers, G. F. C., Cohen, H. and Straznicky, P. V.** (2009), *Gas Turbine Theory*, 6th Ed., Pearson Education Limited.
- Shadid, J. N. and Eckert, E. R. G.** (1991), *The Mass Transfer Analogy to Heat Transfer in Fluids With Temperature-Dependent Properties*, J. Turbomachinery **113**, pp: 27-33.
- Sieverding, C. H.** (1985), *Secondary flows in straight and annular turbine cascades*, ASI 1, (Series E, 97A), pp: 621-664.
- Simon, T. W. and Piggush, J. D.** (2006), *Turbine Endwall Aerodynamics and Heat Transfer*, Annals of the New York Academy of Sciences **934**, pp: 27-36.
- Steiner, P.** (2000), *Application of the Pressure Sensitive Paint Technique to the Turbomachinery Environment*, Ph.D. Thesis 2297, Ecole Polytechnique fédérale de Lausanne, Lausanne
- Sundaram, N., Barringer, M. D. and Thole, K. A.** (2008), *Effects of Deposits on Film Cooling of a Vane Endwall Along the Pressure Side*, J. Turbomachinery **130**, (4), p: 041006.
- Suryanarayanan, A., Mhetras, S. P., Schobeiri, M. T. and Han, J. C.** (2009), *Film-Cooling Effectiveness on a Rotating Blade Platform*, J. Turbomachinery **131**, pp: 011014-1 - 12.
- Takeishi, K., Matsuura, M., Aoki, S. and Sato, T.** (1990), *An experimental study of heat transfer and film cooling on low aspect ratio turbine nozzles*, J. Turbomachinery **112**, pp: 488-496.
- Tropea, C., Yarin, A. L. and Foss, J. F.** (2007), *Springer Handbook of Experimental Fluid Mechanics*, 1st Ed., Springer.
- Vogel, G.** (2002), *Experimental Study on a Heavily Film Cooled Nozzle Guide Vane with Contoured Platforms*, Ph.D. Thesis 2602, EPFL, Lausanne
- Vogel, G., Wagner, G. and Bölcs, A.** (2002), *Transient Liquid Crystal Technique Combined with PSP Film Cooling Measurements*, The 10th International Symposium on Flow Visualization, Kyoto, Japan.

-
- Vogel, G., Graf, A., von Wolfersdorf, J. and Weigand, B.** (2003), *A Novel Transient Heater-Foil Technique for Liquid Crystal Experiments on Film-Cooled Surfaces*, J. of Turbomachinery **125**, pp: 529-537.
- von Kaenel, R.** (2003), *Large-eddy simulation of compressible flows using the finite-volume method*, Swiss Federal Institute of Technology, ETH, Zürich
- von Wolfersdorf, J., Hoecker, R. and Sattelmayer, T.** (1993), *A Hybrid Transient Step-Heating Heat Transfer Measurement Technique using Heater Foils and Liquid-Crystal Thermography*, J. Heat Transfer **115**, pp: 319-324.
- von Wolfersdorf, J., Ott, P. and Weigand, B.** (2006). *Temperature and Pressure Sensitive Coatings, Flow Phenomena in Nature, Volume 2 - Inspiration, Learning and Application*, WIT Press, pp: 747-766.
- von Wolfersdorf, J.** (2007), *Influence of lateral conduction due to flow temperature variations in transient heat transfer measurements*, Int. J. Heat and Mass Transfer **50**, (5-6), p: 1122.
- Wagner, G.** (2007), *Experimental investigations of showerhead film cooling on the leading edge of a turbine blade*, Ph.D. Thesis 3755, EPFL, Lausanne
- Wagner, G., Schneider, E., von Wolfersdorf, J., Ott, P. and Weigand, B.** (2007), *Method For Analysis of Shower Head Film Cooling Experiments on Highly Curved Surfaces*, J. of Experimental Thermal and Fluid Science **31**, pp: 381-389.
- Weideman, J. A. C.** (1994), *Computation of the Complex Error Function*, SIAM J. Numerical Analysis **31**, pp: 1497-1518.
- Weigand, B.** (2010), *Convective Heat Transfer at High Velocities*, 2nd Ed.
- Wright, L. M., Blake, S. and Han, J. C.** (2007), *Effectiveness Distributions on Turbine-Blade Cascade Platforms Through Simulated Stator-Rotor Seals*, J. of Thermophysics and Heat Transfer **21**, (4), pp: 754-762.
- Wu, P. S. and Chang, S. F.** (2007), *Vane Endwall Heat Transfer for Smooth and Stepped Inlet Using Streamwise and Cross Stream Film Injection*, Turbo Expo, GT2007-27850.
- Wunderlin, J.** (2006), *Validation of the PSP Measurement Technique for Determination of Film Cooling Effectiveness on a Flat Plate*, Diploma Work EPFL, Lausanne
- Zanker, A.** (2008), *Measurement and Analysis of Heat Transfer on a Turbine Vane Platform*, Diploma Work EPFL, Lausanne
- Zhang, L. J. and Jaiswal, R. S.** (2001), *Turbine Nozzle Endwall Film Cooling Study Using Pressure Sensitive Paint*, J. Turbomachinery **123**, pp: 730-738.

Appendix A

Derivation of Adiabatic Film Cooling Effectiveness

The following is a description of the application of the heat and mass transfer analogy for oxygen pressure measurements using PSP. In order to express Equation (15) in terms of partial pressure of oxygen, the mass fractions are converted into molecular fractions by introducing the molecular weights of the gas species and mixture at the wall:

$$\eta_{energetic} = \frac{\frac{\xi_{g,O_2} \mathcal{M}_{O_2}}{\mathcal{M}_g} - \frac{\xi_{w,O_2} \mathcal{M}_{O_2}}{\mathcal{M}_w}}{\frac{\xi_{g,O_2} \mathcal{M}_{O_2}}{\mathcal{M}_g}} = 1 - \frac{\mathcal{M}_g}{\mathcal{M}_w} \frac{\xi_{w,O_2}}{\xi_{g,O_2}} \quad (44)$$

With the known molecular concentration of oxygen in air ($\xi_{g,O_2} = 0.21$), this reduces to:

$$\eta_{energetic} = 1 - \frac{\mathcal{M}_g}{\mathcal{M}_w} \frac{(p_{O_2}/p)_w}{(p_{O_2}/p)_g} = 1 - \frac{\mathcal{M}_g}{\mathcal{M}_w} \frac{(p_{O_2}/p)_w}{0.21} \quad (45)$$

Since air is used as main fluid, the molecular mass of the gas is

$$\begin{aligned} \mathcal{M}_g &= \xi_{N_2} \mathcal{M}_{N_2} + \xi_{O_2} \mathcal{M}_{O_2} \\ &= 0.79 \mathcal{M}_{N_2} + 0.21 \mathcal{M}_{O_2} \end{aligned} \quad (46)$$

and the unknown molecular mass at the wall can be expressed by

$$\mathcal{M}_w = \xi_c \mathcal{M}_c + \xi_{N_2} \mathcal{M}_{N_2} + \xi_{O_2} \mathcal{M}_{O_2}. \quad (47)$$

The relative molecular fractions of Nitrogen and Oxygen remain constant when the mainstream mixes with the injected coolant ($\xi_{N_2} = 79/21 \xi_{O_2}$). Therefore, the molecular fraction of coolant at the wall is rewritten in terms of the molecular fraction of oxygen:

$$\begin{aligned}\xi_c &= 1 - \xi_{N_2} - \xi_{O_2} \\ &= 1 - \frac{79}{21} \xi_{O_2} - \xi_{O_2} \\ &= 1 - \frac{100}{21} \left(\frac{p_{O_2}}{p} \right)_w\end{aligned}\tag{48}$$

As validated by Wunderlin (2006), inserting Equations (46 – 48) into Equation (45) results in the following expression for the adiabatic film cooling effectiveness when the main-flow is air:

$$\eta_{energetic} = 1 - \frac{1}{\left[\frac{21}{100} \left(\frac{p}{p_{O_2}} \right)_w - 1 \right] \frac{\mathcal{M}_c}{\mathcal{M}_g} + 1}\tag{49}$$

Pressure sensitive paint is then used to determine both the static pressure p in Equation (49) and the partial pressure distribution of oxygen in the presence of foreign gas injection.

Appendix B

Heat Release Distribution

Figure 58 contains an experimental comparison of the non-dimensional heat release distribution modelled with the Finite Element Solver (Comsol®).

Transient TLC

Flow experiment
Transient TLC

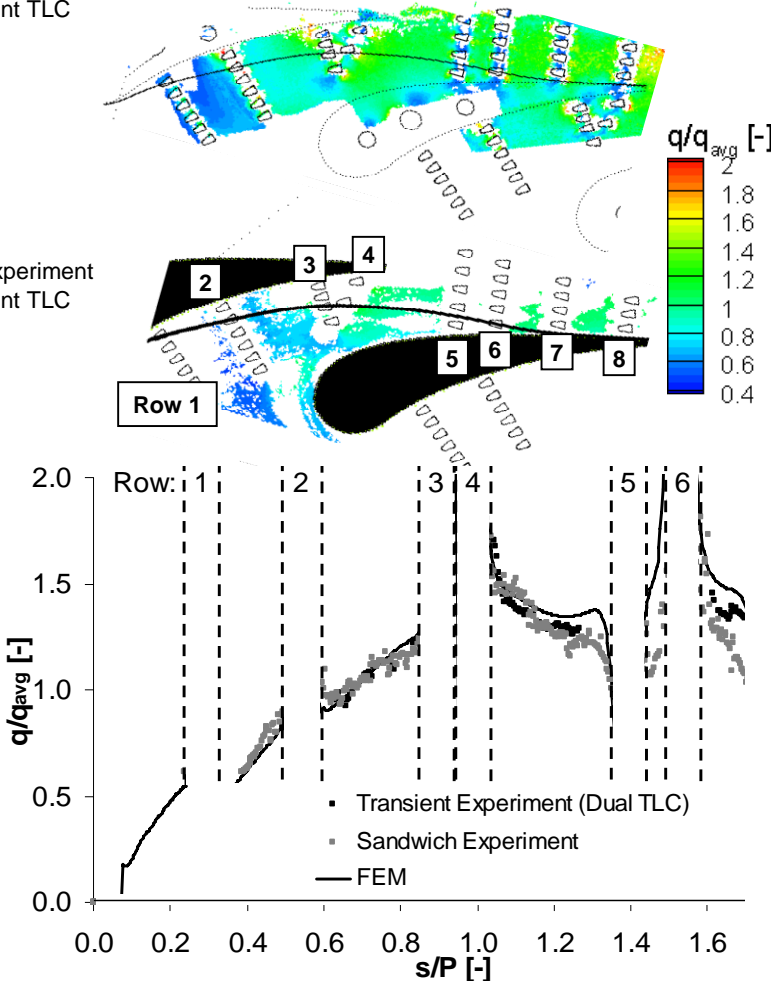


Figure 58: Heat release distribution in the heater foil

Appendix C

In-Situ Calibration Procedure

Figure 59 shows an example procedure in order to measure the PSP-intensity at known reference conditions (pressure and temperature). A slow temperature reduction in the test facility after the end of the flow measurements is used to calibrate the global temperature sensitivity of the PSP in-situ. The test temperature range is covered by raising the mainflow temperature somewhat before switching off the air supply.

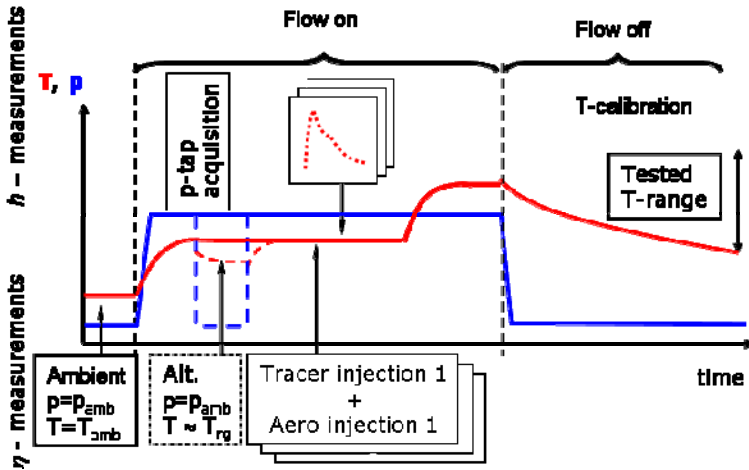


Figure 59: Measurement and in-situ calibration procedure

Appendix D

Boundary Layer Modelling (TexStan)

In boundary layer flows, only the upstream information is required to find the solution in each streamwise position. This parabolic nature of the boundary layer equations allows to start the integration at the inlet in the downstream direction. Airfoil mid-span results at the suction side is used for illustration of a representative boundary layer without film cooling injection.

Influence of Thermal Boundary Conditions (2D)

Figure 60 shows a local variation of heat transfer coefficients due to different thermal boundary conditions.

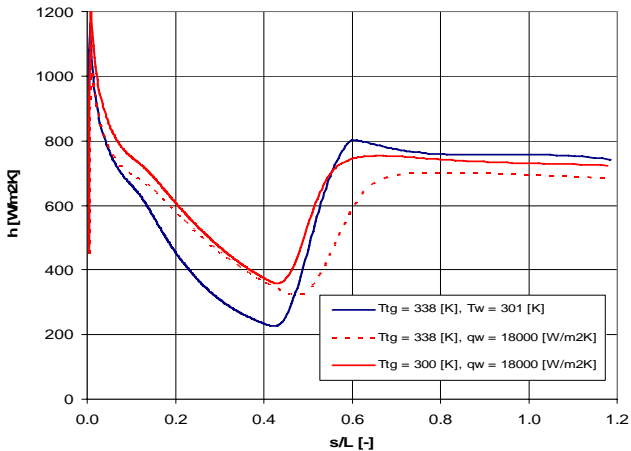


Figure 60: Comparison of wall boundary conditions using TexStan

Simulation of Transient Heat Transfer Experiment

Having demonstrated the sensitivity to thermal boundary conditions for the steady steady-state situation, this section attempts to assess this effect on the transient heat transfer experiments where it is assumed that the heat transfer coefficients are constant in time. Because the time-response of the wall is determined by the heat transfer coefficient, the thermal boundary conditions along a surface vary in time in the presence of large h -gradients. Figure 61 shows the wall temperature evolution of the suction-side example. Theoretically, this leads to an offset between steady and transient heat transfer results due to varying thermal boundary conditions observed in the vicinity of the laminar to turbulent transition region. However, this effect is small in fully turbulent boundary layers—especially when the distribution of the thermal boundary condition is as smooth as in this smooth-wall case. Gradients are significantly larger in the film cooled case.

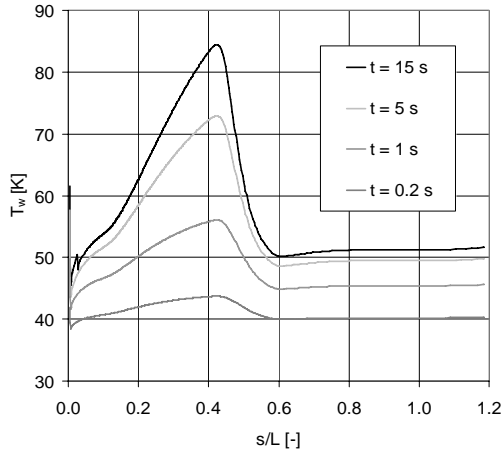


Figure 61: Transient evolution of wall temperature

Appendix E

Inlet Boundary Layer Characterization

The incoming boundary layer has been measured with a Dantec 55M01, constant temperature anemometer and a standard single hotwire probe (5 μ m wire diameter). The small size of hot wire anemometers makes them suitable for near-wall measurements. The velocity is derived from the convective heat transfer between the hot wire and the colder flow. The probe was calibrated for velocity measurements using a laminar free-jet device as in the work by Erber (2007). The calibration range was extended with in-situ data (obtained with a Pitot probe) due to mass flow limitations of the compressed air supply for the free-jet. In fact, the inlet flow Mach number is too high to apply King's law since it is valid for incompressible flows. Therefore, a 3rd order least-square curve fit of the Reynolds number as a function of probe voltage (heat transfer factor) is applied according to Figure 62. The fitted calibration curve spans the range of tested Reynolds numbers. This is similar to the work of Drost and Bölcs (1999).

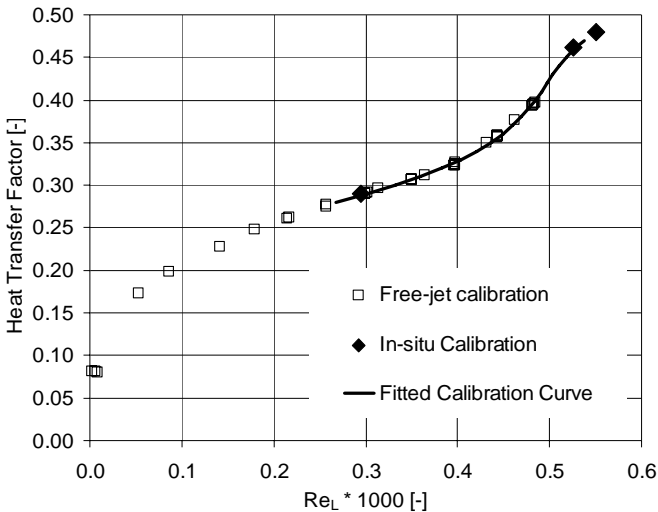


Figure 62: Hot-wire calibration

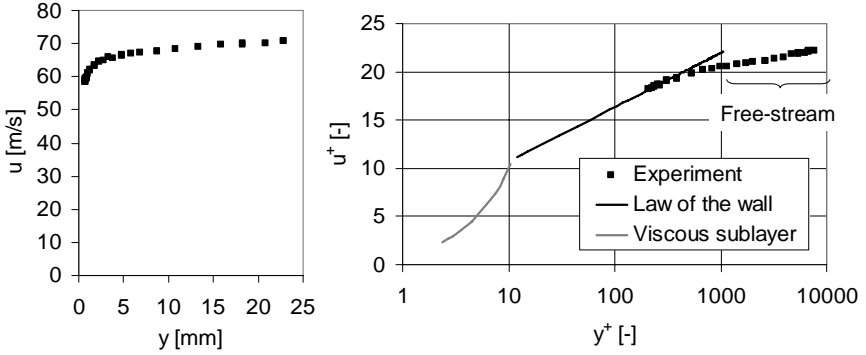


Figure 63: Inlet velocity profile on the endwall

The support structure holding the probe limits the minimum achievable distance to the wall. Approaching the wall further might require additional corrections for thermal interactions with the wall according to Bruun (1995). The standard procedure is to extrapolate the measured velocity distribution with boundary layer theory. As presented in Figure 63, this is done by comparing the results to the law of the wall for a turbulent layer:

$$u^+ = \frac{1}{\kappa'} \ln(y^+) + C^+ \quad (50)$$

Presenting the normal wall coordinate (y) in a semi logarithmic plot allows to better visualize the velocity distribution in the boundary layer. The wall coordinate is expressed in terms of the non-dimensional wall distance according to:

$$y^+ = \frac{u_\tau y}{\nu} \quad (51)$$

with the local kinematic viscosity of the fluid and the shear velocity:

$$u_\tau = \sqrt{\frac{|\tau_w|}{\rho}} \quad (52)$$

The non-dimensional velocity distribution in the boundary layer is defined with respect to the characteristic shear velocity:

$$u^+ = \frac{u}{u_\tau} \quad (53)$$

Equation (50) also contains the von Karman constant ($\kappa' = 0.41$) and another constant for smooth walls ($C^+ = 0.51$). The theoretical curve given by Equation (50) is matched to the experimental data of Equation (53) by adjusting the shear velocity at the wall. Good agreement can be observed at $u_\tau = 3.2$.

From Figure 63 it is judged that the outer boundary layer limit is at $y^+ = 1'000$. This is equivalent to a boundary layer thickness of 3.5 mm. The velocity distribution that can be seen outside of the boundary layer is considered to be part of the free-stream and most likely due to the upstream turbulence grid. The corresponding displacement and momentum loss thicknesses are estimated by integrating over the boundary layer:

$$\delta_1 = \int_{y=0}^{3.5mm} \left(1 - \frac{u}{u_\infty}\right) dy \quad (54)$$

$$\delta_2 = \int_{y=0}^{3.5mm} \frac{u}{u_\infty} \left(1 - \frac{u}{u_\infty}\right) dy \quad (55)$$

Appendix F

CFD Modelling

In order to assess the impact of the incoming boundary layer and other parameters, fully turbulent CFD-calculations have been carried out on similar platform configurations — the numerical details are given by Charbonnier et al. (2009). Mesh generation was performed with *ICEM-CFD* and calculations with the *ANSYS-Fluent* solver. The domain included in the model is visualized in Figure 64.

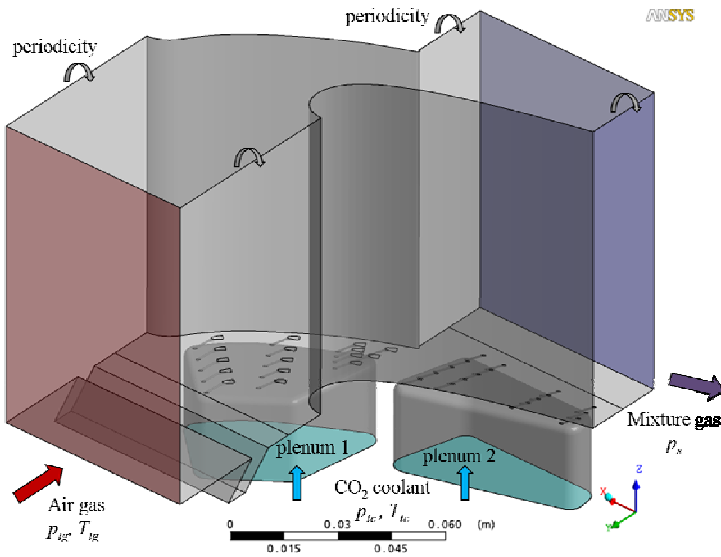


Figure 64: CFD (3D-RANS) model and mesh of a platform test case

Influence of Thermal Boundary Conditions (2D)

A couple of parameter studies related to the present thesis are detailed below:

1. The first section treats the impact of the thermal boundary conditions and their distribution on the wall on the heat transfer measurements.
2. The 3D capability of CFD allows for assessment of the impact of a radial temperature distribution of the incoming flow, and how this affects the adiabatic wall temperature on the platform.

3. The analogy between heat and mass transfer is verified using the capability to model multiple species.
4. A brief comparison of calculated and measured adiabatic film cooling effectiveness results.

Figure 65 shows the impact of heat release distribution on the predicted convective heat transfer coefficients. A constant heat flux (top-left) and spatial variation (top-right) as determined by FE-modelling are applied in the CFD model. The resulting heat transfer coefficients (bottom) show local differences close to the cooling holes. This is due to the complex thermal boundary conditions at the wall generated by the heater foil. It illustrates the effect of un-heated/over-heated starting lengths. However, the effect appear to be relatively local in nature.

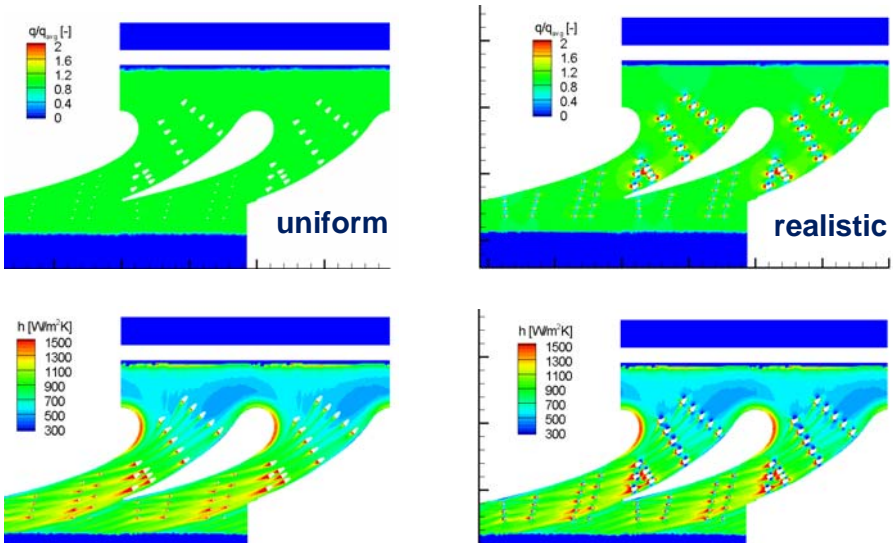


Figure 65: Predicted heat release (top), heat transfer coefficients (bottom)

Sensitivity of heat transfer coefficients to inlet boundary layers has been assessed with the CFD model. Figure 66 shows results with constant radial distribution of total pressure at inlet (left) and measured distribution (right). The 2D results have been averaged in the pitch-wise direction and plotted along a streamwise coordinate normalised by the total length of the averaging box (Figure 67). Differences in the predicted heat transfer coefficients between the two computations are visible only on the surface near the inlet of the cascade (just downstream of the slot). This is attributed to the restarting action that the slot has on the boundary layer.

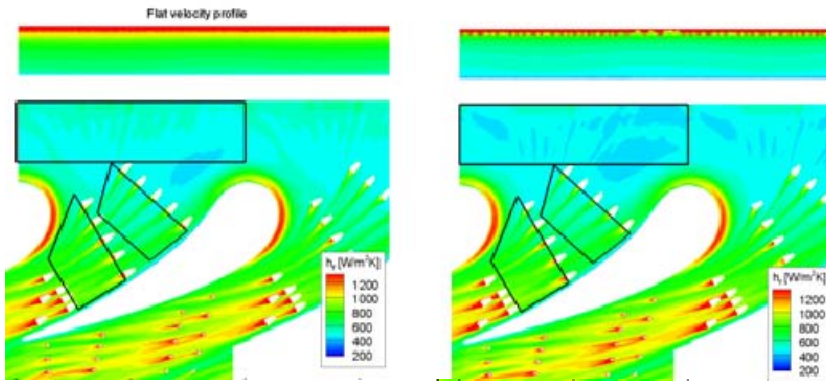


Figure 66: Impact of inlet boundary layer on heat transfer coefficients

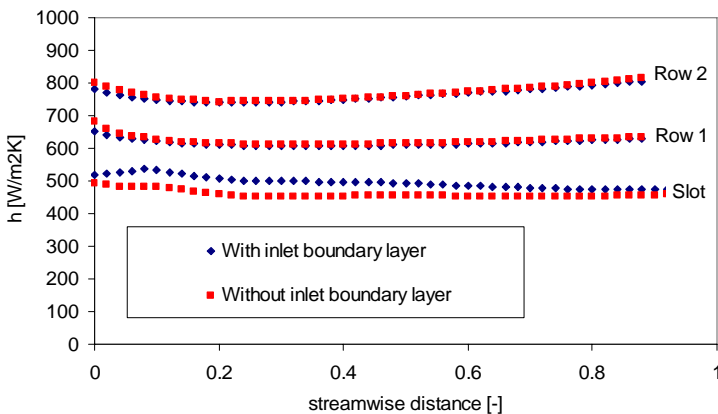


Figure 67: Sensitivity to inlet boundary layer on convective heat transfer

Figure 68 shows numerical results of adiabatic film cooling effectiveness (left). This test case includes injection through the upstream slot in addition to cooling holes. A comparison of the three definitions of η employed in this thesis is provided on the averaged results (right). It can be seen that the impermeable effectiveness (mass concentration) agrees with the energetic definition of the adiabatic film cooling effectiveness according to the analogy between heat and mass transfer. The temperature-based definition is offset according to Equation (26).

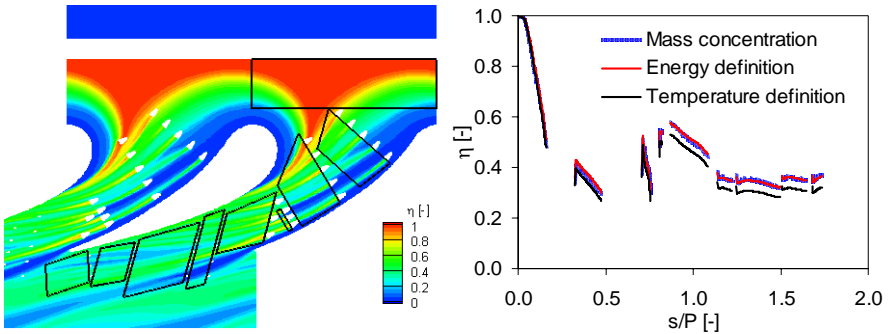


Figure 68: Calculated adiabatic film cooling effectiveness

Figure 69 show a comparison between measured and computed adiabatic film cooling effectiveness. The surface result has been averaged in the lateral direction over the regions depicted in the plot.

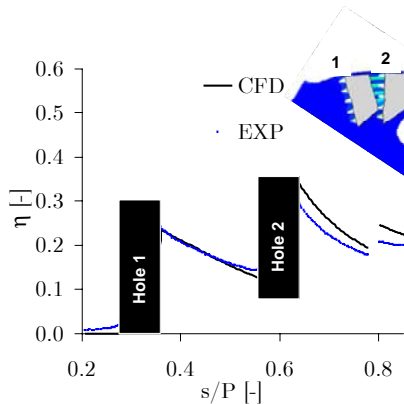


Figure 69: Numerical comparison of adiabatic film cooling effectiveness

Appendix G

Film Cooling Flow Parameters

In order to determine the losses inside the holes as well as pressure recovery induced by the exit diffusers of the shaped holes, the discharge coefficients have been measured. Based on the low impact of the mainstream reported by Gritsch et al. (2000), the tests were done without any mainstream, i.e. dumping into ambient pressure. An advantage of this procedure is that all holes can be measured simultaneously. Since all holes are of the same shape, it is assumed that they have the same discharge characteristics. Therefore, each plenum chamber was measured separately to ensure a common feed pressure. The coolant mass flow, that is determined by laminar flow elements, is normalised by the ideal flow rate:

$$C_d = \frac{\dot{m}}{\dot{m}_{is}} \quad (56)$$

$$\dot{m}_{is} = A_{c,cylindric} \rho_c u_{is,c} \quad (57)$$

where the ambient back pressure is used until sonic choking is predicted. This is done by computing the isentropic coolant Mach number according to:

$$Ma_{is,c} = \min \left(1.0, \sqrt{\frac{2}{\kappa_c - 1} \left[\left(\frac{p_g}{p_{tc}} \right)^{-\frac{\kappa_c - 1}{\kappa_c}} - 1 \right]} \right), \quad \kappa_c = 1.28 \text{ (CO}_2\text{)} \quad (58)$$

followed by the derivation of the static cooling gas conditions:

$$p_c = p_{tc} \left(1 + \frac{\kappa_c - 1}{2} Ma_{is,c}^2 \right)^{-\frac{\kappa_c}{\kappa_c - 1}} \quad (59)$$

$$T_c = T_{tc} \left(1 + \frac{\kappa_c - 1}{2} Ma_{is,c}^2 \right)^{-1} \quad (60)$$

$$\rho_c = \frac{p_c}{R_c T_c}, \text{ where } R_c = 188.92 \text{ J/kgK (CO}_2\text{)} \quad (61)$$

Therefore, when $Ma_{c,is} = 1.0$ the isentropic flow rate is solely a function of the feed pressure (P_{tc}). The isentropic coolant velocity is then calculated,

$$a_g = \sqrt{\kappa R_g T_g} \quad (62)$$

$$u_{is,c} = Ma_{is,c} a_c \quad (63)$$

This ideal coolant mass flow is the same as the more compact expression as long as the pressure ratio does not exceed the critical level.

$$\dot{m}_{is} = A_{c,cylindric} \frac{p_{tc}}{\sqrt{R T_{tc}}} \left(\frac{p_c}{p_{tc}} \right)^{\frac{1}{\kappa}} \sqrt{\frac{2\kappa}{\kappa-1} \left[1 - \left(\frac{p_c}{p_{tc}} \right)^{\frac{\kappa-1}{\kappa}} \right]} \quad (64)$$

The resulting discharge coefficients of the holes are used to derive the cooling gas quantities for each row in the same manner. In detail, the static dump pressures are obtained by linear interpolation of the external isentropic Mach number distribution of the main-flow at the cooling-hole positions. The isentropic Mach numbers have been obtained from an un-cooled CFD calculation validated with pressure tap measurements. For simplicity, an averaged Mach number is extracted for each row of holes which is a good approximation since the holes are, in this case, positioned roughly along isobar lines on the platform. With the isentropic Mach numbers of the main-flow available, the external static pressure at the individual row locations are derived:

$$p_g = p_{tg} \left(1 + \frac{\kappa-1}{2} Ma_{is}^2 \right)^{-\frac{\kappa}{\kappa-1}} \quad (65)$$

The other main-flow properties are also needed for reference purpose:

$$T_g = T_{tg} \left(1 + \frac{\kappa-1}{2} Ma_{is}^2 \right)^{-1} \quad (66)$$

$$\rho_g = \frac{p_g}{R_g T_g}, \text{ where } R_g = 287.22 \text{ J/kgK} \quad (67)$$

$$a_g = \sqrt{\kappa R_g T_g} \quad (68)$$

$$u_{g,is} = Ma_{is} a_g \quad (69)$$

Then the conditions are computed according to Equations (59) to (64). Based on coolant total temperature measurements inside the plenum chambers and the assumption of adiabatic walls inside the holes, the static coolant

temperatures are determined for each hole. Density ratio (DR), blowing (M) and momentum ratios (I) can then be calculated according to:

$$DR = \frac{\rho_c}{\rho_g} \quad (70)$$

$$M = C_d M_{is} = C_d \frac{\rho_c u_{c, is}}{\rho_g u_{g, is}} = \frac{\rho_c u_c}{\rho_g u_{g, is}} \quad (71)$$

$$I = \frac{M^2}{DR} \quad (72)$$

The transfer between isentropic and real properties is done by multiplying with the measured discharge coefficient of the cooling holes. Finally, the total coolant mass flow is obtained from the sum of all flows:

$$\dot{m}_{c, tot} = \sum_{j=1}^N \left(C_d A_{c, cylindrical} \rho_c u_{c, is} \right)_j \quad (73)$$

Acknowledgements

The presented work has been conducted at the “Laboratoire de Thermique Appliquée et de Turbomachines” (LTT) of EPFL. The research project has been financially supported by the European Commission via the industrial/academic research project TATEF2 (Turbine Aero-Thermal External Flows 2). The active participation of Alstom Switzerland in the present task was highly appreciated.

First of all, I would like to thank my thesis director Dr. Peter Ott for giving me the chance to carry out this thesis and showing me trust and support. Furthermore, I would like to express my gratitude to the thesis jury. Prof. Daniel Favrat and Prof. John Thome made very valuable efforts at the final stage of the thesis. A special thank to Prof. Bernhard Weigand for the regular and enriching discussions on turbulence, mixing and more down-to-earth topics such as crème brûlée. I deeply appreciated collaborating with Dr. Jörg Krückels for all the fruitful feedback and putting the results in perspective —throughout the TATEF2 project duration — and beyond.

The assistance of Prof. Jens von Wolfersdorf was of great value, including hands-on experiments, analysis, discussions and writing on the topic of heat transfer. I am also grateful to Dr. Gregory Vogel for defining the research project and introducing me to the fascinating domain of cooling. Many thanks to Dr. Guillaume Wagner for teaching me how to find my way amongst the lab equipment, measurement techniques and skiing tricks (I haven’t tried them all yet).

I enjoyed the inspiring and helpful work that was going on with my diploma students Jens Wunderlin, Andreas Erber as well as Achim Zanker who became part of the LTT-team. Many thanks to Prof. Michael E. Crawford for introducing me to the art of boundary layer analysis and for setting up the interactive guide to TexStan. Thanks also to Dr. Trong-Vien Truong for lending me his equipment and expertise in the most critical moments.

Then I would like to thank all my colleagues at the lab who gave me inspiration, support and friendship. This work would not have been possible without our fruitful discussions as well as coffee-breaks and BBQ’s. Many thanks to Dr. Dominique Charbonnier for the precious collaboration on film cooling including the impressive meshing work related to such geometries.

Acknowledgements

Thanks to Dr. Stefan Kristukat for the frisbee lessons and biking company up to Lausanne. Dr. Arrigo Beretta gave me early kick-off advice on lab work. Dr. Samantha Pavon introduced me to high performance cameras and was always available to assist in everything from starting a megawatt-compressor to finding the right glue to secure items exposed to near-sonic flow velocities. Elia Colombo and Virginie Chenaux, from the sunny side of the corridor, shared their time and experiences (e.g. on how to setup a pressure gauge device with 80 channels — or were there more?). Dr. Cécile Deslot helped me out with computers and the French language. Alexandros Terzis taught me a lot about aero-engines and accepted to share office with me during the last intense phase of my thesis! I appreciated the interesting chats I had with Sami Goekce and Philip Peschke that often tended to end up in discussions about interdisciplinary spin-off possibilities. I am very grateful to Annick Despont and Stina Zufferey for assisting with the administrative science even on short notice.

Many thanks to the technicians Marc Salle, Bernhard Savary, Jean-Pierre Rougnon, Laurent Chevalley, Jean-Pierre Rudaz and Nicolas Jaumin. A special thank to Christophe Zurmühle for the continuous collaboration, especially for showing me how to mount very thin heater foils on platforms!

My deepest gratitude goes to my family and friends for inspiring me during this work and also for accepting temporary absences during intense laboratory periods. I very much appreciated the advice from my parents gave me on how to tackle big tasks (piece-by-piece). Finally, I owe my wife Justine a lot for her love, understanding and support throughout this work — thank you!

Magnus

Curriculum Vitae

Name: Magnus JONSSON
Date of birth: June 17, 1976
Place of birth: Umeå, Sweden
Phone: +41 76 509 46 69
E-mail: m@jonsson.ac
Nationality: Swedish
Status: Married



WORK EXPERIENCE

- 2005 - 2010 **Swiss Federal Institute of Technology (EPFL)**, Lausanne, *PhD-student*, Laboratory of Applied Thermodynamics and Turbomachinery (LTT), PhD-thesis: “Application of Photoluminescent Measurement Techniques for Quantitative Assessment of Turbine Film Cooling”
Collaboration within a European research project (*TATEF-2*)
- 2001 - 2004 **ALSTOM Power Turbo Systems**, Baden, Switzerland, *Development engineer* in the Gas Turbine Department
Aerodynamic design of highly cooled turbine blades
- Summer 1999 **SAAB Aerospace**, Linköping, Sweden, *Internship*

EDUCATION

- 2005 - 2008 **Swiss Federal Institute of Technology (EPFL)**, Lausanne
Courses within the Energy Program of the Doctoral School
- 1996 - 2001 **Royal Institute of Technology (KTH)**, Stockholm, Sweden
MSc. Eng. in Aeronautical Engineering. Diploma thesis: “Simulation of a turbine cascade using the NSMB flow solver”
- 1998 - 1999 **University of Bristol**, UK, *Erasmus exchange student (3rd year)*
- 1995 - 1996 **Swedish Air Force**, Luleå, *Military service as flight mechanic*

LANGUAGES

- Swedish: Mother tongue
English: Excellent knowledge
French: Fluent
German: Good knowledge